ESTIMATION OF SEISMIC ATTENUATION FROM VSP DATA IN TWO COOPER/EROMANGA BASIN WELLS USING THE SPECTRAL RATIO METHOD.

A THESIS SUBMITTED TO

THE NATIONAL CENTER FOR PETROLEUM GEOLOGY AND GEOPHYSICS,

FOR PARTIAL FULFILMENT OF THE M.SC. DEGREE

IN PETROLEUM GEOLOGY AND GEOPHYSICS,

BY

PAUL SIFFLEET.

1994

TABLE OF CONTENTS

TABLE OF CONTENTS (Cont.)

TABLE OF CONTENTS (Cont.)

This work contains no material which has been accepted for the award of any other degree or diploma in any university or other tertiary institution and, to the best of my knowledge and belief, contains no material previously published or written by another person, except where due reference has been made in the text.

I give consent to this copy of my thesis, when deposited in the University Library, being available for loan and photocopying.

PAUL B. SIFFLEET

1ST AUGUST 1994

ABSTRACT

Anelastic or intrinsic attenuation is the loss of energy through frictional processes from a propagating seismic wave, resulting in both a decrease in amplitude and a change in frequency content. Laboratory and in-situ measurements indicate that, within the bandwidth of conventional seismic data, attenuation obeys a negative exponential law, the exponent of which is a linear function of frequency and may be parameterised by a dimensionless quantity, Q, a constant for any particular rock.

The spectral ratio method is commonly used to estimate attenuation from vertical seismic profile data. The technique involves comparing the amplitude spectrum of a reference signal with successive downhole VSP first arrival spectra to determine cumulative attenuation. Q is then calculated from the rate at which cumulative attenuation increases with depth. The attenuation measured in this way is a combination of both the intrinsic attenuation, due to rock properties, and the apparent attenuation resulting from short-period multiple reflections.

Attempts to estimate attenuation using the spectral ratio method were made on VSP data recorded in two wells penetrating representative Cooper and Eromanga Basin sediments in South Australia and Queensland. Measured attenuation from one of these wells, Watson #1, implies Q values ranging from 26 to over 400. Synthetic VSP's created from log data, both with and without multiples provide the method to determine the apparent attenuation, which appears to be responsible for between 4% and 82% of the measured attenuation. In particular, cyclic coal sequences encountered in the Permian give rise to very high apparent attenuation rates.

Spectral ratios for the second well, Tirrawarra #22, could not be interpreted for Q, due to severe notching in the spectra of the downhole data.

The accuracy of the intrinsic attenuation estimates over small depth intervals is insufficient to make correlations with lithology, particularly in reservoirs of limited vertical extent. A Q log constructed from intrinsic attenuation and interval velocity is compared with known geological information.

Attention to data acquisition procedures, the minimizing of noise and "ghosting" effects, are necessary in recording data of a quality suitable for analysis. The use of a far field signature to compute the spectral ratio for each VSP level is shown to give a better result than using a shallow VSP trace as the reference signal.

The attenuation measurements presented here should prove useful in quantifying the known problem in collecting wide bandwidth seismic data in the area, and in the design of inverse-Q filters.

LIST OF FIGURES

LIST OF TABLES

CHAPTER 1

INTRODUCTION

Hydrocarbon exploration of the Cooper and Eromanga Basins, that make up the largest onshore hydrocarbon area in Australia, is mainly performed by seismic methods. These involve introducing a seismic signal at, or close to, the earth's surface, and recording the reflections, refractions, and direct arrivals of the propagating signal. The energy content of all such signals diminishes as they propagate. This loss of energy is due to spherical divergence, transmission losses, mode conversion, scattering, dispersion, and attenuation.

Seismic wave attenuation, in the context of this study, is defined as the anelastic loss of energy, through frictional processes, from a seismic signal as it propagates through the earth. Measurements of attenuation are most commonly given as Q values. Lower Q values imply greater rates of attenuation. Q is an intrinsic property of materials, and is the ratio of stored energy to dissipated energy (Johnston and Toksoz, 1981).

Other terms commonly used in conjunction with attenuation measurements are; i) the logarithmic decrement δ; ii) the reciprocal of Q; iii) the coefficient of attenuation α, which is the exponential decay constant of the amplitude of a plane wave propagating in a homogenous medium. These terms are related as follows (Johnston and Toksoz, 1981).

$$1/Q = \alpha v/\pi f = \delta/\pi \qquad \ldots 1$$

Here v and f are velocity and frequency respectively.

The attenuation of a seismic signal is known from laboratory studies to be affected by pore fluids, saturation, confining pressure, porosity, and temperature (Toksoz et al. 1979; Mavko and Nur, 1979; Winkler and Nur, 1979; Johnston and Toksoz, 1981). The possibility of determining attenuation from seismic data and correlation of such values with lithology makes Q estimation highly desirable. This is particularly so in hydrocarbon bearing zones, where such estimates may yield valuable information about reservoir properties.

Because most exploration activity is dependent on seismic reflection techniques, a detailed understanding of the behaviour of a propagating seismic wavelet is desirable. With an understanding of the attenuation a signal undergoes, an improvement in acquisition and processing may be possible, particularly in relation to collecting wide bandwidth data and inverse-Q filtering.

Laboratory and in-situ measurements of attenuation show that its effect is to reduce both the amplitude and the frequency content of a propagating seismic wavelet. The results of McDonal et al. (1958), Tullos and Reid (1969), and Stainsby and Worthington (1985) all support the theory that attenuation obeys a negative exponential law in which the exponent is a linear function of frequency. Consequently the hypothesis of a constant-Q model, that is Q independent of frequency, is often adopted.

With a constant-Q model, a method to quantify attenuation can be designed using the amplitude spectra of a propagating wavelet recorded at successive depths. This forms the basis of a method known as the spectral ratio technique. Unfortunately conventional reflection seismic data is unsuitable for this method of analysis. However, vertical seismic profiling does provide usable data. VSPs are unique in that by assuming an identically repeatable seismic pulse, seismic wave propagation can be monitored vertically through the geologic column over the depth of a borehole.

The spectral ratio method involves determining the amplitude spectrum for each direct downhole arrival of the VSP and then constructing the spectral ratio between each downhole

signal and a reference signal, or signals. This results in a measure of the cumulative attenuation between the reference and successive downhole signals. A value of the cumulative attenuation for each successive downhole signal, plotted against depth, gives a measure of the rate of attenuation over any interval, and is related to Q by:

$$\pi/Q = v_X k_X \qquad \ldots 2$$

where v_X is the interval velocity, and k_X is the rate of attenuation.

From several studies, including those of Schoenberger and Levin (1974), it is known that the observed or effective attenuation is the sum of the intrinsic and apparent attenuation. The intrinsic attenuation is that due directly to lithology, while the apparent attenuation is a result of short-period multiple reflections. By determining the effective attenuation from VSP data, and the apparent attenuation from model data, an estimate of the intrinsic attenuation can be made.

Using the estimates of intrinsic attenuation, Q-logs may be computed and compared to the geological information available, with particular reference to the mechanisms of attenuation that are responsible.

Two VSP data sets recorded in the Cooper and Eromanga Basins of Australia, and selected as representative of these basins, were analysed to determine estimates of attenuation. VSP data may be acquired with signals generated from a variety of seismic sources, and the two selected sets used airgun and Vibroseis* sources.

In order to progress this study in a logical manner a series of goals were set, and methods to realize them followed.

* Registered trademark of Conoco Inc.

Goals:

1. To determine realistic values of Q for the Cooper and Eromanga basin rocks.

2. To determine if the spectral ratio method is appropriate for the estimation of Q from VSP data.

3. To determine, via synthetic VSPs, the proportion of the observed attenuation that is attributable to short-period multiple activity.

4. To determine if rock properties, particularly over hydrocarbon reservoir zones, can be deduced from intrinsic attenuation estimates.

5. To investigate how attenuation estimates can be used to improve the acquisition, processing, and interpretation of seismic data.

Methods:

1. Carry out a comprehensive literature search to locate all relevant studies on attenuation with particular reference to mechanisms, measurement techniques, and VSP data.

2. Describe the Cooper and Eromanga basins with respect to both seismic response and stratigraphy.

3. Using borehole log data, construct models, and generate synthetic VSPs both with and without multiples.

4. Develop a reliable processing route to estimate the attenuation of a propagating seismic wavelet using the spectral ratio technique and VSP data. Ascertain the sensitivity of the estimates to changing input parameters.

5. Generate a Q log that can be correlated with conventional log data.

CHAPTER 2

AN OUTLINE OF THE GEOLOGY AND GEOPHYSICS OF THE STUDY AREA

2.1 Geology

The Cooper Basin is an intracratonic downwarp of Permian-Triassic age extending over an area of 127,000km^2. It unconformably overlies earlier Palaeozoic basins and is in turn unconformably overlain by Jurassic and Cretaceous sediments of the Eromanga Basin, which extend over an area of 1,000,000 km^2. The location of these basins within the Australian continent is shown in Figure 1.

A stratigraphic column for the Cooper and Eromanga Basins is shown in Figure 2. The boundary between the basins occurs in the Early Jurassic to Late Triassic. The figure gives a description of the prevailing environments, and the lithology of the sediments. The following paragraphs offer a brief outline of the basins.

The sediments of the Cooper Basin, deposited on eroded Proterozoic and Palaeozoic sediments, are lacustrine shales, fluvial sandstones, and fluvio-deltaic coals. Part of the sequence was deposited in large bodies of standing water that may have had distant connection with the open sea (Stuart 1976). The Cooper sequence can exceed a thickness of 2000m, and the depth to its top varies from 1200m along the southern margin, to greater than 3000m in the Nappamerri and Patchawarra Troughs. Throughout the Early Permian, localised uplift and erosion occurred with the Daralingie unconformity representing a major, basin wide, structural event. Apart from this, there was some re-activation of Pre-Permian faults along the flanks of structures. Deposition in the Cooper Basin ceased in the Middle to Late Triassic and was followed by a period of uplift and erosion.

Location Map

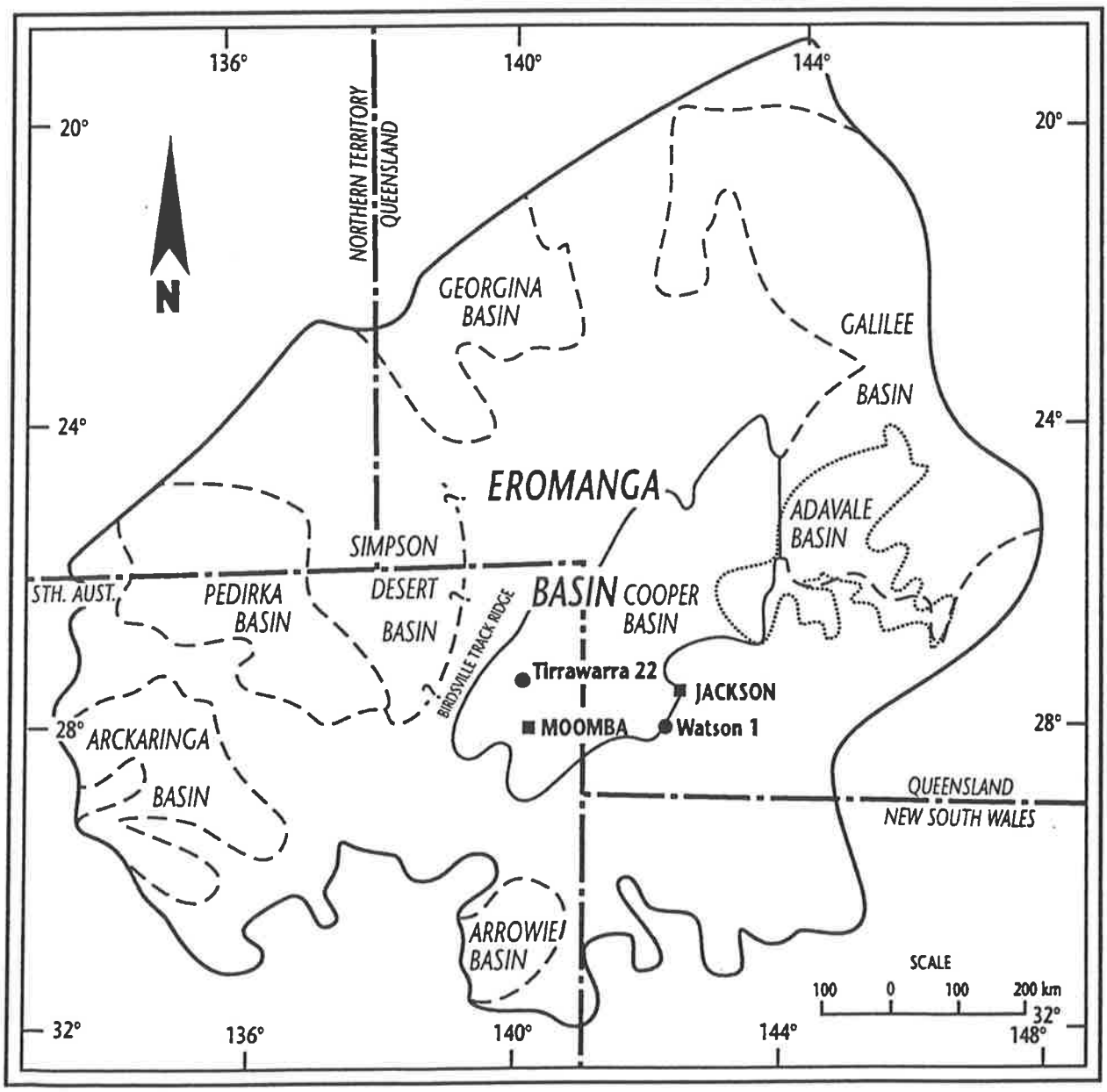

Fig. 1

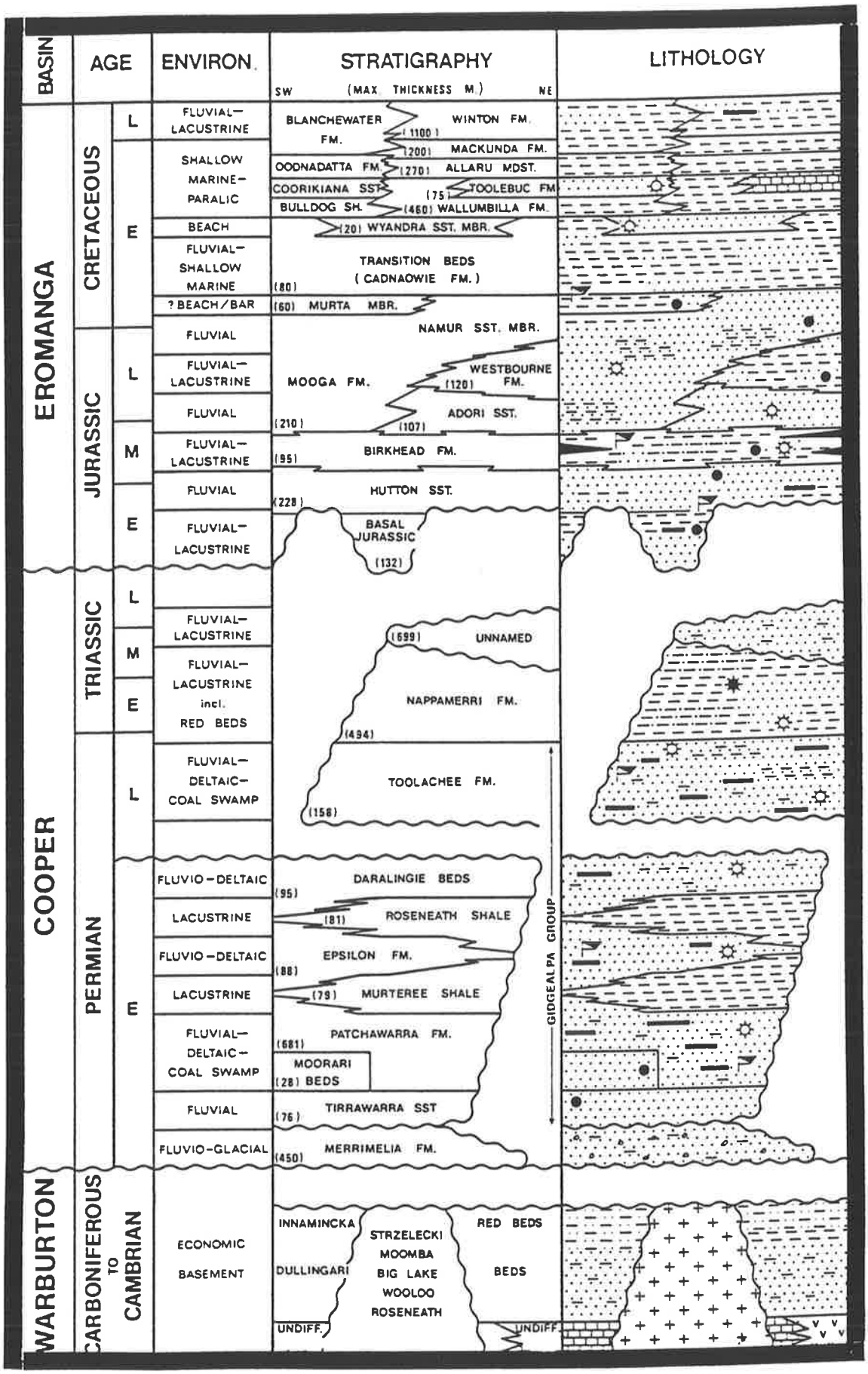

Lithostratigraphic column (Kantsler, et al, 1983)

Fig. 2

The Eromanga Basin is Australia's largest onshore hydrocarbon province by area, with up to 3000m of sediment preserved (Gravestock and Alexander, 1986). The sediments comprise a basal dominantly non-marine sequence overlain by shallow marine deposits, in turn overlain by a fluvial and lacustrine coal swamp series. They have been subjected to very little disturbance since their deposition. The structure of the basin was influenced by the older basins below, and shows relief with very low dips.

2.2 Seismic Response

The reflection seismic data recorded over the Cooper and Eromanga Basins is of good quality in comparison with other Australian basins. Figures 3 and 4 are normal polarity (SEG standard) migrated seismic sections through the selected wells. Strong reflections are seen over the vertical extent of the sections down to economic basement, with many reflections being laterally continuous. Hydrocarbon accumulations are found in reservoirs from the Cretaceous Cadna-Owie formation down to economic basement. The response of the reflectors within the Jurassic section varies from easily interpretable (Cadna-Owie, Namur), to more difficult transitional type reflections (Birkhead). Within the Cooper sequence, the highly reflective coals of the Toolachee and Patchawarra formations degrade the quality of the seismic data, from this level down. This is evidenced by a decrease in the dominant frequency and signal strength. Reflections from below the Cooper sequence are usually weak and difficult to interpret.

The vast majority of the reflection seismic data recorded over the basins has been shot using Vibroseis sources, with CMP fold ranging between 12 and 120. There are two major problems with this data. The first is an apparent inability to acquire adequate signal strength at high frequencies (above about 60 Hz). As a result, the data do not have sufficient bandwidth to resolve the detail necessary in the search for stratigraphic traps. Attenuation measurements should help to locate and quantify the source(s) of this problem. The second difficulty is the calculation of accurate static corrections due to the complex velocity structure of the near surface.

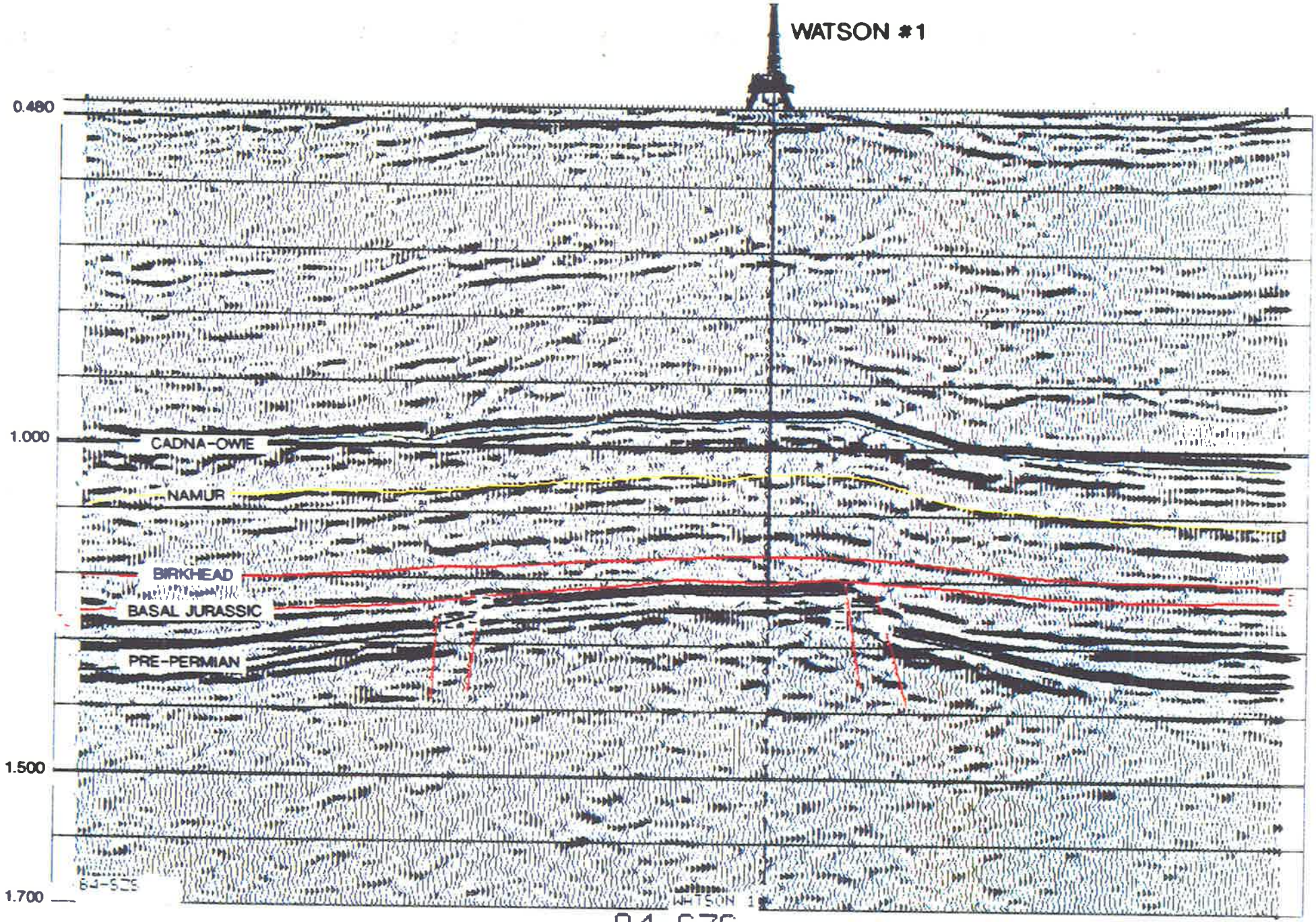

84-SZS

Surface seismic at Watson #1

Fig. 3

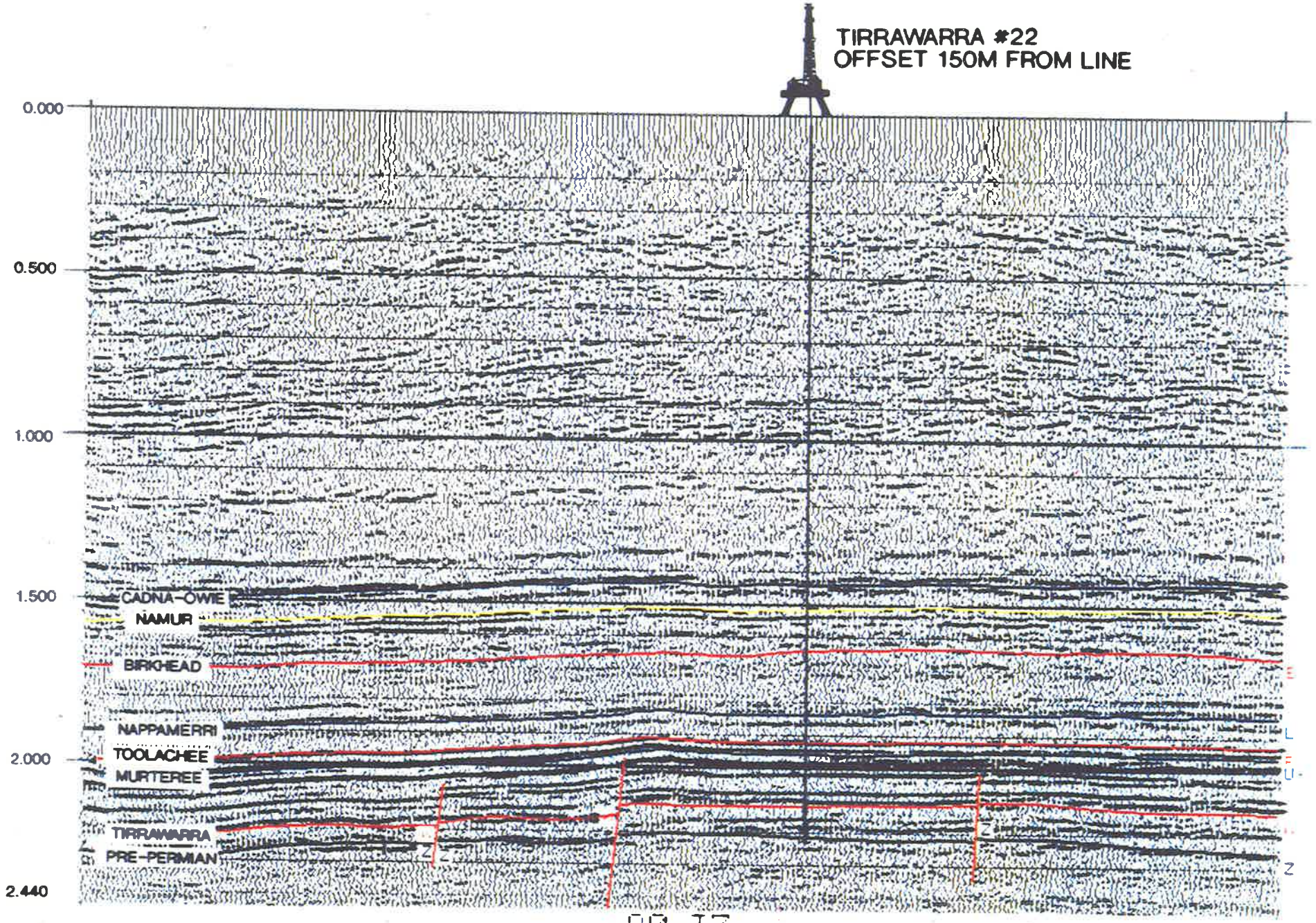

80-17

Surface seismic at Tirrawarra #22

Fig. 4

2.3 Selection of VSPs

Several wells from both the Cooper and Eromanga Basins have had a vertical seismic profile recorded. After an inspection of the data available, the VSPs acquired in Watson #1 and Tirrawarra #22, were chosen for analysis. The location of both these wells is shown in Figure 1.

Stratigraphically, Watson #1 encounters a complete Eromanga sequence but this sits directly on Pre-Permian economic basement. To investigate the Cooper sequence, Tirrawarra #22 was selected, since this well encounters both the Eromanga and Cooper sequences before penetrating economic basement.

The two VSP's selected as representative of the basins were also shot using different sources. The Watson #1 VSP was recorded with a Vibroseis source, and was designed with attenuation analysis as a possible goal. 3 types of geophone were used to monitor the source signature, and the downhole geophone recordings were made in open hole.

Conversely, the Tirrawarra #22 VSP was recorded using an airgun positioned in a water-filled pit. The aim was correlation with the surface seismic data, and over half the downhole recordings were made in cased hole. The source signature was monitored using a hydrophone. The selection of these VSPs allows for comparison to be made between different recording techniques, the two source types, and between recordings in open and cased hole.

The effect of attenuation upon the seismic response of the basins can only be discussed qualitatively prior to the analysis. It will decrease the amplitude and frequency content of the reflected signal. This may contribute to the difficulty in interpreting transitional type reflectors. The coal sequences encountered in the Permian section will reduce the energy of the propagating seismic pulse, by both intrinsic (anelastic) and apparent attenuation (caused by intrabed multiples). Quantifying these effects is a major goal of the analysis.

CHAPTER 3

SEISMIC WAVE ATTENUATION

3.1 Introduction

Attenuation is a general term applied to the phenomenon observed in all seismic experiments that the energy density of an elastic wave decreases as it propagates away from the source. This manifests as a decrease in amplitude and a change in waveform. Attenuation is therefore an important factor in seismic exploration. Most importantly, it sets limits on the depth of penetration and the resolution obtainable in a seismic survey. On a more positive note, measurements of attenuation may possibly provide information on lithologies, pore fluids and other rock properties of interest.

A number of mechanisms cause attenuation. These are the expansion of the wavefront, inhomogeneities in the earth's elastic properties, and conversion of the wave's energy into heat due to the imperfect elasticity of rocks. The latter two processes cause attenuation effects which are frequency dependent, and are the subject of this investigation.

This chapter presents an outline of the attenuation mechanisms, concentrating in particular on the anelastic processes, which give rise to the effects termed "intrinsic attenuation" in this project.

3.2 Attenuation, Mathematical Relationships

i) Spherical divergence

The energy from a seismic source is distributed across a wavefront which moves away from the source with time. For a point source in a constant velocity medium, the wavefront is an expanding sphere. If the medium is also perfectly elastic, the total energy in the wavefront

will be conserved. However, this energy will be spread over an increasingly large surface area as the wavefront expands, causing the energy density to decrease with time. This leads to a decay in wave amplitude termed spherical divergence, which has, in the simple case discussed, the form

$$A_X = A_O(x_O/x) \qquad \ldots 3$$

Here A_X and A_O are amplitudes measured at distances x and x_O from the source respectively. In an earth where the velocity is layered, the spherical divergence can be described approximately by

$$1/(V^2(t).t) \qquad \ldots 4$$

where t is the two-way traveltime and V(t) is the rms velocity of the primary reflections (Newman, 1973).

Provided that traveltimes and velocities in the earth are known, the attenuation caused by spherical divergence can be computed and removed from seismic data. Note also that spherical divergence is independent of frequency and so does not alter the shape of the propagating wave.

ii) Transmission losses and multiple activity

The product of bulk density and propagation velocity is termed an impedance, and energy will be scattered from a wave whenever it encounters a change in impedance. If the change occurs across a boundary which is smooth relative to the wavelength of the incident signal, a specular reflection results; part of the energy in the wave is reflected back from the interface, and the remainder is transmitted through it. In addition, and in general, mode conversion occurs, further partitioning both reflected and transmitted energy into compressional and shear wave modes. Transmission and reflection coefficients are defined as

the ratio of the amplitude (or energy) of a given transmitted or reflected wave relative to that of the incident wave.

For a plane wave incident on a planar impedance boundary, continuity of displacement and stress across the interface define the Zoeppritz equations (Zoeppritz, 1919) which can be solved for the transmission and reflection coefficients in terms of the compressional and shear wave impedances, and the angle of incidence. For normal incidence, there is no mode conversion, and the solutions simplify to the well known zero offset transmission and reflection coefficient equations.

$$T_c = 2\,\rho_1 V_1/(\rho_2 V_2+\rho_1 V_1) \qquad \ldots 5$$

and $$R_c = (\rho_2 V_2-\rho_1 V_1)/(\rho_2 V_2+\rho_1 V_1) \qquad \ldots 6$$

There is therefore, a decrease in the energy transmitted downward through the section. In the multi-layered case observed in the earth, the upward reflected waves are partially reflected back downwards from the undersides of the overlying impedance boundaries. Short-period multiple reflections generated in this way interefere with the transmitted seismic wave, thus resulting in a redistribution of energy in the propagating signal. Although the reflection and transmission coefficients for a single interface are independent of frequency, Schoenberger and Levin (1974) showed that the effect of short-period multiples is to progressively diminish the high frequencies in the spectrum of the transmitted wavelet. This frequency dependent attenuation is termed apparent attenuation.

iii) Intrinsic Attenuation

Earth materials are not perfectly elastic. Hence, as a wave propagates, its mechanical energy is gradually converted to heat via a number of frictional processes. This mode of attenuation is termed intrinsic attenuation in the following chapters, and is also commonly referred to as anelastic attenuation or absorption. It is a property of the rock materials

themselves, rather than of the arrangement of bedding or the geometry of the wavefront, as are the mechanisms previously outlined. For this reason, it is the intrinsic attenuation in which we are interested when attempting to obtain rock property information from attenuation measurements. Intrinsic attenuation is frequency dependent, as will be discussed in detail below. Indeed it is this property which forms the basis of the spectral ratio method used to quantify it.

In common with many physical phenomena, the loss of amplitude by absorption from a seismic wave is exponential with distance (Sheriff et al, 1976). The exponential decay is supported by several in-situ studies, including the classical study on wavelet propagation by Ricker (1953), and a study by Kolsky (1955). The latter study shows that pulse shapes can be predicted for a mechanical pulse introduced into polymer rods by assuming an exponential decay law.

Empirically, therefore, intrinsic attenuation in a homogenous medium can be described by the equation

$$A_x = A_0 e^{-\alpha x} \qquad \ldots 7$$

Here A_x is the amplitude of the wave after it has travelled a distance x from a reference point where the amplitude was A_0, and α, the coefficient of attenuation, is a positive number.

Rearranging equation 7, the coefficient of attenuation in nepers per unit length, is given by

$$\alpha = (1/x) \ln(A_0/A_x) \qquad \ldots 8$$

(The neper is the natural logarithmic analogue of the bel :
1 neper = 20 log e = 8.686 dB).

If, in equation 7, the distance is expressed in wavelengths, the appropriate attenuation coefficient to use is the logarithmic decrement, δ. By definition, δ is the ratio, expressed in nepers, between the amplitudes at two points on an attenuating sinusoidal signal separated by one wavelength. Hence

$$\delta = \ln(A_0/A_\lambda) = \alpha \lambda \quad \ldots 9$$

and 7 can be expressed as

$$A_X = A_0 e^{-\delta x/\lambda} \quad \ldots 10$$

Another measure of attenuation is the quality factor, Q, (Knopoff and McDonald, 1958), which is defined in terms of the energy dissipated per cycle of an harmonic excitation (ΔE) and the elastic energy stored at maximum stress (E_0) by

$$Q = 2\pi(E_0/\Delta E) \quad \ldots 11$$

Attewell and Ramana (1966), show that δ (nepers/wavelength) and Q are related by

$$\delta = \pi/Q \quad \ldots 12$$

Substituting 9 gives the relationship between Q and α:

$$\alpha = (\pi f/Qv) \quad \ldots 13$$

To this point nothing has been assumed about the dependence of the various attenuation parameters upon the frequency of the propagating wave.

The coefficient of attenuation, α, has been shown, by numerous laboratory experiments over a wide range of frequencies, to be a linear function of frequency (Toksoz et al, 1979). Similar conclusions have been drawn from field experiments (e.g. Wuenschel, 1965). This result implies that Q and δ are independent of frequency. Studies by Attewell and Ramana (1966), Tullos and Reid (1969) and Hamilton (1972), amongst others, indicate the general validity of the constant-Q model. Such a model also has the practical virtue that Q becomes a fundamental rock property, alongside density and compressional and shear velocities, and has similar diagnostic value in characterizing a rock.

Several other measures of attenuation will be introduced later in the discussion of the spectral ratio method.

iv) Dispersion

A propagating seismic pulse travels with a velocity referred to as its "group velocity", whilst a point of constant phase within the pulse travels with a "phase velocity". If the phase velocity is constant for all frequencies that comprise the pulse, the group velocity equals the phase velocity, and the wave propagates without changing its pulse shape (ignoring the attenuation mechanisms discussed previously). However, if the phase velocity varies with frequency the medium is said to be dispersive. The wave will change shape and attenuate with distance, as different frequencies travel with different velocities, "stretching" the pulse out over a longer distance.

The principle of causality, when applied to the constant-Q model for intrinsic attenuation, requires that the medium be dispersive. This is discussed in detail by Futterman (1962), who concludes that "for a linear theory, the existence of absorption implies dispersion", and that "the phase shift resulting from dispersion depends upon a non-zero low frequency cut off".

Quantitative studies of absorption and dispersion combined are few in number and inconsistent in their results. However, within the range of frequencies used for seismic exploration, differences in phase velocity appear to be negligible. This is illustrated by the results of Wuenschel (1965), who processed the experimental data obtained in the Pierre Shale by McDonal et al (1958) to derive absorption and dispersion values. His results support a frequency independent Q value, and showed an increase in phase velocity of just 2.6%, from 6720 ft/s at 25Hz to 6860 ft/s at 400Hz.

In this study of attenuation, dispersion is assumed to be small, and its effect on the shape of the propagating wavelet is ignored.

3.3 Attenuation Mechanisms

The mechanisms responsible for intrinsic attenuation are an area of continuing research. This involves looking at the rocks in terms of their microstructure, which is several orders of magnitude smaller than seismic wavelengths. Mavko et al (1979) consider the mechanisms in two groups: those that involve pore fluids, and those that do not. The first group includes attenuation attributable to fluid flow and the interactions between the pore fluid and rock matrix. The second group includes attenuation that is attributable directly to anelasticity of the mineral grains and the effects of grain boundaries, and also the losses attributable to cracks. The majority of mechanisms have been studied using laboratory methods, which usually concentrate on one mechanism. It is apparent that attenuation is a complex phenomenon, and cannot generally be attributed to a single mechanism (Johnston and Toksoz, 1981).

Biot (1962) developed a comprehensive theory for the static and dynamic response of linear porous materials containing compressible fluids. He attributed the dissipation of energy to the relative motion between the rock matrix and pore fluid. As both P and S waves propagate through the saturated rock, the matrix is accelerated, but the acceleration of the pore fluid lags behind the matrix. This causes the development of stresses between the rock and

liquid, resulting in viscous dissipation of mechanical energy. Tittmann et al (1972) increased the understanding of the mechanisms involving fluids with their discovery that very small amounts of water are required to dramatically alter Q values in lunar rocks. Stoll (1974) concluded that Biot's theory can reproduce most of the behaviour seen in saturated sediments, but due to a lack of laboratory experiments conducted at frequencies below 10kHz, it is questionable whether the results can be extrapolated down into the seismic frequency range. The studies by Johnston et al (1979) suggest that Biot flow may be important for sedimentary rocks at ultrasonic frequencies only, and negligible in all but highly permeable rocks.

Walsh (1966) discusses the effects of friction between the two faces of a thin crack. Lubrication occurs if fluid fills the crack, and energy is dissipated as the faces slide past each other when a shear stress is applied across the crack. At low frequencies, Mavko and Nur (1975), and O'Connell and Budiansky (1977) describe a mechanism termed squirting flow, or intercrack fluid flow. This flow is induced between adjacent cracks, by a change in relative volume caused by a stress wave. The result of the flow of fluid is the dissipation of energy.

Attenuation may also be caused by fluid flow induced by a pressure gradient. If a uniform stress is applied across a saturated crack of variable width, then there will be instantaneous pressure variations along the crack. High pressure will be found where the crack is narrow, and low pressure where it is wide (Mavko et al, 1979). This pressure gradient will cause the fluid to flow and consequently energy will be dissipated. Mavko and Nur (1979), investigating wave attenuation in partially saturated rocks, showed that the presence of at least a small fraction of gaseous phase permits fluid to flow freely when the pore spaces are compressed under wave excitation. The flow is attributed to the lower induced pressure in the compressible gas giving rise to a large pressure gradient and thereby enhancing fluid flow. This leads to viscous shearing in the fluid and high energy dissipation. The resulting Q values are extremely sensitive to the pore and fluid droplet shape, with the Q value increasing for flatter pores and droplets. Attenuation is greater in a partially saturated rock than in the same rock when fully saturated (Winkler and Nur, 1979).

The thermoelastic attenuation of elastic waves is a mechanism that has been described by Savage (1965). The results are based on laboratory studies on dry rocks containing cracks. At depth however, such cracks could not exist unless fluid filled, so this mechanism is unlikely to operate.

Whilst the mechanisms associated with fluid flow are important, some of the observed attenuation is attributable to mechanisms that do not involve fluids. This statement is justified by the observation that attenuation is not zero at zero saturation (Mavko et al, 1979). A detailed review of such mechanisms associated with attenuation at high temperature and pressure, and to polycrystalline solids, is given by Jackson and Anderson (1970). They consider high-frequency atomic scale relaxations, intergranular thermoelastic relaxation, grain-boundary relaxation, high temperature background, and partial melt, as mechanisms likely to cause seismic attenuation.

Relaxation occurs when a change in the state of a solid is caused by applying a stress, and on reversal of the stress the change is also reversed. Energy is absorbed during the first half of the change and given up on reversal. An example of a relaxation mechanism is thermoelasticity, where a rock is heated and cooled by the application of a soundwave. If the change in the rock is totally reversible, then there is zero attenuation. Should the change not be totally reversible, a percentage of the sound energy will be converted to thermal energy, resulting in attenuation.

Partial melting, associated with volcanic regions, has been suggested as a reason for the increase in absorption seen during seismic studies in these areas. Partial melting is possibly important to the low frequency attenuation that is observed in the upper mantle.

The above review is not a complete list of possible mechanisms. Considering that a rock is a complex structure, it is unlikely that a single mechanism is responsible for attenuation, but rather a combination of mechanisms. This contributes to the difficulty in extrapolation from laboratory data to in-situ seismic experiments.

3.4 Measurement Techniques

Measurements of attenuation fall into two distinct categories; those made in the laboratory and those made in-situ. Problems exist with both, as will be highlighted in the text.

The laboratory methods involve taking samples of rock and subjecting them to different conditions of pressure, saturation, temperature, etc, while measuring the propagation of a pulse through the sample. In the laboratory a very wide range of frequencies can be generated and the amount of data resulting from such methods far exceeds that from in-situ techniques. A review of laboratory methods is given in Appendix 2.

The in-situ measurements vary from those in the laboratory mainly in the frequencies that can be used and the level of resolution. Almost all involve the use of a seismic pulse with frequency content limited to at best a few hundred hertz. The resolution is dependent on the number of, and interval between measurements. The latter is generally of the order of 50 to 100 feet. Interpretation of the measurements may be very subjective because of the complexity of the real earth, and the difficulty in isolating accurately the intrinsic attenuation effects in the data.

3.4.1 In-situ Techniques

In-situ techniques to measure attenuation have received a great deal of attention following laboratory work showing the effects of pore fluids and saturation on attenuation. However, the number of field measurements reported in the literature is small. The technique for measuring attenuation almost always uses the direct transmission of a seismic pulse.

McDonal et al (1958) made attenuation measurements on the Pierre Shale in Colorado. They used vertically travelling compressional waves generated by explosive shots, recorded by 5 detectors positioned in a cluster of boreholes, and from Fourier analysis estimated the

coefficient of attenuation for the Pierre Shale to be $\alpha = 0.12f$, where α is the attenuation in dB per 1,000 ft, and f is the frequency in Hz.

Tullos and Reid (1969) measured attenuation in Gulf Coast sediments using blasting caps as a source, offset from a borehole, with geophones cemented in place at depths between 100 and 1000 feet. With 34 geophones and 5 shot locations, a large number of recordings were made. The analysis of the data was based on the concept that if "two inline observations of an outgoing pulse in a homogenous isotropic medium were corrected for geometric spreading, the ratio of the spectrum observed at the second point to the spectrum at the first point would describe the decay of the frequency components between the two points", (Tullos and Reid, 1969). This is the basis of the spectral ratio technique and will be detailed later in this section. The results from the analysis ranged from 13.1 dB/wavelength over the top 10 feet to 0.1508 dB/wavelength within the section.

In the above two studies source repeatability does not present a problem because the same shot was recorded by multiple detectors. Hauge (1981) measured attenuation from vertical seismic profiles (VSPs), where a single geophone was used to record multiple shots at successive levels in the borehole. In this case, source repeatability is important. The spectral ratio technique gave results ranging from 0.1 to 0.9 dB/wavelength, with evidence that porous sands cause more attenuation than neighbouring shales. Stainsby and Worthington (1985) also used VSP data to determine attenuation. They compared results using spectral ratio, pulse amplitude, pulse width and zeroeth lag autocorrelation analysis methods.

Tonn (1991) compared the spectral ratio method with nine other commonly used methods for determining attenuation, using both synthetic and real data. He concluded that in the absence of noise, the spectral ratio method gives results that are reliable but inferior to those determined using either the analytical signal or forward modelling methods. Examination of Q values determined for synthetic data with known Q in 12 separate layers

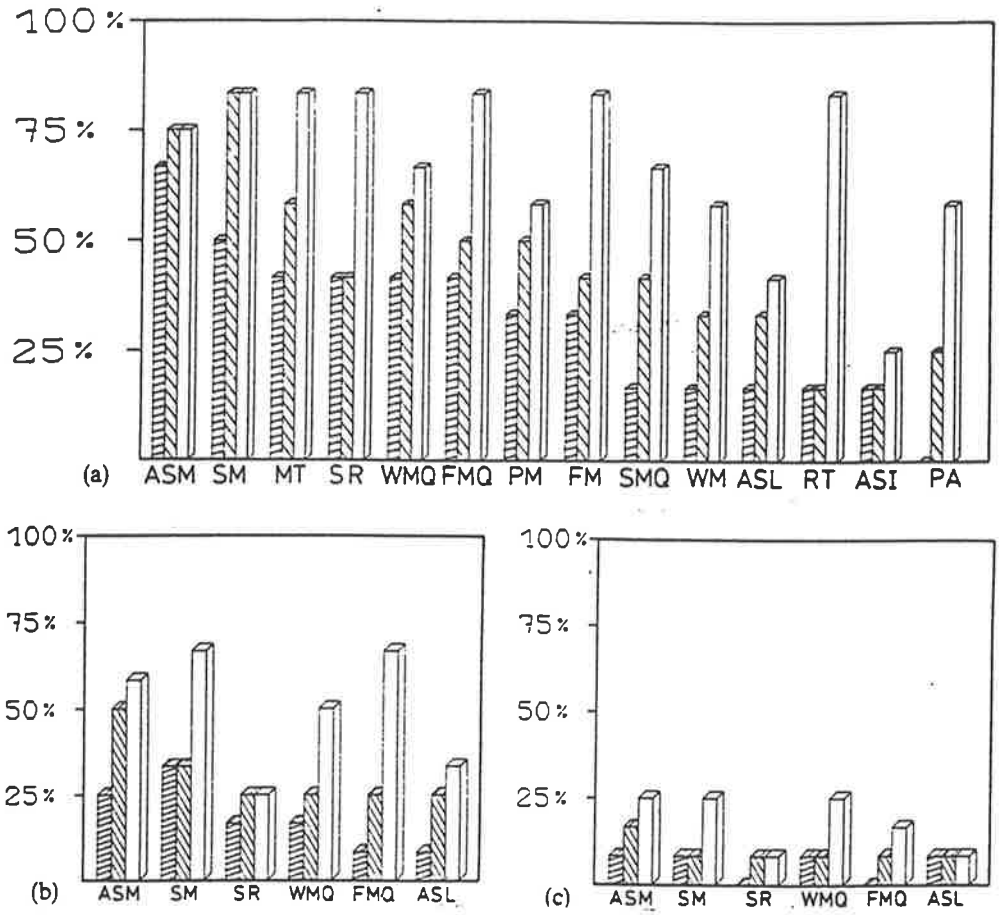

Fig. 5

Comparison of the percentage of the correct layer-Q estimates for various methods a) noise free case, b) minor noise, c) intensive noise (Tonn, 1991)

Figure 5 (Tonn, 1991) illustrates the results of determining Q for individual layers using the methods listed below:

ASM:	analytical signal (maximum method)
ASL:	analytical signal (linear approximation)
ASI:	analytical signal (averaging method)
SM:	spectral modelling (minimization in the L_1, norm)
SMQ:	spectral modelling (minimization in the L_2, norm)
WM:	wavelet modelling (minimization in the L_1, norm)
WMQ:	wavelet modelling (minimization in the L_2, norm)
FM:	frequency modelling (minimization in the L_1, norm)
FMQ:	frequency modelling (minimization in the L_2, norm)
PM:	phase modelling (minimization in the L_1, norm)
PA:	pulse amplitude
RT:	rise time
MT:	matching technique
SR:	spectral ratio method

and in the absence of noise gave a reliability factor of 60% for the spectral ratio method, reducing to 10% in the presence of intense noise. In Figure 5, the three bars shown for each method give the percentage of calculated Q values which are within, from left to right, 10%, 20% and 50% of the true value. For the cases with added noise, only the six best methods are illustrated. The spectral ratio method compares favourably in all cases, but all methods appear to give random and unreliable results in the presence of intense noise. The results illustrated in Figure 5 may have been improved if the apparent Q had been determined and subtracted from the observed Q. The paper suggests that this was not done.

The majority of reported field techniques are limited by the usable frequencies which a conventional source can generate. The attenuation to be measured is a small fraction of the total energy loss, and the effects of spherical divergence and losses at reflecting boundaries are always far greater. Multiple activity can have a large effect on measurements. For example, Hauge (1981) reported that short-period multiples contribute 10 to 40% of the total estimated attenuation.

3.4.2 Analysis of In-Situ Measurements

Figure 6a illustrates a simple earth model with 3 homogenous layers, each with a different Q value. A borehole penetrates the model, and located within the borehole is a series of receiver locations. A seismic pulse is generated at the surface of the model and recorded at each receiver location in turn. Ignoring all but the direct transmission from source to receiver, a set of data recording the propagation of the pulse from depth x_0 to x_n is obtained. The recorded pulses will all be copies of the input progressively modified in amplitude and shape by the combination of attenuation mechanisms.

The attenuation of the pulse in the above model can be determined by analysing either the pulse shape or signal attributes. Pulse shape methods include the spectral ratio technique used by several authors including Ganley and Kanasewich (1980), Hauge (1981), and Stainsby and Worthington (1985). Toksoz et al. (1979) applied the same method in

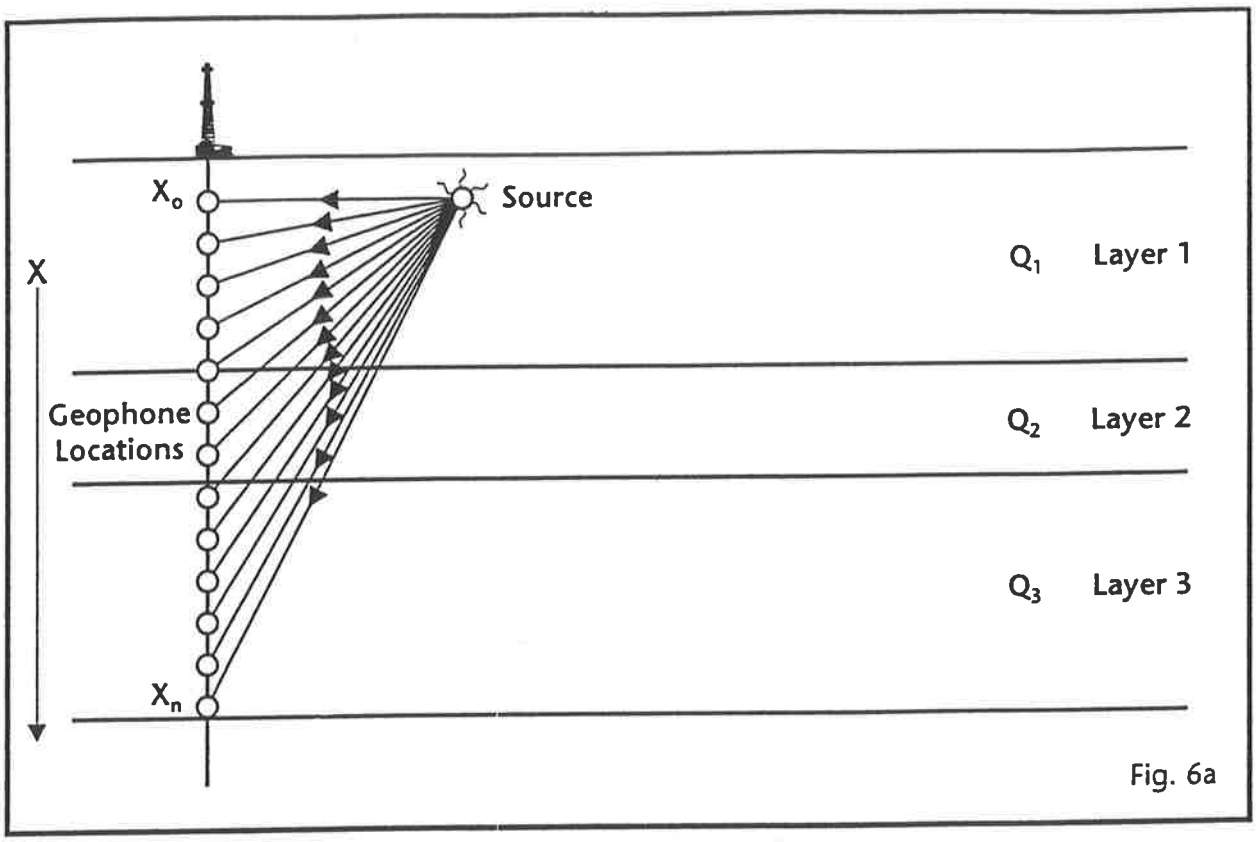

A 3-layer earth model

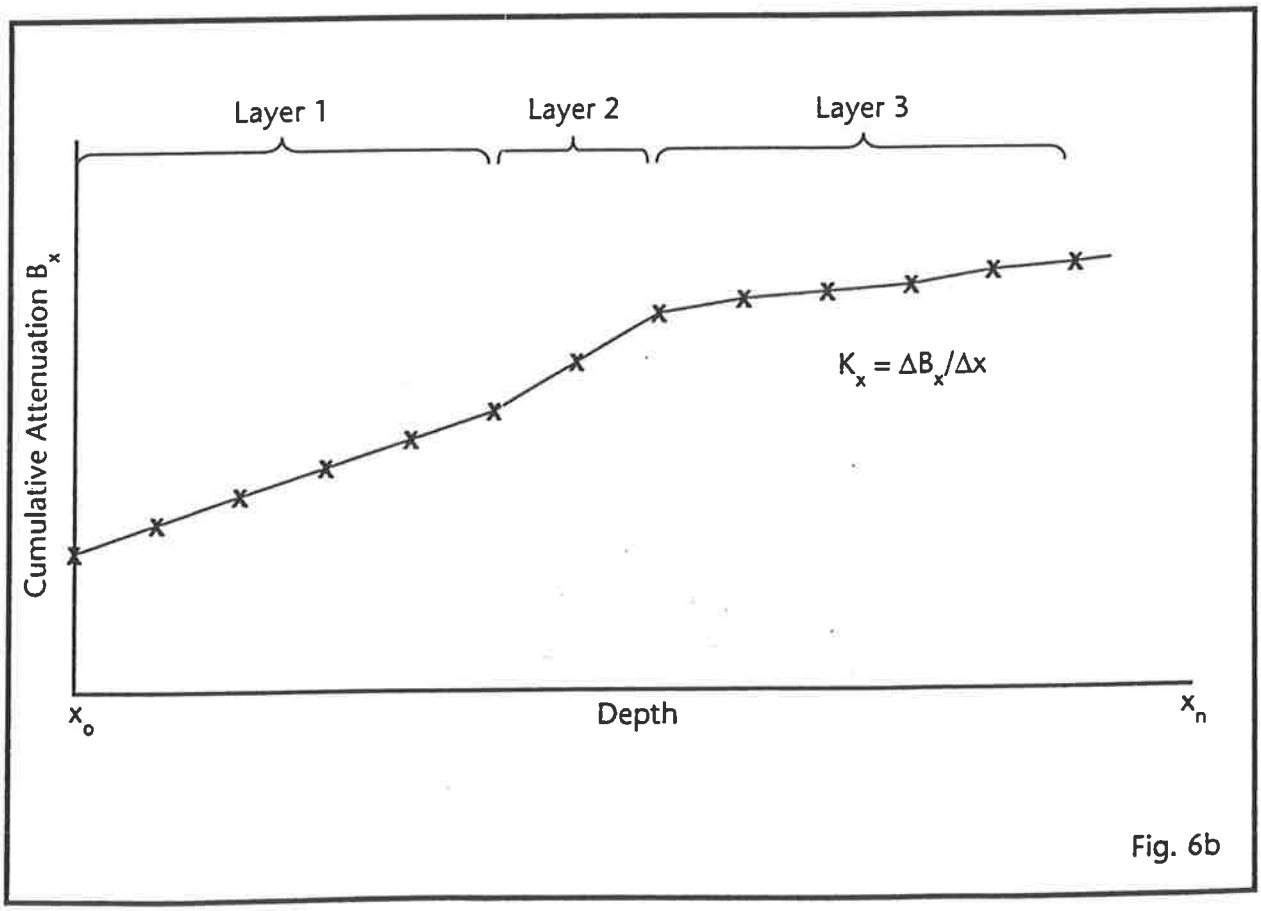

Schematic of the cumulative attenuation for the model in Fig 6a

laboratory studies. Since this is the method of analysis used in this project, it is discussed in some detail in the following paragraphs.

Assuming negative exponential attenuation, with the exponent being linear with frequency, the amplitude spectra of a propagating seismic pulse at different depths x and x_o are related by, (Hauge 1981);

$$A_x(f) = G_x A_o(f) \exp(-B_x f) \quad \ldots 14$$

A_x and A_o are the amplitude spectra at depths x and x_o respectively. G_x is a frequency independent term which accounts for changes in pulse magnitude resulting from factors including spherical divergence, variations in recording gain, changes in source and receiver coupling, and the dependence of pulse magnitude on rock impedance. B_x is the cumulative attenuation between depth x_o and x. Taking natural logarithms of both sides, equation 14 becomes

$$\ln(A_x(f)/A_o(f)) = -B_x f + \ln G_x \quad \ldots 15$$

Since G_x is a constant for any particular pair of observation points, a plot of the natural logarithm of the spectral ratio against frequency should yield a straight line of slope $-B_x$ nepers/Hz. In practice, for each observation level, x, the log spectral ratio is computed using a common reference signal from depth x_o. A straight line is fitted by least squares to each set of spectral ratio data. A set of B_x values, one for each observation point, can then be determined from the slopes of the fitted lines. Plotting B_x against x should give a graph resembling Figure 6b. If the value of Q is constant with depth, B_x vs x is a straight line. Equating the exponential terms in equations 7 and 14 gives

$$\alpha (x - x_o) = B_x f \quad \ldots 16$$

Defining the interval attenuation k_X as

$$k_X = B_X/(x - x_o) \text{ (nepers/Hz/metre)} \quad \ldots 17$$

the relationship between α and frequency becomes

$$\alpha = k_X f \quad \ldots 18$$

In the more realistic case illustrated in Figure 6a, which contains a series of layers with different Q values, the B_X vs x plot will consist of a set of straight line segments, each segment corresponding to a layer, as shown in Figure 6b. The interval attenuation for each layer is just the slope of its corresponding line segment, and, generalizing (17),

$$k_X = \Delta B_X/\Delta x \quad \ldots 19$$

Schoenberger and Levin (1974) defined interval attenuation by using the travel time difference (Δt) rather than the depth separation (Δx). This form of interval attenuation, denoted by α_X, is given by

$$\alpha_X = \Delta B_X/\Delta t \text{ (nepers)} \quad \ldots 20$$

Since the interval velocity over the interval Δx is given by $v_X = \Delta x/\Delta t$, the relationship between the two forms of interval attenuation is

$$\alpha_X = v_X k_X \quad \ldots 21$$

Substituting for k_X from equation 18 gives

$$\alpha_X = (v_X \alpha)/f = \alpha\lambda = \delta \quad \ldots 22$$

Hence α_X is equal to the logarithmic decrement δ, defined in the previous chapter. Q can be computed from equation 12 by substituting from equations 19, 20 and 22 to give

$$Q = \pi/(k_X v_X) \qquad \ldots 23$$

$$= (\pi \Delta x)/(\Delta B_X v_X) \qquad \ldots 24$$

If the spectral ratios are measured in dB rather than nepers, the conversion factor of 8.686 dB/neper results in the replacement of π in equations 23 and 24 by the factor 27.3. Hauge (1981) notes that the spectral ratio method requires only that k_X, but not α_X or Q, be independent of frequency. For example, in a dispersive medium, the variation in interval velocity v_X would result in a frequency dependent α_X. In practice, dispersion is negligible over typical seismic bandwidths, so v_X, α_X and Q are frequency independent.

The second group of methods involve the analysis of signal attributes, and includes the rise-time, period, and shape index techniques. These attributes will be defined using the symbols adopted by Mari (1989), and are illustrated in Figure 7.

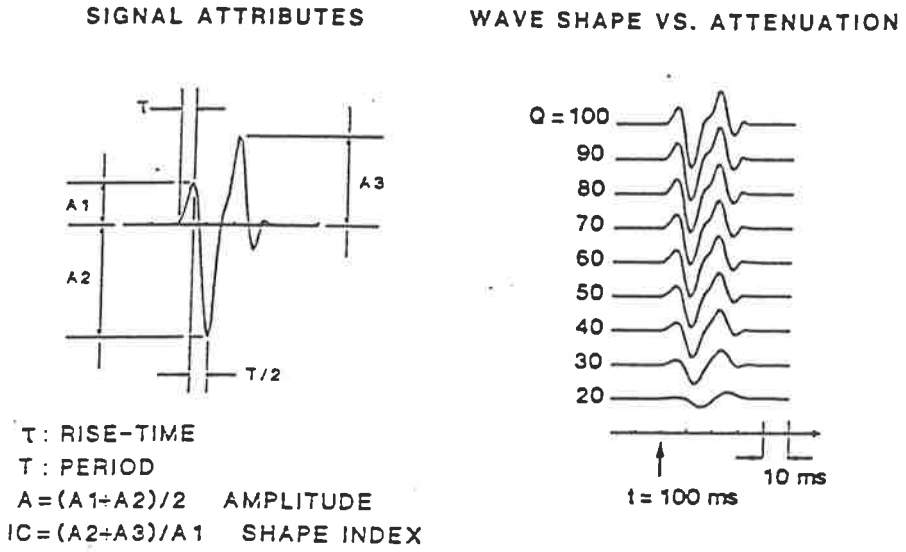

Fig. 7

Seismic attenuation introduces modifications in the waveshape. These may be quantified using signal attributes (Mari, 1989)

Mari defined the rise-time of a pulse, τ, as the difference between the true first break time and the first-extremum time of the equivalent minimum-phase pulse. Gladwin and Stacey (1974) used the rise-time technique to measure in-situ attenuation. They related the rise time τ of the displacement signal and Q by the empirical equation

$$\tau = \tau_o + C_\tau \int_o^t Q^{-1}\, dt \qquad \ldots 25$$

For the case of constant Q, this reduces to

$$\tau = \tau_o + C_\tau\, t/Q \qquad \ldots 26$$

where τ_o = the initial rise time (for t = 0)

t = travel time

C_τ = constant

C_τ is dependent upon the source type (i.e. displacement, velocity, acceleration) and also upon the material itself (Tonn, 1991). It is therefore a rather unknown quantity. Kjartansson (1979) showed that C_τ is only constant for $Q \leq 20$; otherwise it is a function of Q. Tarif and Bourbie (1987) list C_τ as varying between 0.203 to 0.53.

Mari defined the period of the pulse, T, as twice the difference between the times of the first two opposite polarity extrema following the true first break, and related the period T and Q by the equation

$$T = T_o + C_T\, t/Q \qquad \ldots 27$$

where T_o = the initial period (for t = 0)

C_T = a source dependent constant

Additionally, the shape index, Ic, is defined as the sum of the amplitudes of the second and third extrema divided by that of the first extremum, and is related to Q by the equation

$$Ic(t) = (Ic)_o + C_1\, t/Q + C_2\, (t/Q)^2 \quad \ldots 28$$

where $(Ic)_o$ = initial shape index

C_1 and C_2 = source dependent constants

By allowing Δt to be the travel time variation in ms between two receiver locations in the model, $\Delta\tau$ the rise-time variation in ms, ΔT the variation in period in ms, and ΔIc the shape index variation, then

$$Q = C_\tau\, \Delta t/\Delta\tau \quad \ldots 29$$

$$Q = C_T\, \Delta t/\Delta T \quad \ldots 30$$

$$Q = (2C_2\, \Delta t)/(C_1\, (B-1)) \quad \ldots 31$$

$$\text{where } B^2 = 1 + ((4\, \Delta Ic)\, C_2)/(C_1) \quad \ldots 32$$

Tarif and Bourbie (1987) and Tonn (1991), made comparative studies of the spectral ratio and signal attribute techniques and came to the following conclusions:

1. The spectral ratio method is more reliable in the presence of noise. However, where the first arrival is badly affected by later arrivals the rise-time method may be more suitable as the measured parameters are restricted to the first quarter period of the pulse.

2. Determining source dependent constants is a complex task, and the relationships between τ, T, Ic and t/Q are dependent on the experimental set up, coupling functions and the medium under investigation.

3. Based on the complexities outlined in 2, the spectral ratio method is easier to implement after determining a reliable reference signal.

Based on these results, it was decided to use the spectral ratio method to analyse the Cooper/Eromanga basin data in this project.

By far the majority of attenuation measurements in the field have been made using data acquired by the vertical seismic profile (VSP) technique. A detailed description of the technique is given in Chapter 4.

CHAPTER 4

VERTICAL SEISMIC PROFILES

4.1 Introduction.

Vertical seismic profiling is an exploration technique designed so that a signal generated at the earth's surface is recorded by geophones placed at various depths within a borehole. It is an extension of the seismic reflection technique with the geophones placed vertically rather than horizontally (Figure 8). The vertical orientation of the geophones allows for the total response of the earth from the surface to a distance below the total depth of the borehole to be measured as both a function of time and depth.

The recording of vertical seismic profiles as an exploration tool has only been pursued outside of the former USSR since the 1970's. Prior to this, Soviet geophysicists realised the potential for the technique and developed the technology for recording and processing the data. A large volume of technical data and a number of documented studies were built up in the Soviet Union during the 1950's, 60's, and 70's. Gal'perin (1974) illustrated the extent of the Soviet technology, and his published work lists a large number of Soviet references available at the time. The increased awareness of vertical seismic profiles in the West is illustrated by the number of VSPs recorded, the amount of literature available and an increase in the body of research into the technique. A number of non-Soviet geophysicists have shown that VSP can be of benefit in exploration and have published comprehensive works. These include Kennett and Ireson (1977, 1981, 1982); Kennett et al (1980); Balch et al (1982) and Hardage (1983).

Vertical seismic profiles can be recorded in vertical and deviated boreholes, either on land or offshore, using a variety of repeatable sources. The configuration of source and downhole geophones can be varied to highlight areas at or away from the borehole. With the use of the multi-component geophone, the total wavefield can be recorded, including both P

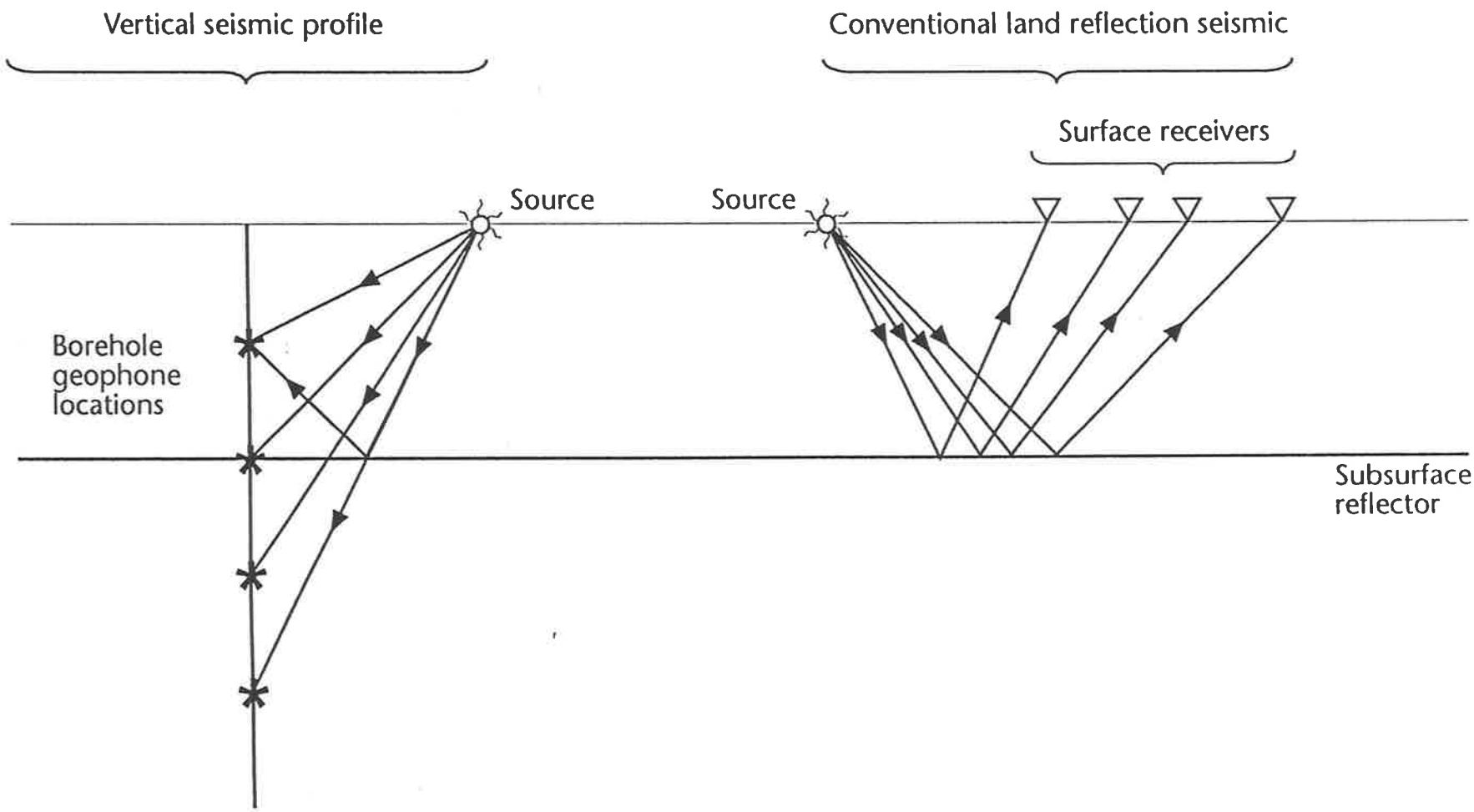

Schematic comparison between VSP and conventional seismic acquisition

Fig 8

and S-waves. Research is well advanced into using this information to define subsurface properties.

4.2 Basic Principles.

In the surface seismic reflection technique, a line of receivers placed horizontally on the earth's surface records seismic waves returning to the surface after reflection from below. A distinction often cannot be made as to whether the arrival is a primary or multiple reflection. The path of a seismic wave is approximately known, but the effect the geologic section has on the propagating wave is unknown. Lateral mapping of the reflecting interfaces is accomplished relatively easily, and this property has accounted for the success and popularity of the seismic reflection technique in hydrocarbon exploration.

With geophones placed vertically, a distinction between upward and downward travelling waves is possible, the nature of the change in the seismic wavelet as it propagates through the geologic section is observable, and the location of interfaces both in time and depth together with the determination of the origin and propagation of multiples can be made.

Figure 9 shows the simplest configuration for recording a VSP. A repeatable source (e.g. airgun, watergun, or Vibroseis) is placed near the wellhead, the offset being small compared to the depth of the borehole. A geophone is locked into position against the borehole wall and the source activated. Recordings are made at the surface of the time break, the source signature, and several seconds of seismic arrivals received at the geophone. Each level may be recorded a number of times and the signals added to improve the signal to noise ratio. The geophone is then unclamped from the borehole wall and moved to the next position. Levels may be separated by equal depth intervals (generally 20-50m), or by equal time intervals derived from a borehole sonic log. The first recording is generally made just below the surface casing. The geophone is then lowered to the deepest level and the survey recorded upwards to ensure greater depth control. A check is made on the accuracy of the recording by

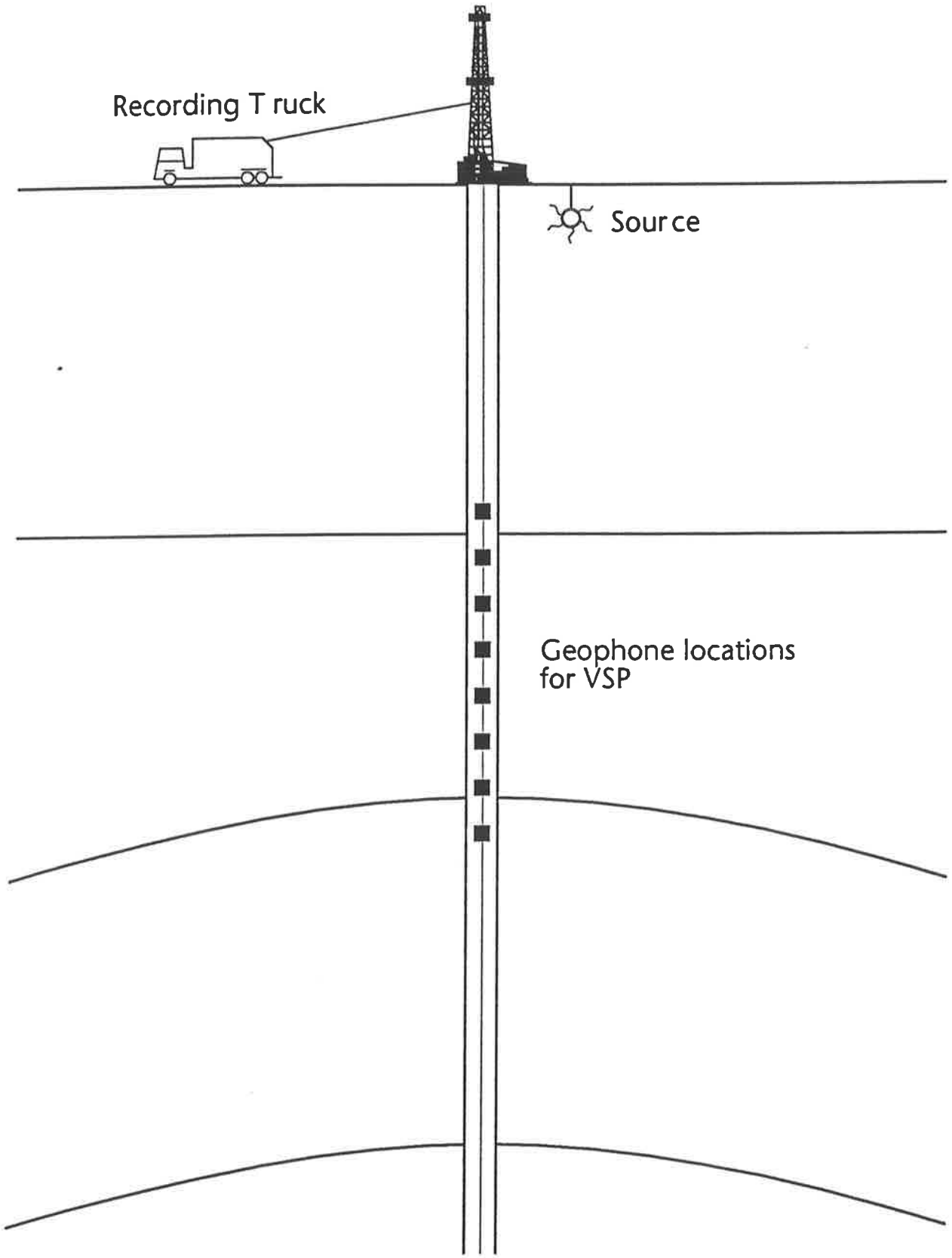

Schematic of a simple VSP recording configuration

Fig. 9

re-recording the first level. Several checks can be made if more than one level is recorded while running into the borehole.

This basic configuration may be varied in a number of ways: moving the source to a larger offset (Offset VSP), moving the source to a number of offset positions traversing the borehole while leaving the geophone fixed (Walkaway VSP), and the recording of surveys in deviated boreholes. Recording offshore is achieved by suspending the source either from the rig or a vessel.

Figure 10a (Kennett and Ireson,1982), illustrates diagramatically the events generated by the interfaces P1 and P2, and recorded by a VSP. For ease of explanation two geophone locations are shown to distinguish between the upward travelling reflections and multiples (yellow and blue respectively), and the downward travelling direct wave and multiples (black and red respectively). Figure 10b (Kennett and Ireson, 1982), illustrates how the events generated by the two interfaces, together with the direct arrivals, would appear on a VSP display. From the diagrams it can be seen that;

1) the direct arrival slopes in the opposite direction from the reflections.
2) in a horizontally layered case, as the geophone is moved deeper, the source to receiver spacing increases, while the spacing to the reflector decreases until the geophone is deeper than the reflector.

Each upgoing wave consists of reflections that are scaled reproductions of the downgoing wavetrain just prior to reflection. Upgoing and downgoing wavefields can be separated in processing either in the frequency-wavenumber (f-k) domain, or using a median filter followed by subtraction in the time-space domain. The upgoing wavefield contains both primary and multiple reflections. The multiples may be removed by deconvolution using an operator determined from the downgoing wavefield, which is known precisely. This method of deconvolution should theoretically give total multiple suppression up to, and including, multiples generated by the last primary reflector above the geophone. Comprehensive

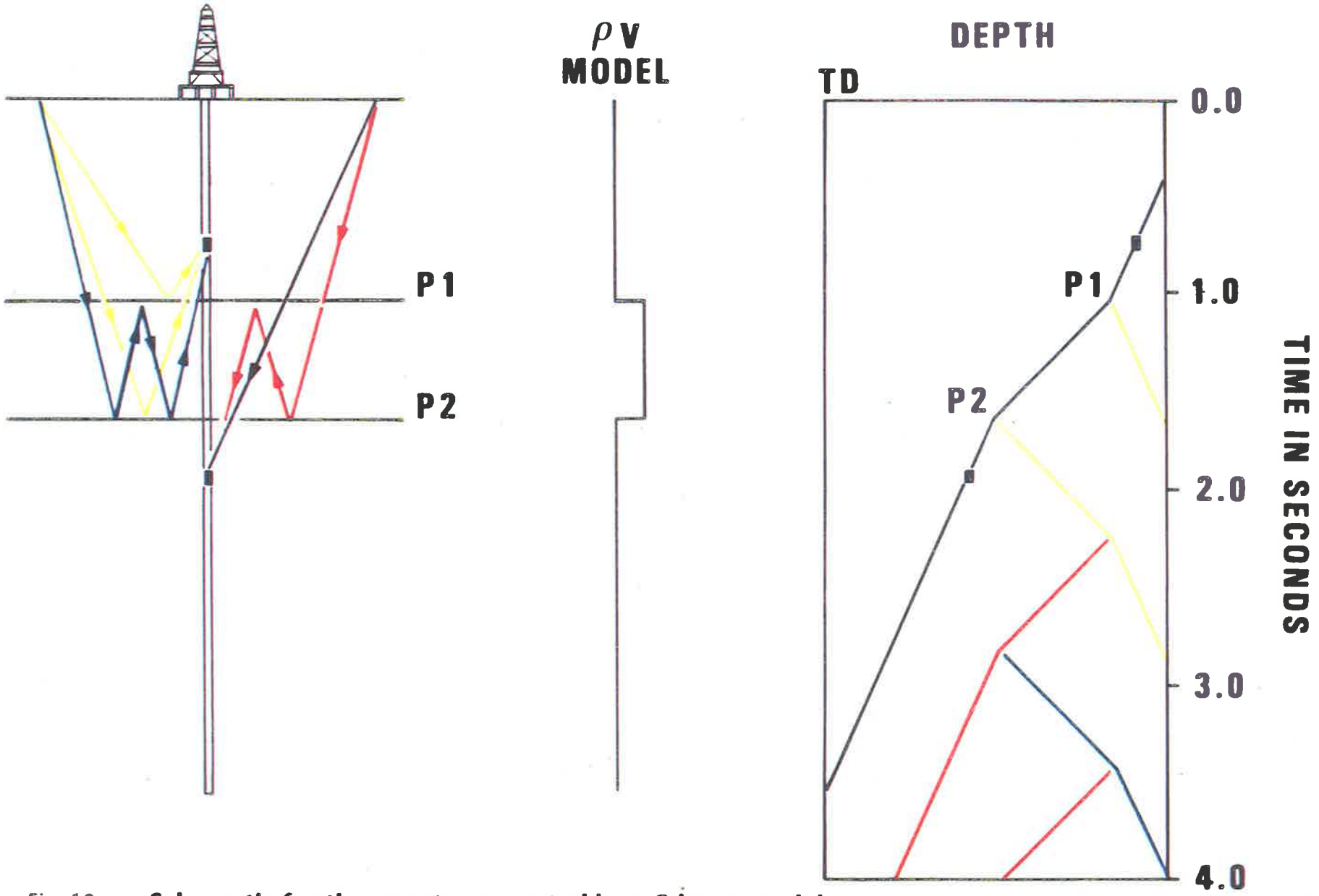

Fig. 10a **Schematic for the events generated by a 2-layer model**

Fig. 10b **VSP display for the 2-layer model (Kennett & Ireson, 1982)**

descriptions on wavefield separation and deconvolution are available in the literature, e.g. Kennett and Ireson (1982) and Hardage (1983). With respect to attenuation measurements, the VSP allows us to study the evolution of the downgoing wave with depth. This wave is not recorded on surface seismic data.

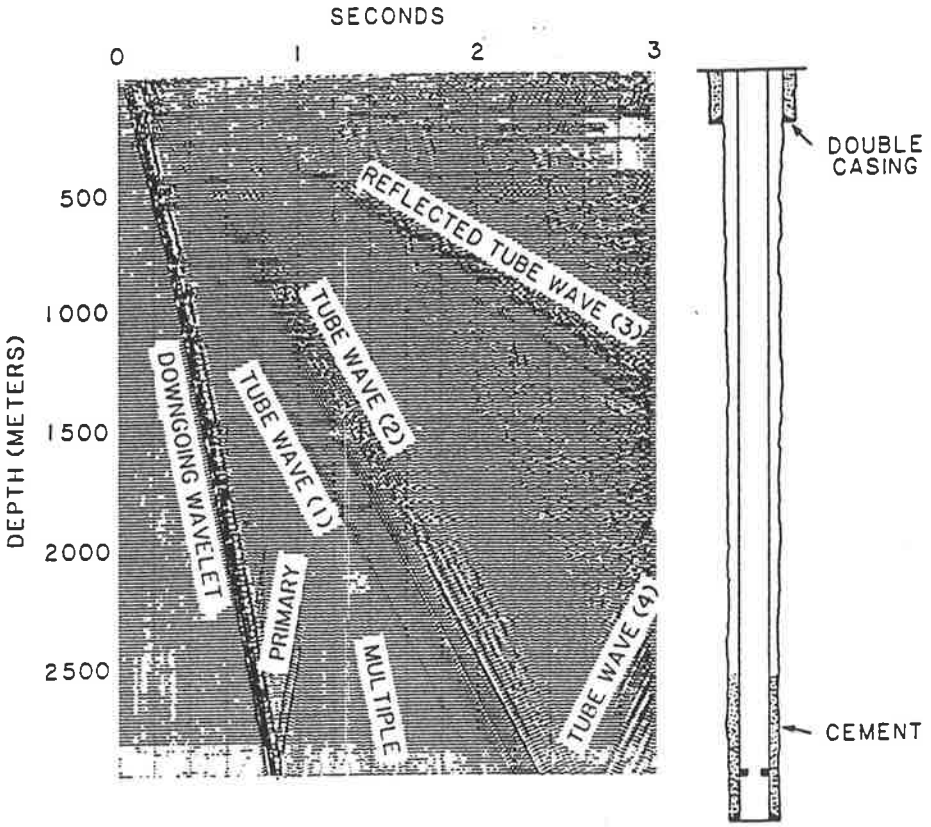

Fig. 11

Tube waves (Hardage, 1983)

There are a number of technical difficulties in acquiring a VSP and many are evident as noise problems in the recorded data. At each of the survey levels the downhole geophone tool is clamped to the borehole so that the geophone is coupled to the formation. Due to cave-in, washout, and the irregular shape of the borehole, perfect coupling is not always achieved, resulting in recordings contaminated with high frequency cable noise. The source may excite waves which propagate down the borehole between the borehole wall and the drilling mud. These are referred to as tube waves. Tube waves are repeated with every source impulse and are coherent, making their removal difficult. They also undergo reflection and refraction, as

shown in Figure 11 (Hardage 1983). Unavoidable random rig noise can be removed in many instances by stacking several records together, however filtering may be required to suppress electrical and mechanical pick up from rig machinery. The seismic source should be continuously monitored to ensure that its output remains consistent. This is accomplished with a hydrophone or geophone placed close to the source.

CHAPTER 5

SYNTHETIC VSP DATA

5.1 Introduction

A suitable data processing sequence giving reliable estimates of attenuation is required that allows for the input of a variety of VSP survey data, and gives repeatable results. In order to achieve this, the software to perform several of the data processing steps, in particular the spectral ratio analysis, had to be written, debugged and tested. Other software used included the SIERRA QUIKLOG (trademark of SIERRA Geophysical) package, and a number of seismic data input/ouput and processing routines written at the National Centre for Petroleum Geology and Geophysics.

The processing route to be used on the real VSP data was determined using synthetic data constructed from the sonic and density logs recorded in the Watson #1 and Tirrawarra #22 wells.

5.2 Spectral Ratio Processing Route

A data processing route for attenuation analysis was determined from several trials and is shown in Figure 12. The route can be divided into two distinct sections, and has been modified to allow for the input of real VSP data.

The first section processes the VSP traces to a suitable level for input to spectral ratio processing. The second section is the spectral ratio processing and analysis itself.

In the first stage, the VSP traces are initially displayed at their recorded one-way time, and an edit performed to remove dead and noisy traces, the latter resulting from poor borehole conditions, cable slip, poor coupling, or pick-up. An option to stack data, where several

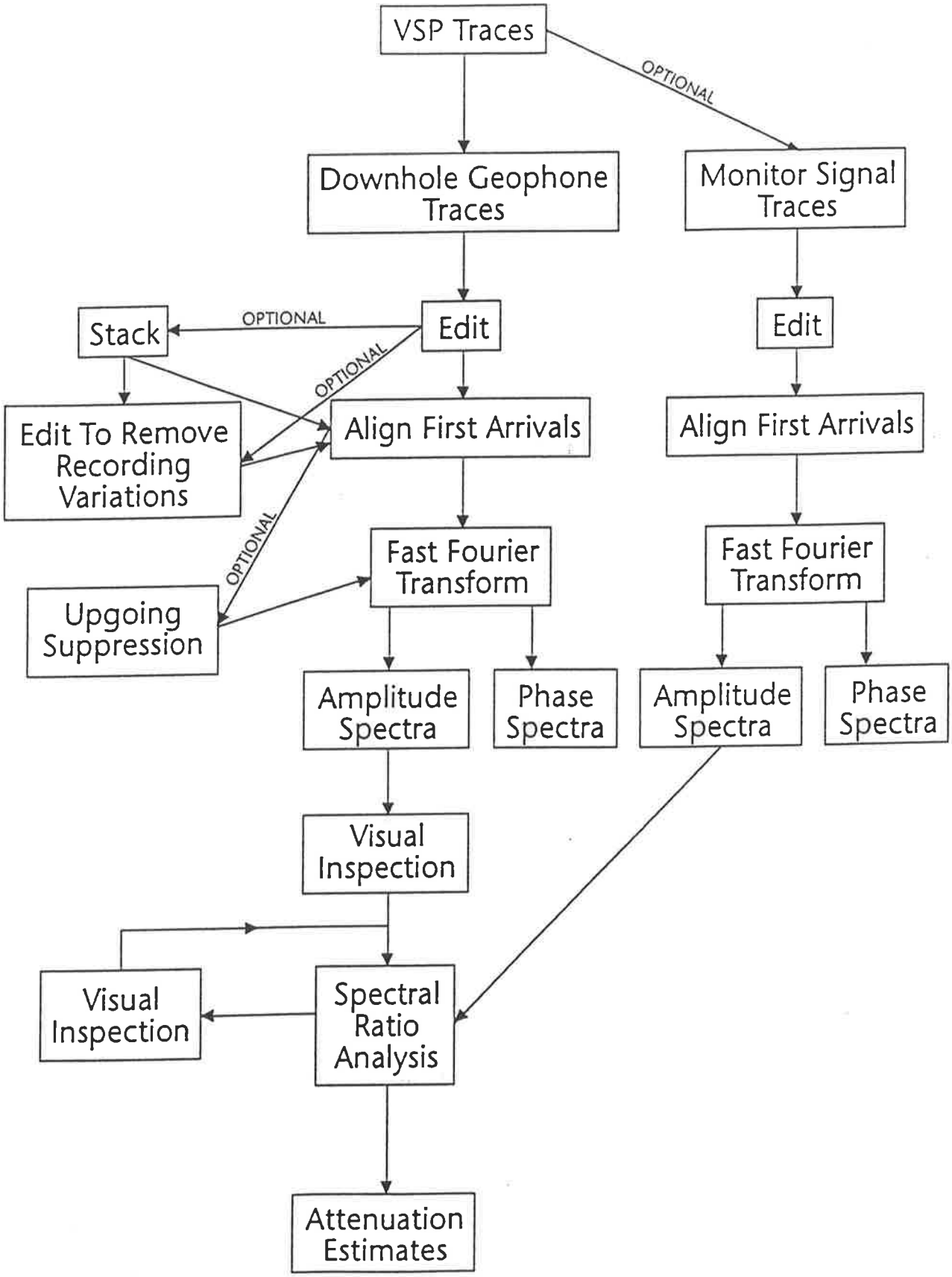

The Spectral-Ratio Processing Route

Fig. 12

recordings are made at a constant depth is included, allowing for an improvement in the signal to random noise ratio.

The edited and optionally stacked data is then shifted to align all the first arrivals at a constant time. The main reason for doing this is convenience. It enables the analysis window for the first arrivals to be the same for all traces, thus simplifying both the programming and the use of the processing code. It also makes the visual comparison of first break waveforms easier for further editing in this stage, and reference trace selection in the next. The alignment can be based on any point of the first arrival waveform, although it is preferable to choose a peak or trough rather than the first break or a zero crossing, since the latter are more sensitive to noise (Dillon and Colyer 1985). Also, in the case of zero phase data (e.g. acquired with a Vibroseis source), a well-defined first break will not exist. In this project, the first arrivals were aligned on the highest amplitude trough.

Two optional steps complete the first processing stage. Firstly, trace to trace amplitude variations may be removed, if their causes are known. Typical examples are changes in recording gain with depth in the well, and changes in vibrator drive level for Vibroseis sources. These corrections are only included for completeness, and are not required for the attenuation analysis, since they do not affect the slope of the spectral ratio plot.

Secondly, the data may be processed to suppress the upgoing waves. The rationale for doing this is to remove the interference effects of the upgoing waves on the first arrivals. Ideally, this results in a "cleaner" first arrival signature, more accurate spectral ratios, and higher resolution of attenuation with depth. The effect of upgoing wave interference and its attempted removal will be discussed later.

Suppression of the upgoing waves is commonly achieved by either f-k (frequency - wave number) or median filtering. In this project, median filtering was implemented as the optional wavefield separation technique. It is performed in the time domain and does not suffer from the mixing and wraparound effects which commonly occur in f-k filtering. Median filtering is

performed by having a moving filter window which looks at a fixed number of samples, re-arranges the samples into ascending order then outputs the median or middle value. The filter has the following two effects (Hardage, 1983):

1. Median filters absolutely reject noise spikes.
2. Median filters pass step functions unaltered.

Applying a median filter along lines of constant time in the VSP data, after the first breaks have been aligned, results in strong suppression of the upgoing wavefield. Point 1 above means that the process acts as a dip filter which passes horizontal events (in this case, the downgoing waves) and attenuates dipping events (the upgoing waves). Because of their dip, the upgoing waves are not horizontally coherent, and are treated by the filter as noise spikes.

The data is now ready to pass to the second stage of the processing sequence. The first step here is to generate an amplitude spectrum for the first break on each trace. This is done by performing a fast Fourier transform (FFT) on a time window containing the first arrival signature. Selecting this time window is a critical step in the spectral ratio technique, and one of its most criticized aspects (Sams and Goldberg, 1990). Ideally, the window should contain the entire first arrival waveform, and nothing else. In practice, the "tail" of the first arrival is often contaminated by short-period downgoing multiple energy, making it unclear as to where the window should end. In addition, upgoing events generated from reflectors immediately below a geophone level will interfere with the first arrival waveform. These factors suggest that the window should be kept short, whilst throwing away as little of the first arrival signature as possible.

The transform itself has two effects which may need to be considered. Firstly, the shorter the time window, the lower will be the resolution of the computed spectrum, since, for a fixed time sampling interval, the frequency sampling interval is inversely proportional to the time window length. For very short windows, there may not be many data points available to the spectral ratio analysis. Extending the time window by padding it with zero values will provide more data points in the spectrum. Such padding is normally required to make the

number of samples input to the FFT an integral power of two. However additional zeros may be added to produce any desired frequency sampling interval. Such padding does not add any new features to the spectrum, but simply smoothly interpolates the more widely spaced points in the spectrum of the unpadded data. In this project, padding was used to obtain a frequency sample interval of approximately 1 Hz for all data sets.

Secondly, the application of a time window to the data results in some distortion of the first arrival spectrum. A smooth taper on each end of the window can be used to minimize this effect. The software used in this project allowed the user to optionally apply a cosine taper of specified length to each end of the window. A 15 ms taper was applied as a matter of course to all the data sets analyzed in the project, although tests showed that its effect on the resulting spectra was very small.

The amplitude spectra of the first arrivals are plotted. This display has the following uses:

1. It provides a final check for any remaining traces that should be discarded from the spectral ratio analysis.

2. The effect of previous parameter choices, such as window position and length, padding and tapering can be evaluated.

3. Parameters for the spectral ratio analysis itself can be chosen. The first of these parameters is the reference trace to be used in computing the spectral ratios, in the case where a signature phone was not recording each shot, or it is not desired to use the signature data. The second parameter is the frequency range over which to perform the analysis. Both of these parameters are critical, as will be illustrated later.

After selecting a reference trace and frequency range, the spectral ratio analysis is performed using programmes developed for this study. The output consists of three data files;

File 1 :"Amplitude Ratio File" : the logarithm of the ratio of the amplitude spectrum of each input trace relative to that of the reference trace, for each frequency in the spectrum.

File 2 :"Line of Best Fit File" : co-ordinates of points defining the ends of the lines of least squares best fit for the amplitude ratio data of File 1 over the selected frequency range.

File 3 :"B_X Value File" : the slope of least squares fit for each trace analysed.

A programme designed to write information into the headers of each trace allows the above 3 files to be constructed in terms of depth or time.

These data files are used to generate a plot of the spectral ratios for each trace with the line of best fit overlain, and a plot of the cumulative attenuation, B_X, for each trace, against depth or time. From these plots, estimates of attenuation are made using the relationships detailed in Chapter 3.

5.3 Modelling

In order to test the software written to process the spectral ratios of real data, and to test the processing route, synthetic VSP data sets were constructed using log data and the SIERRA QUIKLOG package.

The algorithm used by QUIKLOG to compute the synthetic VSP can be sketched as follows. An earth model is constructed which consists of horizontal layers. Within each layer, the impedance is constant, and the time thickness is the same for all layers. The source is vertically above the receivers, giving true zero-offset geometry. All reflecting interfaces then occur at integral multiples of the layer vertical time thickness. This is a computational convenience which allows travel times in the model to be discretised.

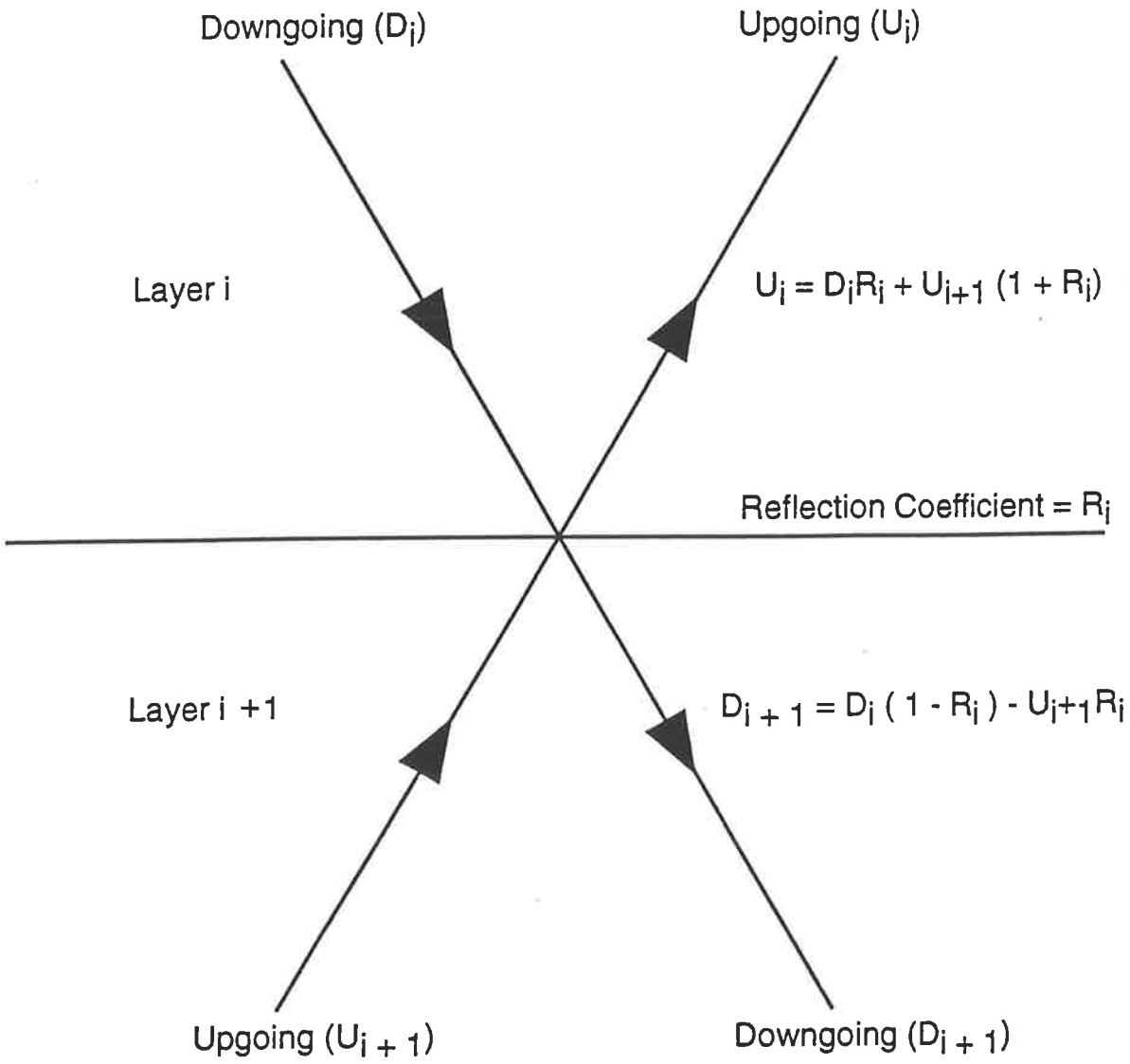

Schematic of upgoing and downgoing waves

Fig. 13

Considering the interface separating layers i and i + 1 in this model, and denoting its reflection coefficient for downgoing waves by R_i, it is apparent from equations 5 and 6 that an incident downgoing wave of amplitude D_i will be split into reflected and transmitted components of amplitude D_iR_i and $D_i(1-R_i)$ respectively. Similarly, an upgoing wave of amplitude U_{i+1} incident on the interface will generate reflected and transmitted components of amplitude $-U_{i+1}R_i$ and U_{i+1} $(1 + R_i)$ respectively. As shown in Figure 13, the upgoing wave above the interface and the downgoing wave below the interface are given by

$$U_i = D_iR_i + U_{i+1}\ (1+R_i) \qquad \ldots 33$$

and $$D_{i+1} = D_i\ (1 - R_i) - U_{i+1}\ R_i \qquad \ldots 34$$

Introducing a spike at time zero at the top of the model, equations 33 and 34 can be solved recursively for all layers, and the process iterated through as many time steps as required, to give the impulse response of the model at the specified detector levels.

The above equations can be used in a model with any number of layers. They generate all upward and downward travelling multiples, in addition to the downgoing wave and primary reflections. Convolution of the impulse response at each detector with an appropriate wavelet will generate the synthetic VSP traces.

The geologic model to be used can be defined by designing a series of layers, separated by equal time intervals, with assigned velocities and densities, or by using wireline log data recorded in a borehole. QUIKLOG provides the facility to block log data into equal travel-time layers whilst preserving traveltime down the well. Reflection coefficients are then calculated from the blocked impedance model or the velocity model alone, if a density log is unavailable. The synthetic is then generated as outlined above.

Sonic and density log data were made available by SANTOS Limited for the two VSP wells, Watson #1 and Tirrawarra #22.

5.3.1 Preliminaries for VSP modelling

The models for the two wells were constructed from the sonic and the density logs. The sonic log measures the time taken for a compressional wave to travel through one foot of formation. It thus provides a measurement of slowness or reciprocal velocity in microseconds per foot. The density log is a porosity log that measures the electron density of the formation. Gamma rays are emitted from the density tool and interact with the electrons of the rock formation, mainly by Compton scattering. The scattering of gamma rays by electrons is related to the density of electrons in the formation, which is a function of the bulk density of the rock.

Logs measure rock properties as a function of depth. However, by integrating the sonic log, depth intervals can be converted to time intervals. This allows comparison between a sonic log (and models derived from it) and a conventional seismic section. After correlation between the sonic log and seismic section, other borehole logs can be related to the seismic response. Unfortunately sonic logs rarely, if ever, correlate perfectly with a seismic section. The main reasons for this are:

i) The sonic log and seismic survey investigate different rock volumes.
ii) Differences in instrumentation
iii) Difference in source parameters and propagation

The sonic log is first edited to remove any effects due to borehole conditions, noise spikes and cycle skip. The transit times are then adjusted so that, when integrated, they agree with the seismic checkshot and VSP times. These adjustments are termed drift corrections.

Drift is the difference between the vertical, datum corrected, checkshot time and the integrated sonic transit time. The check shot survey and sonic log are tied at the first check

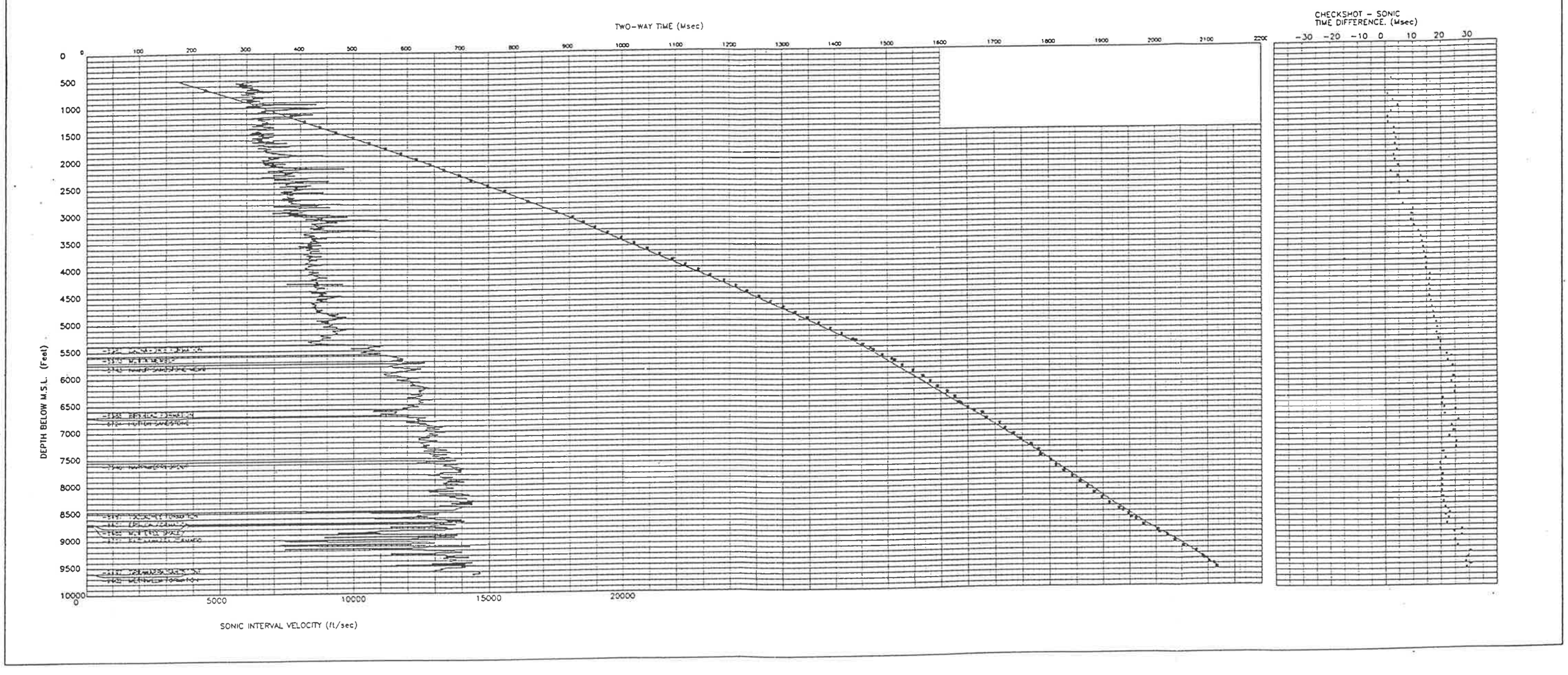

Tirrawarra #22, checkshot data and drift correction

Fig. 14

shot level at or below the top of the sonic log. A plot of the drift with depth allows the calculation of the correction to apply to the sonic log. Drift is negative where the integrated sonic times are longer than the checkshot time intervals, and positive where they are shorter.

Drift corrections to the sonic logs were carried out using the check shot surveys recorded in conjunction with the VSP in both wells. The check shot data and drift applied for Tirrawarra #22 are shown in Figure 14.

The product of the drift corrected sonic and density logs is the acoustic impedance log, from which the synthetic VSP is constructed. A simple Ricker wavelet was used to give the convolved response. The parameters used to model both wells are listed below.

Acoustic model	:	Long spacing sonic (drift corrected)
Density model	:	Density log
Log sample interval	:	1 foot
Wavelet type	:	Zero phase Ricker
Dominant Frequency	:	40 Hz
Wavelet length	:	127 ms
Time sample interval	:	1 ms
Receiver separation	:	100 ft
Polarity	:	S.E.G. Normal

5.3.2 Tirrawarra #22 Synthetic VSP

Figure 15 shows the synthetic VSP response, in one-way time below mean sea level, of the acoustic impedance model for Tirrawarra #22. AGC, of length 500 ms, has been applied to this, and all subsequent VSPs, for display purposes only. Immediately apparent are the downgoing and reflected upgoing wavefields sloping in opposite directions, and the absence of any multiple activity, which has been excluded from this initial model. The downgoing first arrivals slope from right to left and the gradient of the event varies as the velocity of the

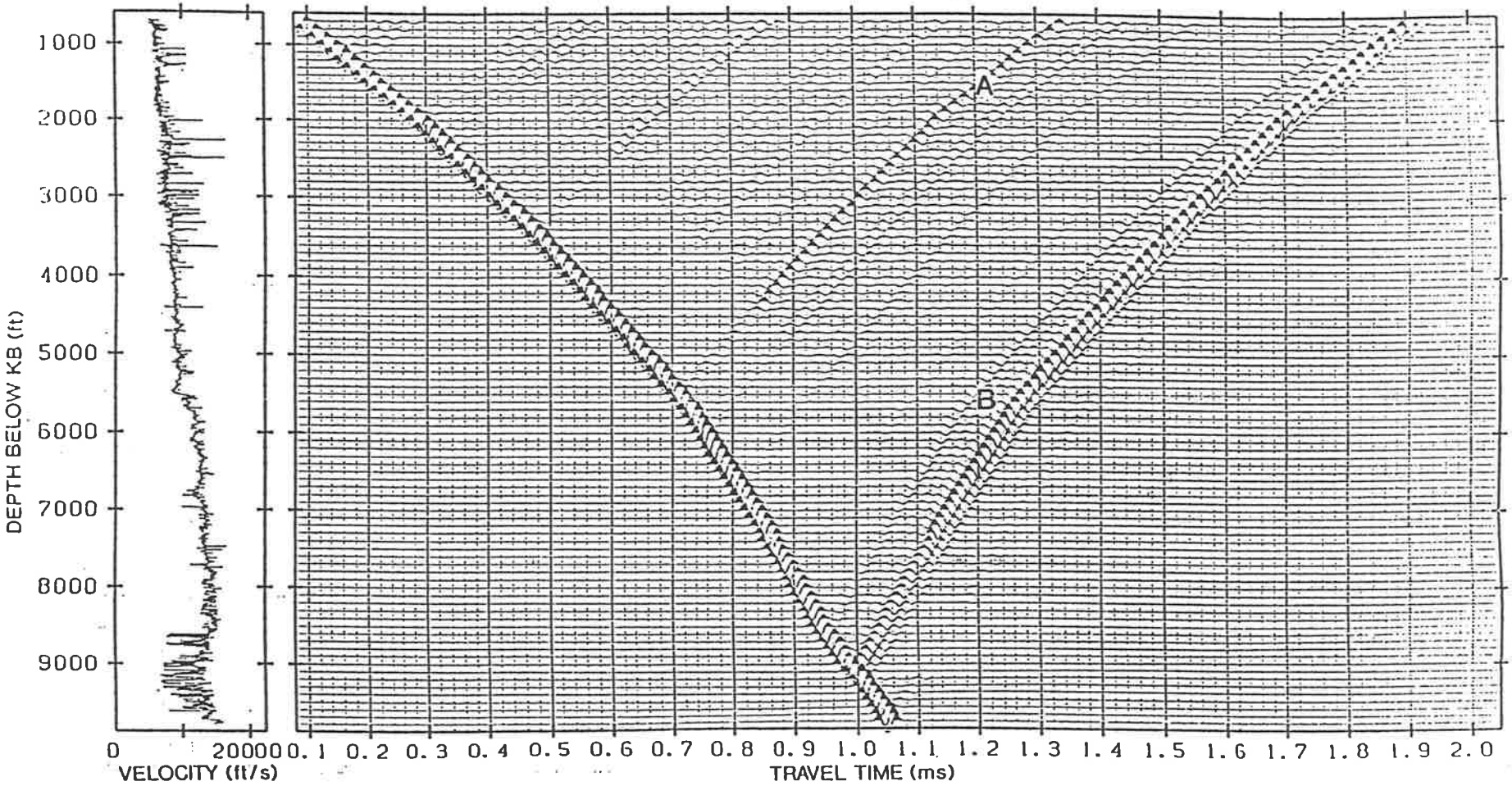

Tirrawarra #22, synthetic VSP without multiples

Fig. 15

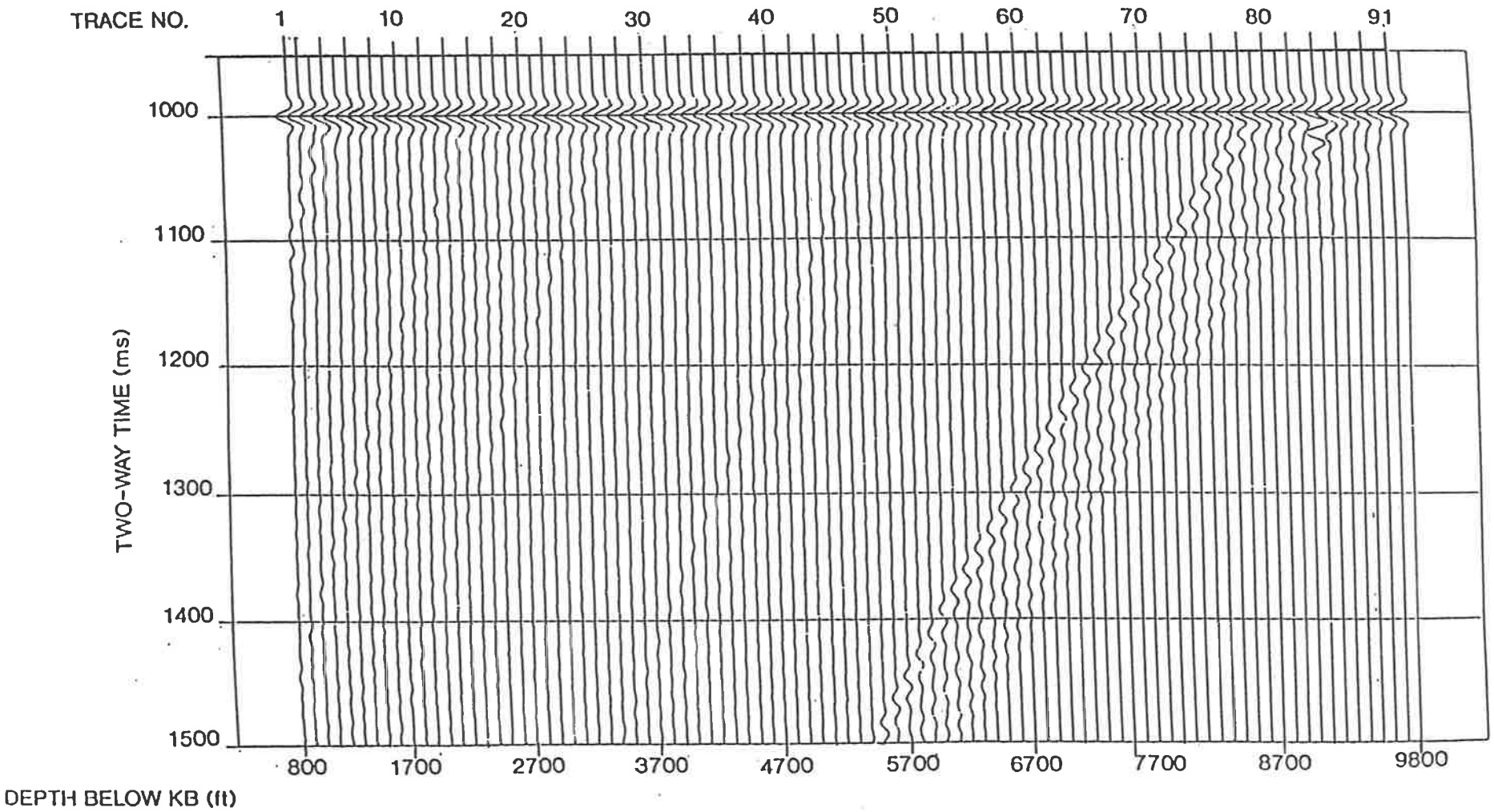

Tirrawarra #22, synthetic VSP traces aligned at 1000ms

Fig. 16

model changes. Sloping from left to right are the upgoing waves. The points where they cut the first arrival curve indicate the depths at which the reflections are generated. The reflection labelled A originates from the interface at 5524 feet (all depths are given relative to KB), and represents the response of the top Cadna-Owie Formation. This interface generates the basin-wide "C" reflection observed on surface seismic data. The upgoing reflections labelled B are generated by the Top Toolachee Formation and coals below and correspond to the "P" and deeper reflections on surface seismic data.

The 91 synthetic VSP traces, shifted to align the first arrivals at 1000 ms, are shown in Figure 16. Based on the length of the wavelet used in the generation of the synthetic, a data window of 127 ms centred on 1000 ms was used in the spectral ratio programme. The trace at 1500 feet was used as the reference trace. The two plots resulting from the analysis are shown in Figures 17 and 18.

5.3.3 Interpretation of the Tirrawarra #22 Synthetic VSP results

The expected result of analysing the synthetic data is that the amplitude ratios should be constant with frequency for each depth, the line of best fit having a slope of zero. This implies that B_X is zero, corresponding to no frequency-dependent attenuation of the propagating signal.

Figures 17 and 18 show that for most of the modelled traces the slope of the line of best fit is very close to the expected value of zero, with an average value for B_X of -.00643 dB/Hz. The desired result of zero attenuation is not obtained because of the scatter in B_X values.

The spectral ratios will be changed if the input parameters are altered. However, the length of the analysis window is correct, being equal to the known length of the wavelet input for the convolution. Changing the frequency range will have little effect, as all frequencies are treated equally and the synthetic traces are noise-free . Changing the reference signal

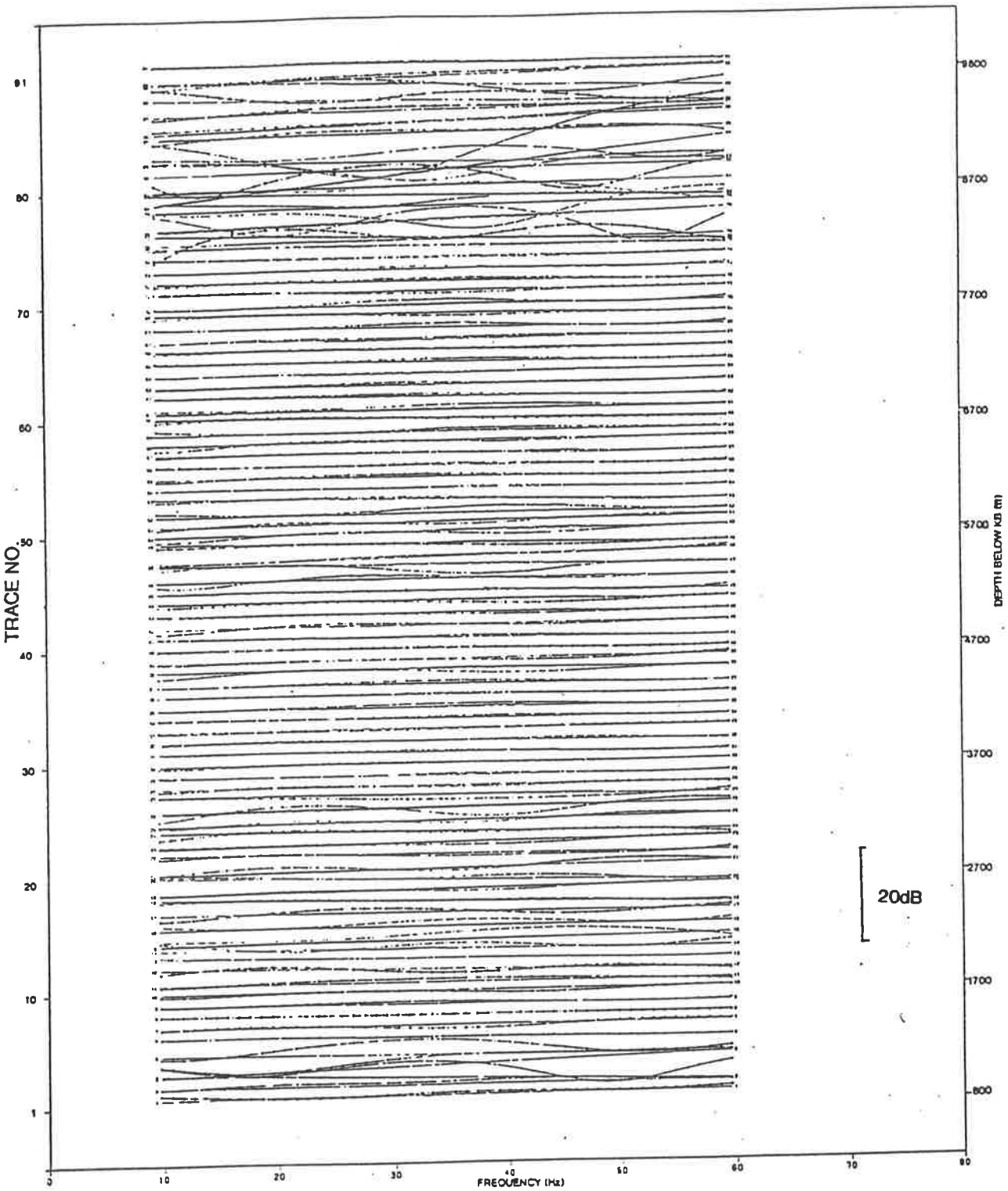

Tirrawarra #22, synthetic data - amplitude ratios between 10-60 Hz

Fig. 17

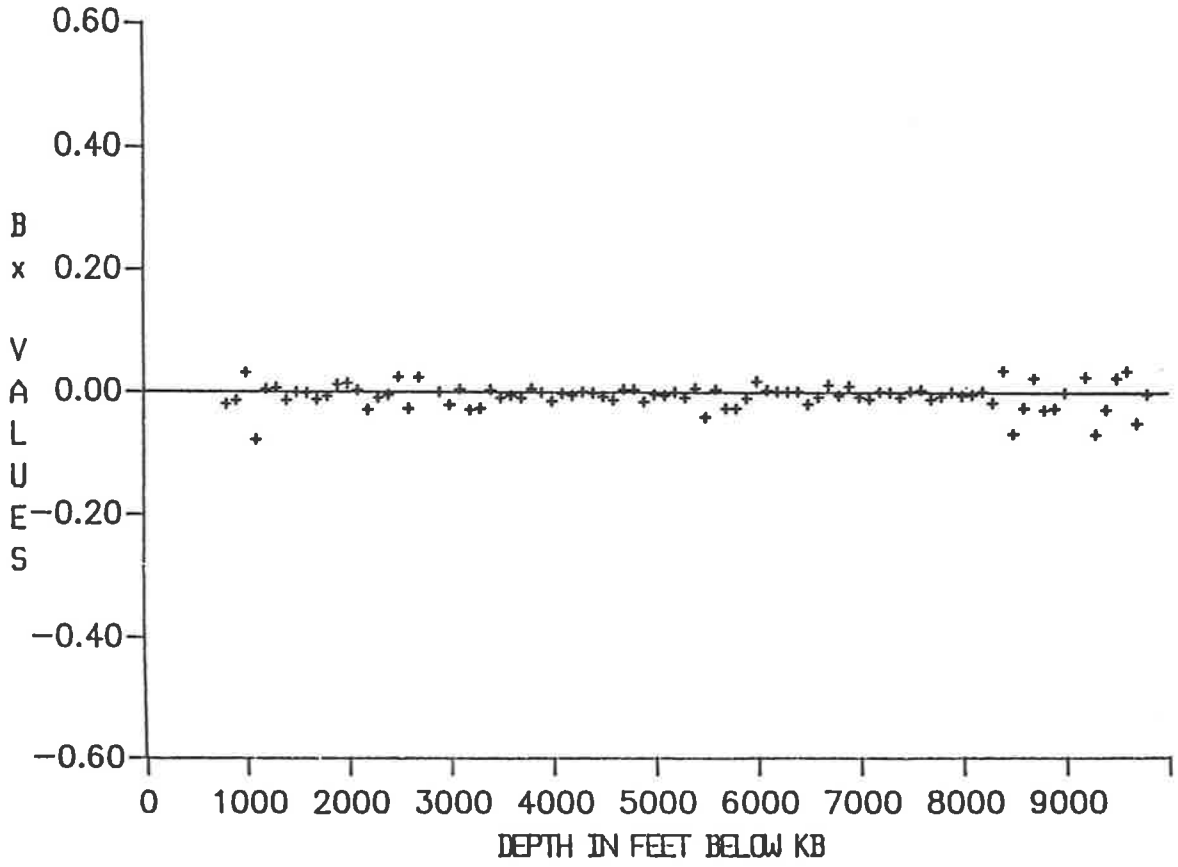

Tirrawarra #22, synthetic data - cumulative attenuation between 10-60Hz

Fig. 18

spectrum to use a trace with a more negative B_X on Figure 18 will bring all the values closer to the zero line, but still show the same scatter.

Several of the B_X values, particularly above 1200 feet and below 8500 feet, show a marked displacement from the zero line. As there is no frequency-dependent attenuation in the modelling algorithm, this displacement must be caused by some other mechanism.

The processing route applied assumes that for each trace the spectrum is that of the downgoing first arrival only. However, synthetic VSP traces above a reflecting boundary include upgoing arrivals. As the detector approaches the boundary, so the time separation between the downgoing and upgoing arrivals shortens, until they begin to interfere with each other. From this depth to the boundary, the first arrivals on a VSP trace will be affected by the superposition of the upgoing reflection.

A comparison between the input acoustic model (Figure 15) and amplitude ratio plot (Figure 17) can be used to explain the larger displacements from zero seen on Figure 18. Where the acoustic model is changing rapidly, the likelihood of locating a geophone level at or very close to a large reflecting interface increases. This is seen by the amplitude ratios above 2000 feet and below 8500 feet. Above 2000 feet the acoustic impedance variation is a result of near surface unconsolidated sediments, and below 8500 feet there is a series of thin coals. The variations in acoustic impedance seen in the intervening depth range are either not large enough to generate reflections of sufficient strength to have a significant effect on the downgoing signal, or, within this interval, no geophone is located close to a strong reflector. For several of the ratio sets that show displacement from a straight line, the least squares fit does show an almost zero slope. It is evident from the model data that the cumulative attenuation measurements will not give meaningful values of attenuation over a small interval. However, over an interval spanning sufficient geophone levels, a best fit to the data appears to give a reliable result. The scatter seen in the plot of cumulative attenuation data shows how sensitive the spectral ratio processing is to any change in the first arrivals of

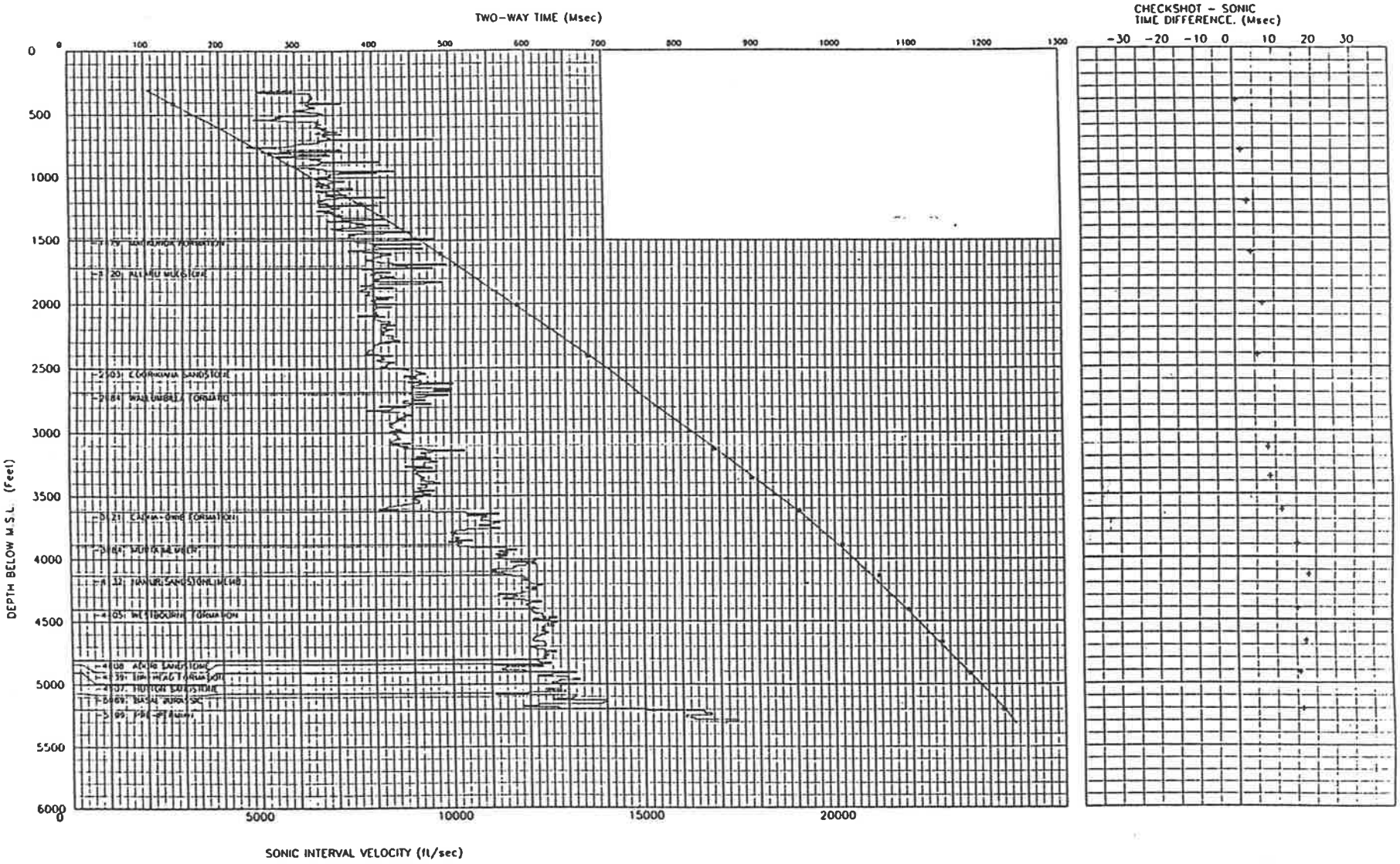

Watson #1, checkshot data and drift correction

Fig. 19

the propagating seismic pulse. Such a change may be a result of interference from upward travelling waves generated by a reflector below the geophone.

Attempts were made to eliminate the upgoing waves by applying a median filter. The data, were initially shifted to align the first downgoing arrivals at 1000ms, and then filtered to eliminate events that exhibited dip. Filters with 5, 7 and 9 points were tested. The median filtering did not reduce the scatter in the cumulative attenuation curve. Hauge (1981) observed a reduction in the scatter, but not of a sufficient amount to improve depth resolution. Because of these results, wavefield separation was not included in the following analyses.

5.3.4 Watson #1 Synthetic VSP

The check shot data and drift correction for this well are shown in Figure 19. The synthetic VSP was generated using the same parameters as for Tirrawarra #22, except for a sample rate of 0.5 ms. The result is shown in Figure 20. Watson #1 is a shallower well than Tirrawarra #22 and does not have the series of coals at depth. The display of the model VSP illustrates how much stronger the amplitude of the downgoing signal is in comparison to the upgoing events which have undergone at least one reflection. The synthetic traces are shown in Figure 21 aligned at 500 ms. Upgoing reflections can be seen dipping at a steep angle.

The synthetic VSP traces were input to the spectral ratio programmes and analysed using identical parameters to Tirrawarra #22. The resulting cumulative attenuation values are shown in Figure 22. The measured values of B_X cluster closely around the expected value of zero. Several values show a significant displacement from zero but can be explained by the vicinity of the geophone to a reflecting interface. The average B_X value is -0.0066 dB/Hz, and the line of best fit has a slope very close to zero.

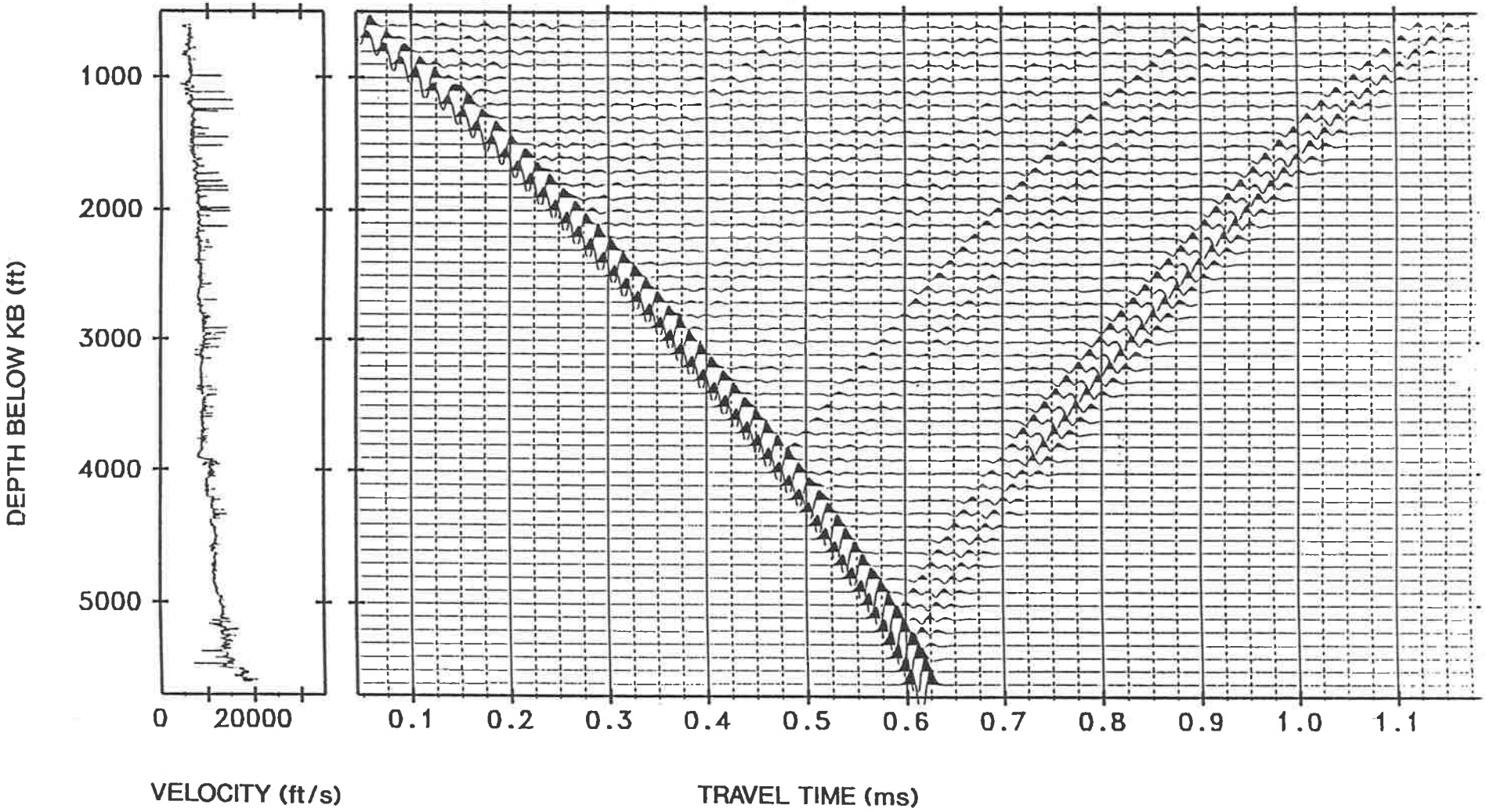

Watson #1, synthetic VSP without multiples

Fig. 20

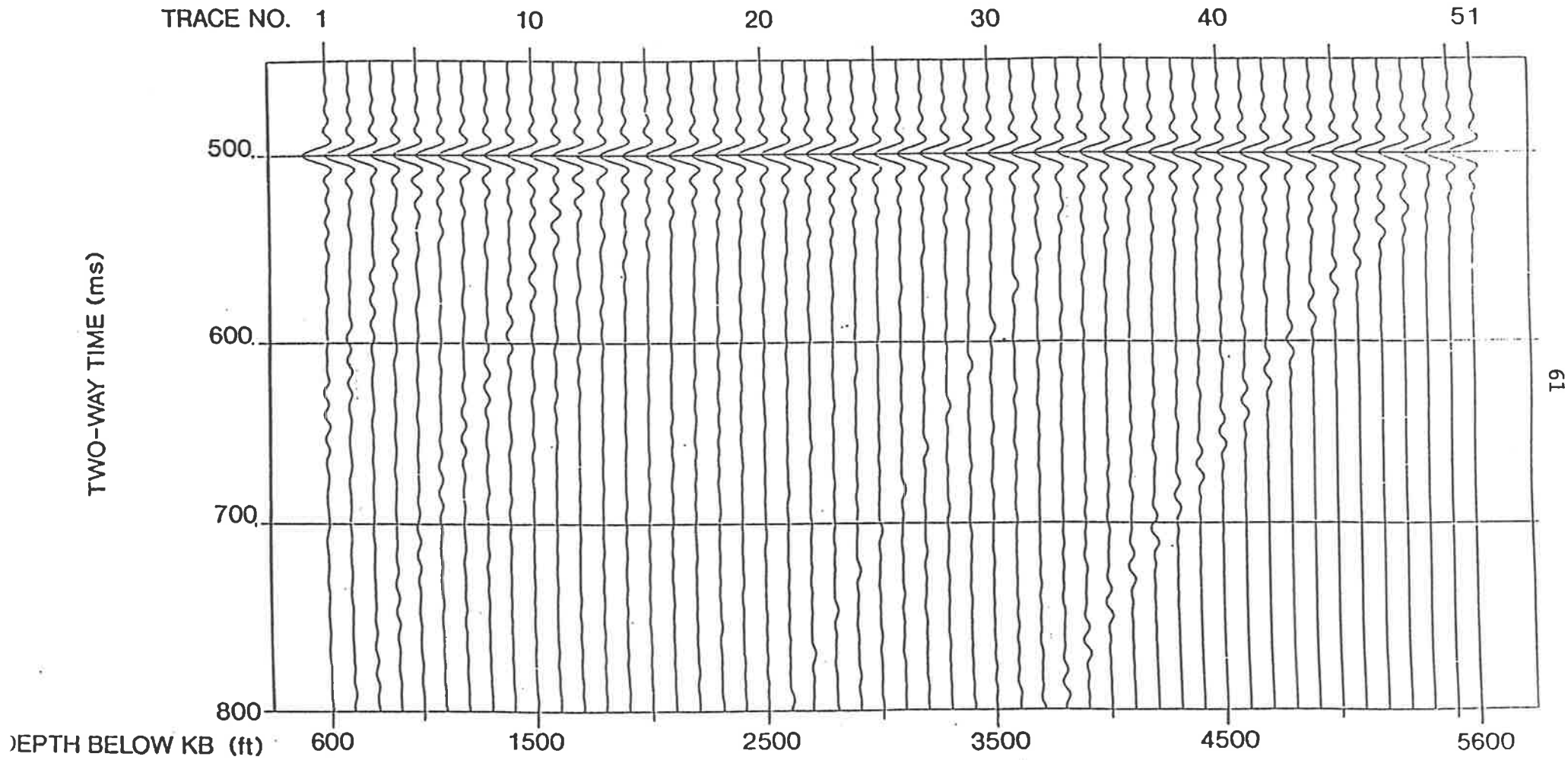

Watson #1, synthetic VSP traces aligned at 500ms

Fig. 21

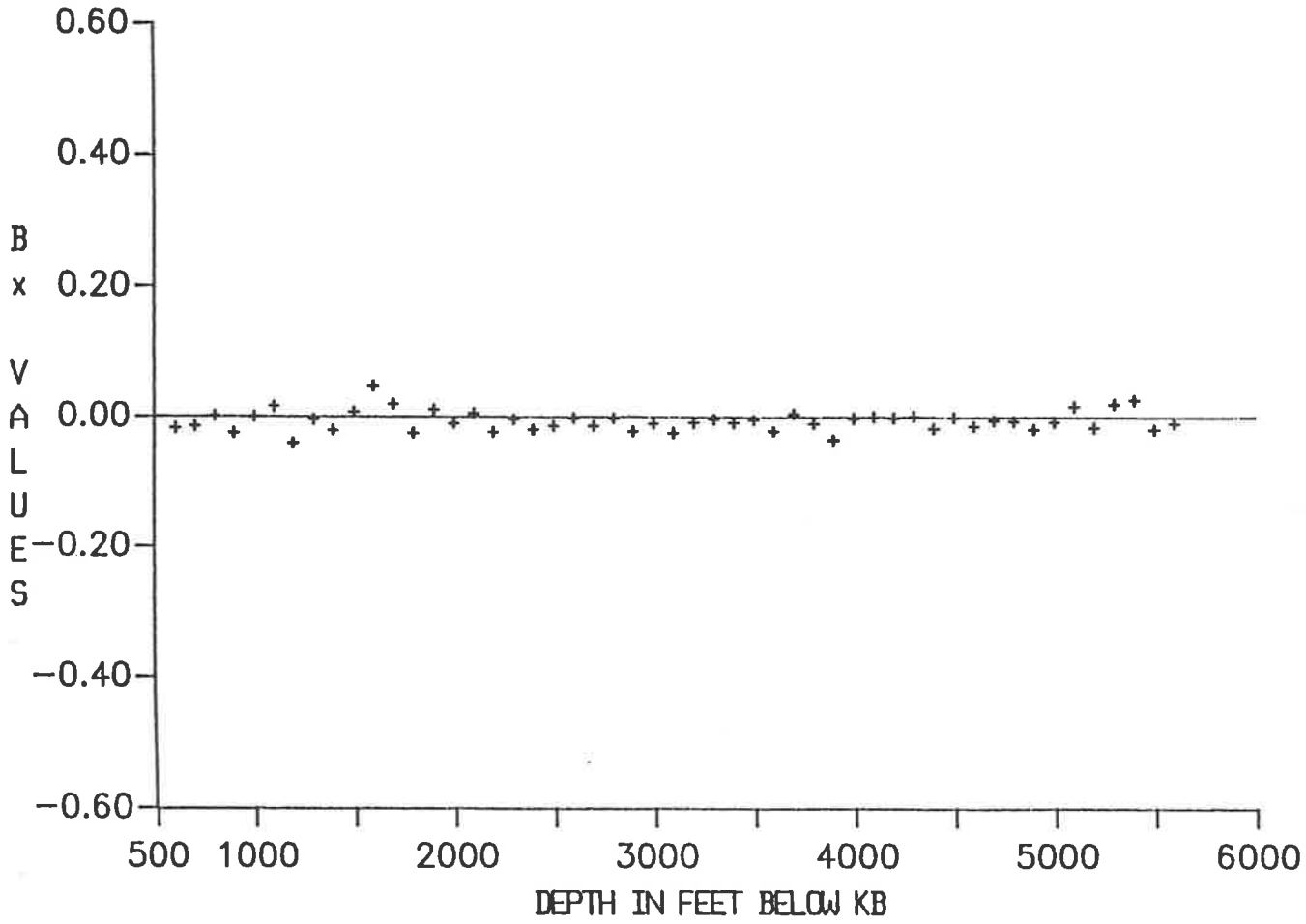

Watson #1, synthetic data - cumulative attenuation between 10-70 Hz

Fig. 22

5.3.5 Summary

The cumulative attenuation calculated from the two synthetic VSPs is very close to the expected value of zero. Modelling has shown the sensitivity of the spectral ratio technique to events interfering with the first arrivals. In a real VSP, other factors not present in model data will compound the problem. These factors will include signal variations, geophone coupling, and noise.

Selection of a reference trace is an important step in the analysis . If a trace was chosen where the first arrival was contaminated by a strong upgoing event, the amplitude ratios are likely to be distorted. With model data this problem is immediately evident, but for real data, a careful inspection of the VSP traces and their locations relative to signficant impedance changes will have to be made prior to selecting a reference trace.

The scatter in the B_X values evident in the foregoing analyses of synthetic data raises two problems associated with analysing real data; i) attenuation may be masked by scatter, particularly over short intervals and zones of low attenuation and, ii) scatter may be mis-interpreted as attenuation. The model VSP results provide a lower limit on the scatter likely to be encountered in the real data. For Tirrawarra #22, ignoring depths below 8300 feet, all B_X values fall within ± 0.035 of the true value. In Watson #1 all but one value fall within the same range. This degree of scatter will be assumed in interpreting cumulative attenuation plots for subsequent data sets.

CHAPTER 6

THE EFFECT OF MULTIPLE ACTIVITY

6.1 Introduction

O'Doherty and Anstey (1971) observed that the attenuation of a propagating seismic pulse is the sum of intrinsic attenuation resulting from anelastic earth behaviour, and apparent attenuation due to intrabed multiple activity. In order to isolate the intrinsic component it is necessary to estimate the attenuation due to multiples so that it can be subtracted from the observed attenuation.

Multiples are events that have undergone more than one reflection, and maybe either upgoing or downgoing. A long-period multiple is one whose travel path is longer than that of its associated primary by a distance such that it appears as a discrete seismic event. A multiple with travel path shorter than this distance is termed a short-period multiple. Intrabed multiples causing apparent attenuation fall into this latter category.

Schoenberger and Levin (1974) used synthetic seismograms to show that intrabed multiples interfere with the first arrival and reflection signals by raising the low-frequency end of the amplitude spectrum and lowering the high-frequency end.

Studies by several authors, including Schoenberger and Levin (1974, 1978), show that the assumption of a constant-Q model is acceptable for attenuation caused by multiple activity, and as a consequence, the spectral ratio technique is applicable. In a study of 8 wells, Schoenberger and Levin (1978) illustrated that the proportion of attenuation attributable to intrabed multiples varies, as shown in Table 1. The values were calculated using synthetic seismograms and the spectral ratio technique. The same method was used by Hauge (1981) to obtain intrabed multiple attenuation estimates, and was used again in this study.

WELL	MEASURED ATTENUATION IN dB/Hz		
	α_1 INTRABEDS	α_2 OBSERVED DATA	(α_1/α_2) 100%
1	0.03	0.21	14%
2	0.04	0.20	20%
3	0.08	0.18	44%
4	0.09	0.35	25%
5	0.15	0.35	43%
6	0.21	0.26	80%
A	0.07	0.20	35%
B	0.04	0.09	49%

Table 1. Percentage of observed attenuation attributable to multiple activity (From Schoenberger and Levin, 1978)

6.2 Tirrawarra #22 Synthetic VSP with Multiples

Using the model parameters described in the previous chapter, a VSP with all order multiples was generated (Figure 23) for Tirrawarra #22. The QUIKLOG modelling package does not allow the user to specify the maximum order of multiple to be included in the synthetic. Consequently, it was not possible to determine the highest order of multiple which still contributes significantly to the synthetic response.

The VSP display with multiples is far more complex than that without multiples. Various discrete events parallel to the first arrival are evident. These are long-period multiples of the downgoing wavefield. The multiple event labelled C, recognized as an artefact of the QUIKLOG model, is a downgoing multiple generated between the surface and a shallow reflector within the model. The software did not permit editing of this event.

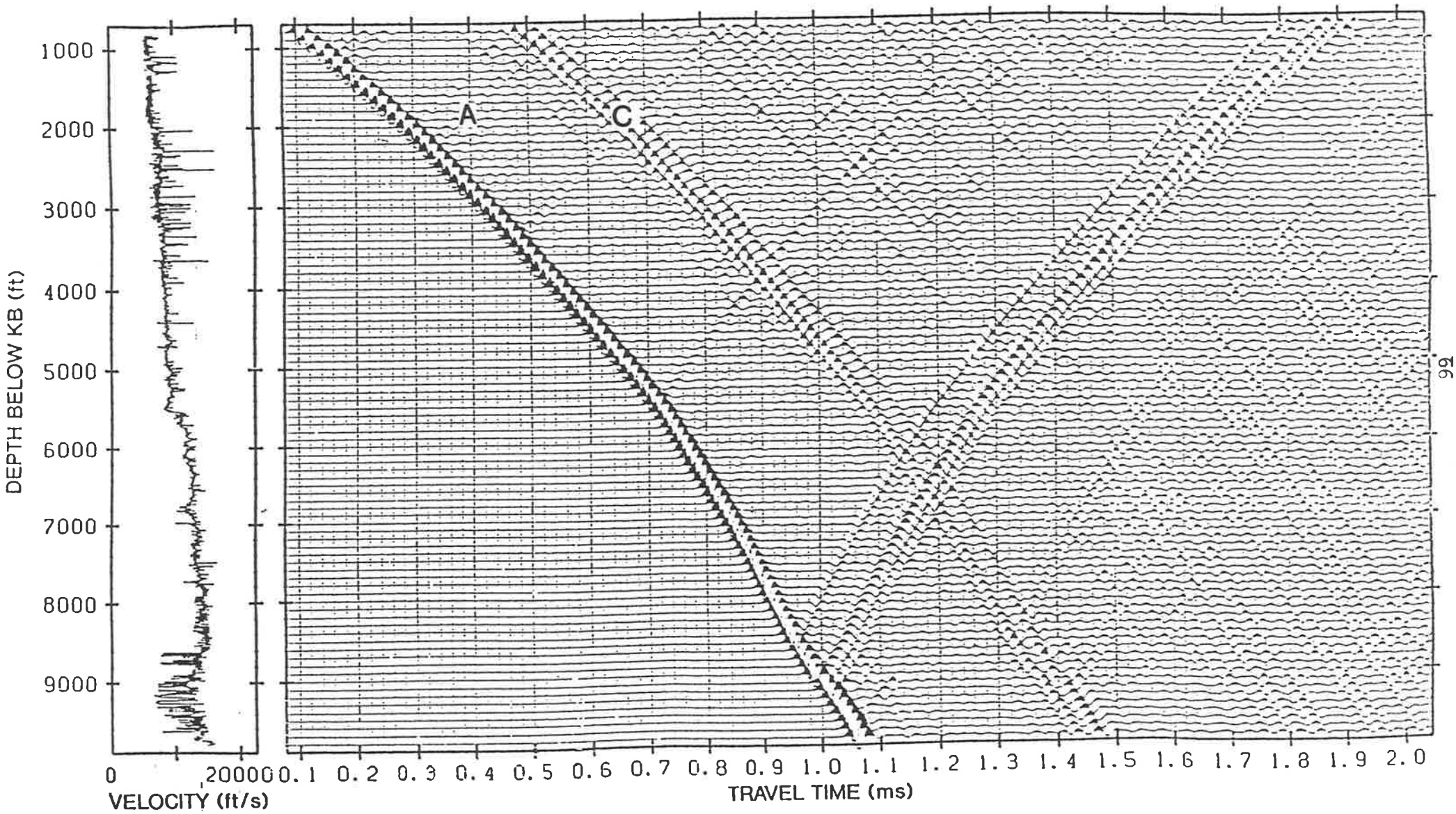

Tirrawarra #22, synthetic VSP with multiples

Fig. 23

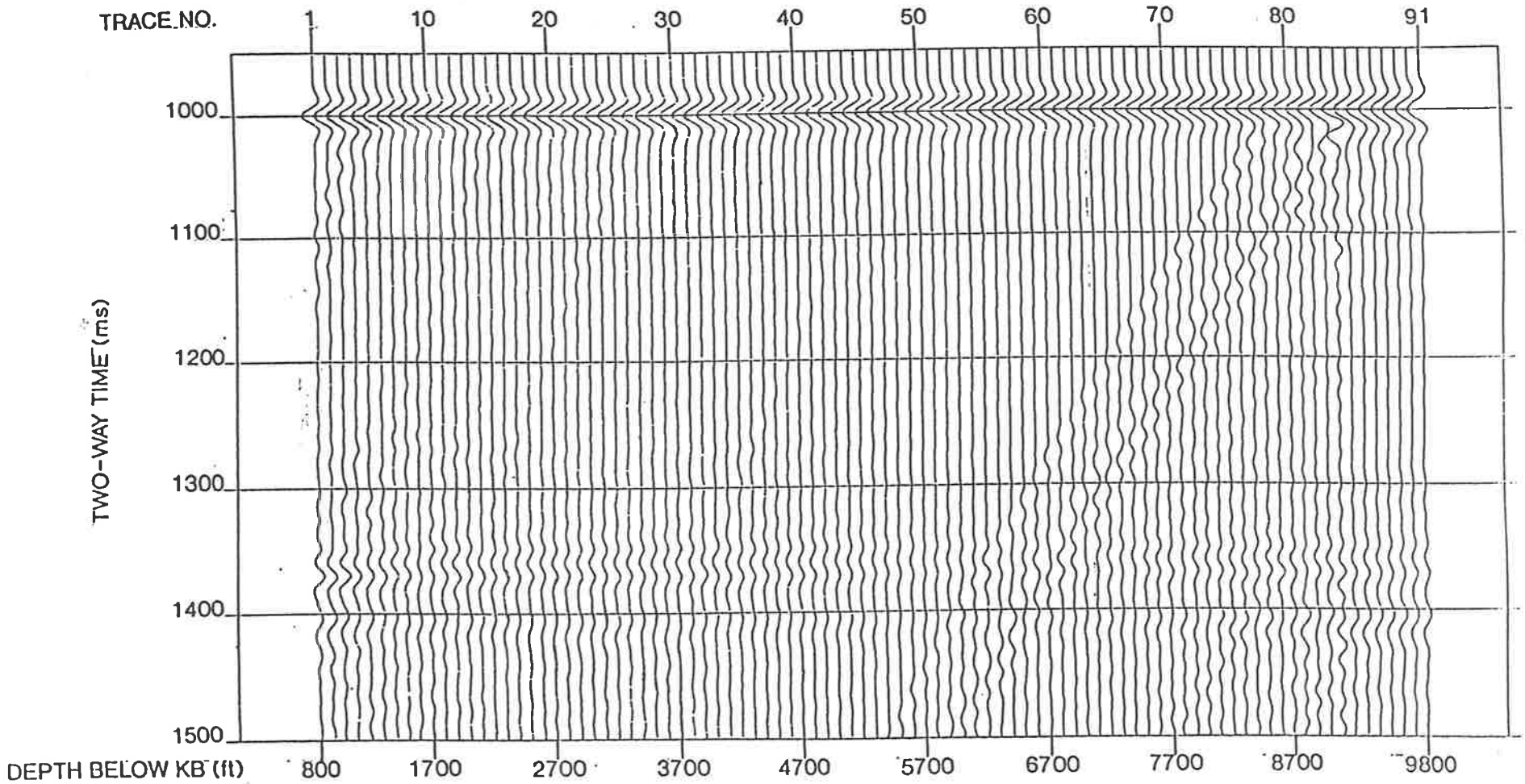

Tirrawarra #22, synthetic VSP with multiples; traces aligned at 1000ms

Fig. 24

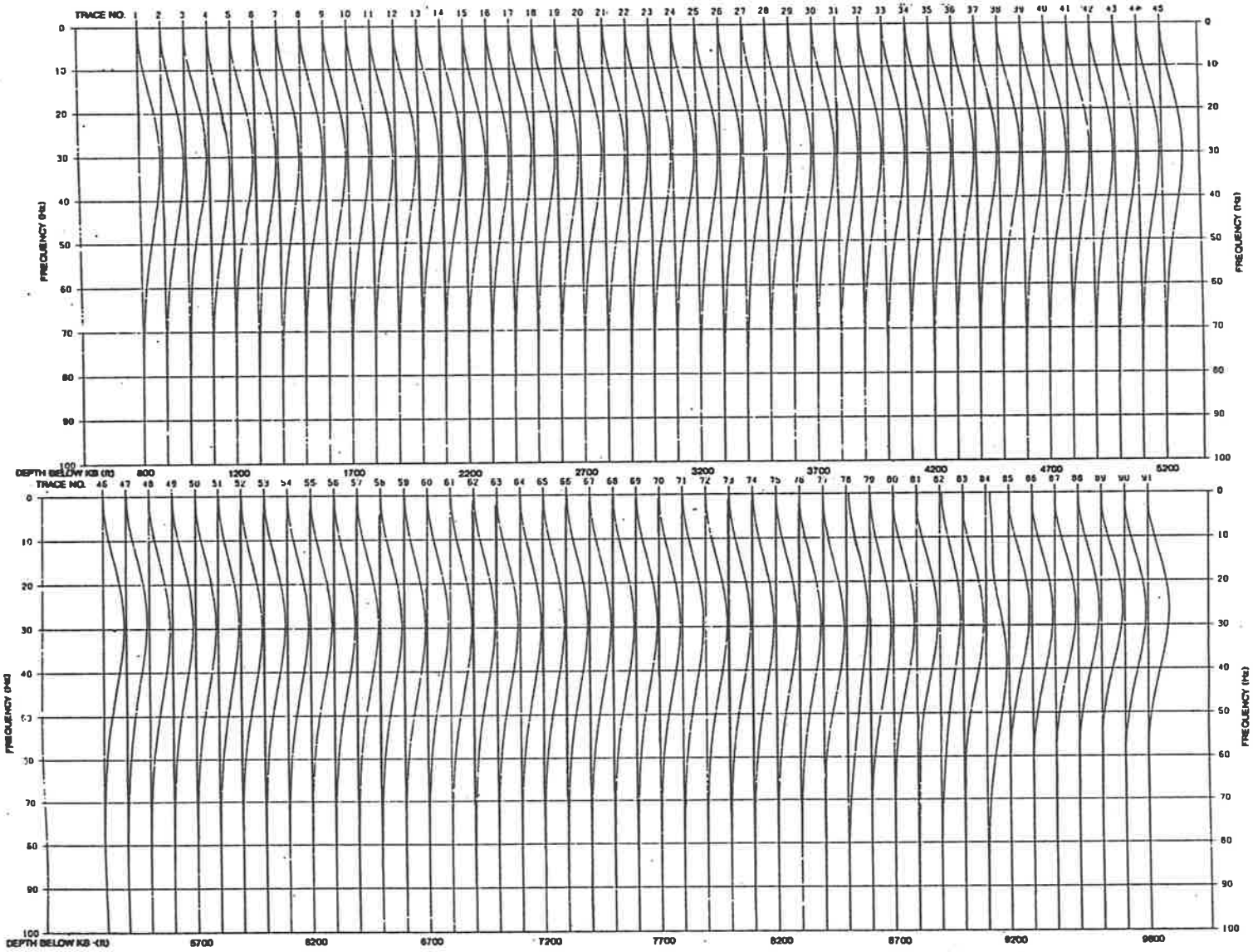

Tirrawarra #22, synthetic VSP with multiples; frequency spectra of the first arrivals

Fig. 25

Upgoing multiples are more difficult to recognize. They manifest as events sloping in the opposite direction to the downgoing wavefield, but they do not intersect the first arrival, as do the primary reflections.

VSP traces with the downgoing first arrival aligned at 1000 ms are shown in Figure 24. The long-period multiple labelled C in Figure 23 is evident as an event aligned at approximately 1360 ms, and strong upgoing reflections are seen on the deeper traces. The first arrival from 9100 feet (trace 84) is distorted in comparison to the other traces. Inspection of the model shows this level to be very close to a thin coal which generates an upgoing reflection that interferes with the first arrival. This interference is also evident on the model without multiples (Figure 16).

The spectra of the first arrivals were then computed, again using the length of the convolved wavelet as the live data length for the transform. The results, normalized by the maximum value for each trace, are displayed in Figure 25. The spectra show the frequency content of the first arrival to be between 5 and 70 Hz, with very little change in character until 8300 feet (trace 76). From there to the bottom of the model the approximate bandwidth of the first arrivals is between 5 and 50 Hz.

The spectral ratios were then calculated using trace 8 at 1500 ft as the reference. Least squares lines were fitted to the ratios, using the data between 10 and 60 Hz. The results are shown in Figure 26. Between 800 and 8300 feet (traces 1 and 76) the amplitude ratios are very consistent and are similar to those for the model without multiples. From 8400 feet (trace 77) down, the amplitude ratios vary dramatically, particularly below 9100 feet (trace 84).

The location of the synthetic trace at 8400 feet (trace 77) is in a section of the model with little acoustic variation. However the amplitude ratios suggest that there is some interference with the downgoing first arrival at this depth. To explain this, it is necessary to consider the input signal. The 127 ms long zero-phase Ricker wavelet used to generate the

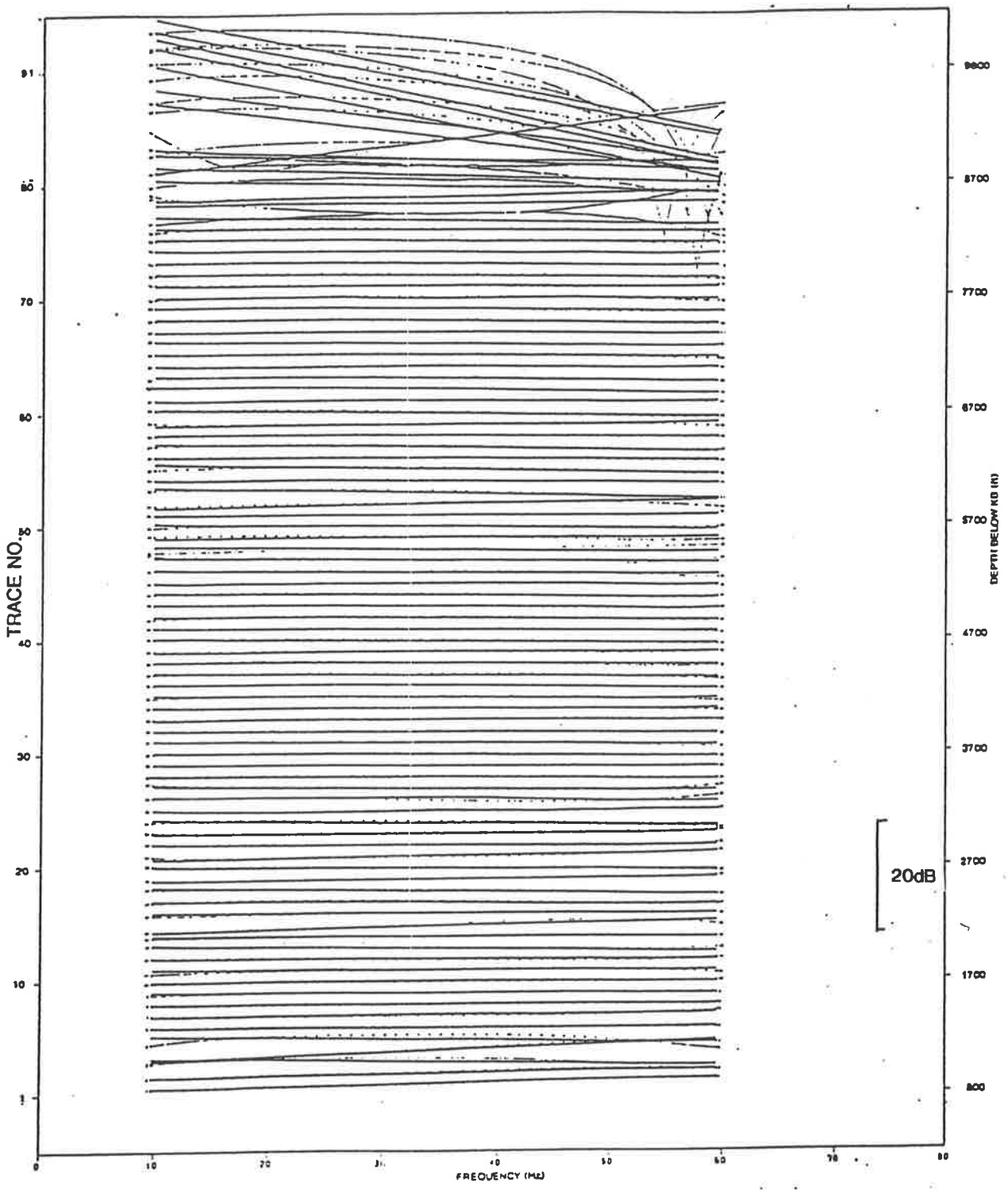

Tirrawarra #22, synthetic VSP with multiples; amplitude ratios

Fig. 26

synthetic has 63.5 ms of signal either side of the ray trace arrival time. Hence, in this model, if a reflection is not to interfere with the first arrival, it must be delayed by at least 63.5 ms. The reflector must therefore be located at a minimum distance below the geophone level corresponding to 31.75 ms of one-way travel time. At 8400 feet, integration of the sonic log shows that this minimum distance is 490 feet. However, inspection of the logs shows that the first large impedance variation is only 210 feet, or 13.75 ms, below the geophone at 8400 ft. Trace 76, at 8300 feet shows little if any affect of the large impedance change which is 21.5 ms below this level. With this larger time separation, only the low amplitudes at the start of the reflected wavelet interfere with the first arrival. Because a downgoing first arrival can be affected by a reflection from some distance below the geophone location the resolution of attenuation measurements will be limited. This example illustrates the need to analyse geophone locations with reference to a sonic log, if the aim of a VSP survey is to measure attenuation.

Decreasing the length of the input to the Fourier transform would reduce the effect of nearby reflectors. However, tests on reducing the window length showed that decreasing the length to less than that of the known input signal cut off part of the first arrival, which in turn distorted the estimates of attenuation.

Referring back to the model without multiples (Figure 17), below the sequence of coals the spectral ratios are once again almost linear with slopes close to zero. As there are only a few minor impedance variations below the coals, this is to be expected. However the results for the model with multiples indicate that within and below the coal sequence there is a large effect on the amplitude ratios. This is in agreement with the results of Schoenberger and Levin (1974, 1978) who observed a spectral bias with a relative lowering of the high frequency end of the spectrum when synthetic seismograms were generated with multiples.

Figure 27 is the plot of the cumulative attenuation from the above analysis. The value of B_X at 9100 feet is plotted, but not used in the following analysis. In comparison with the B_X values for the model without multiples, it is evident that the introduction of multiple

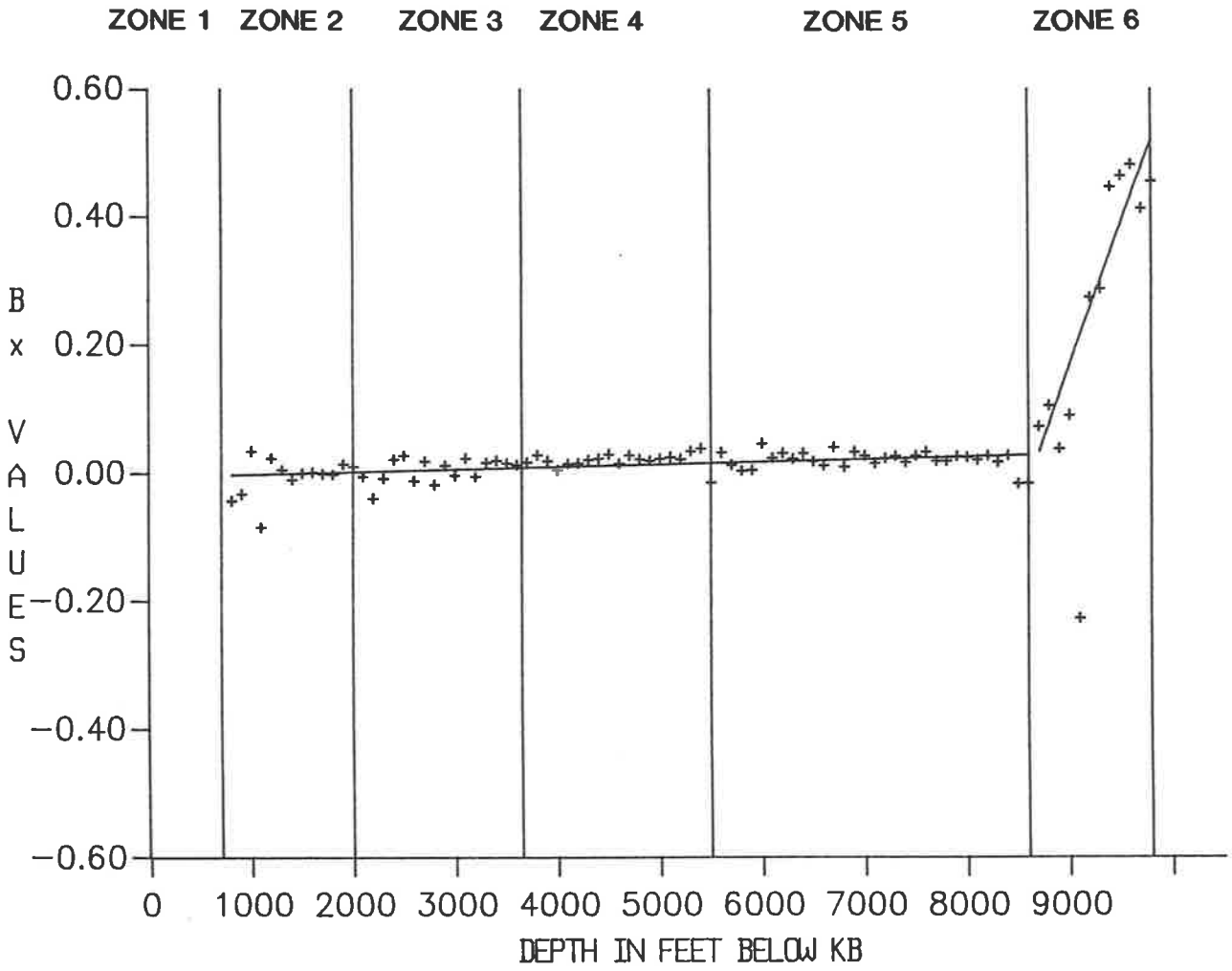

Tirrawarra #22, synthetic VSP with multiples; cumulative attenuation between 10-60 Hz

Fig. 27

TABLE 2 TIRRAWARRA #22 ACOUSTIC MODEL ZONES

ZONE	DEPTH INT. KB	FORMATION RANGE	AGE RANGE	VELOCITY RANGE (ft/sec)	VELOCITY CHARACTERISTICS	DEPOSITIONAL ENVIRONMENT	SEDIMENTS
1	Surface–700	Unnamed surficial to Winton	L. Cretaceous to present		Sonic log not recorded	Fluvial – lacustrine	Interbedded siltstone and claystone
2	700–2000	Winton	L. Cretaceous	5260–10520	Low velocity with small but rapid velocity fluctuations. 3 high velocity intervals between 1000 and 1300 ft.	Fluvial – lacustrine	Interbedded claystone, sandstone and siltstone
3	2000–3650	Winton	L. Cretaceous	5850–15375	Many thin high velocity spikes, caused by stringers of calcite cement	Marine	Interbedded claystone, sandstone and siltstone
4	3650–5500	Mackunda to Wallumbilla	E. Cretaceous	7140–12500	Uniform velocity gradient with few large fluctuations	Marine	Interbedded claystone, sandstone and siltstone
5	5500–8600	Transition Beds to Toolachee	E. Cretaceous to L. Permian	10000–16650	Small high and low velocity fluctuation super-imposed on a significant velocity gradient	Mainly fluvial and lacustrine. E. Cretaceous was a transition from fluvial to marine	Interbedded siltstone, claystone and sandstone
6	8600–TD	Toolachee to Merrimelia	L. Permian to E. Permian	6250–14275	Repeated thin low velocity beds, particularly between 9000 and 9320 feet	Fluvio-deltaic and coal swamp	Interbedded sandstone siltstone and coal

activity has resulted in some apparent attenuation, particularly below 8600 feet. From the top of the model to 8600 feet, a gradual and small increase in B_X value can be discerned, superimposed on a data scatter similar to that observed for the model without multiples.

Prior to further analysis of the B_X values, the input model was divided into zones based on acoustic character. This division was carried out in order to define sonically distinctive zones over which to compute interval attenuation estimates, and to examine the validity of assuming a constant Q value for multiple attenuation over such intervals. The zones are defined both by the average sonic log velocities and by the size and rapidity of changes in these velocities. Table 2 shows the zones and their characteristics. The zones are also indicated on the curves in Figures 27 and 28. The stratigraphic information is given with reference to Figure 2.

In the absence of sonic log data from the surface to 700 feet, the model for the synthetic VSP is incomplete. Over this interval the sedimentary sequence may give rise to an apparent attenuation that has not been modelled.

Inspection of Figure 27 indicates no discernable variations in trend of the B_X values between zones 2 and 5. Either subtle changes are being masked by the scatter of the data, or the multiples are having a consistent effect over this interval of the model. A line of best fit to the data values between 800 and 8600 feet is annotated on Figure 27 and has a slope of 4.0×10^{-6} dB/Hz/ft.

The B_X values over the interval of Zone 6 show a marked difference in trend to the shallower values. Over this interval there is a rapid increase in the cumulative attenuation with depth, showing that multiple activity is having a large effect on the propagating signal. The multiples are generated within and between the coals contained in the repeated sand-shale-coal cycles in Zone 6. The line of least-squares best fit for the B_X values of Zone 6 is plotted and has a slope of 4.4×10^{-4} dB/Hz/ft, i.e. the attenuation rate has increased 100 fold relative to the overlying section.

The results from the model data indicate that multiple activity generated by a 'cyclic' sequence of coals, sands and shales lead to a much higher rate of attenuation than a rapidly changing spikey sequence of thin beds. This may, however, be a consequence of too gross a sample interval for the fine detail of the thin beds. The sample interval is restricted by the QUIKLOG software used.

Schoenberger and Levin (1978), showed that the apparent attenuation estimates for synthetic data increase as the subsurface sampling rate decreases from 4 ms to 1/4 ms. Hauge (1981), determined that a 1 ms sample rate was sufficient for the surveys he examined. The limitations set by the QUIKLOG software resulted in a 1 ms sample rate being used for the Tirrawarra model.

It is apparent from Figure 26 that at depths in excess of 9000 feet (trace 83) the least squares fits to the amplitude ratios are distorted by the high frequency end of the spectrum, in particular 40 Hz and greater. As mentioned previously the addition of multiples decreases the high frequency end of the spectrum, and for Zone 6 of the Tirrawarra #22 model this decrease restricts the usable frequency to a maximum of 40 Hz. This is an important result as the model was designed using realistic source frequencies, and as a consequence suggests that seismic resolution of the Permian section of the Cooper Basin is restricted not by the field acquisition parameters but by the multiple activity.

The B_X values plotted in Figure 28 are calculated from the least squares fit to the amplitude ratios over the frequency range 10-40 Hz. Above 8600 feet (Trace 79) the B_X values between the 10-60 Hz and 10-40 Hz analyses are very similar. Below 8600 feet the B_X values are quite different for the two frequency ranges, however both show an increase in the

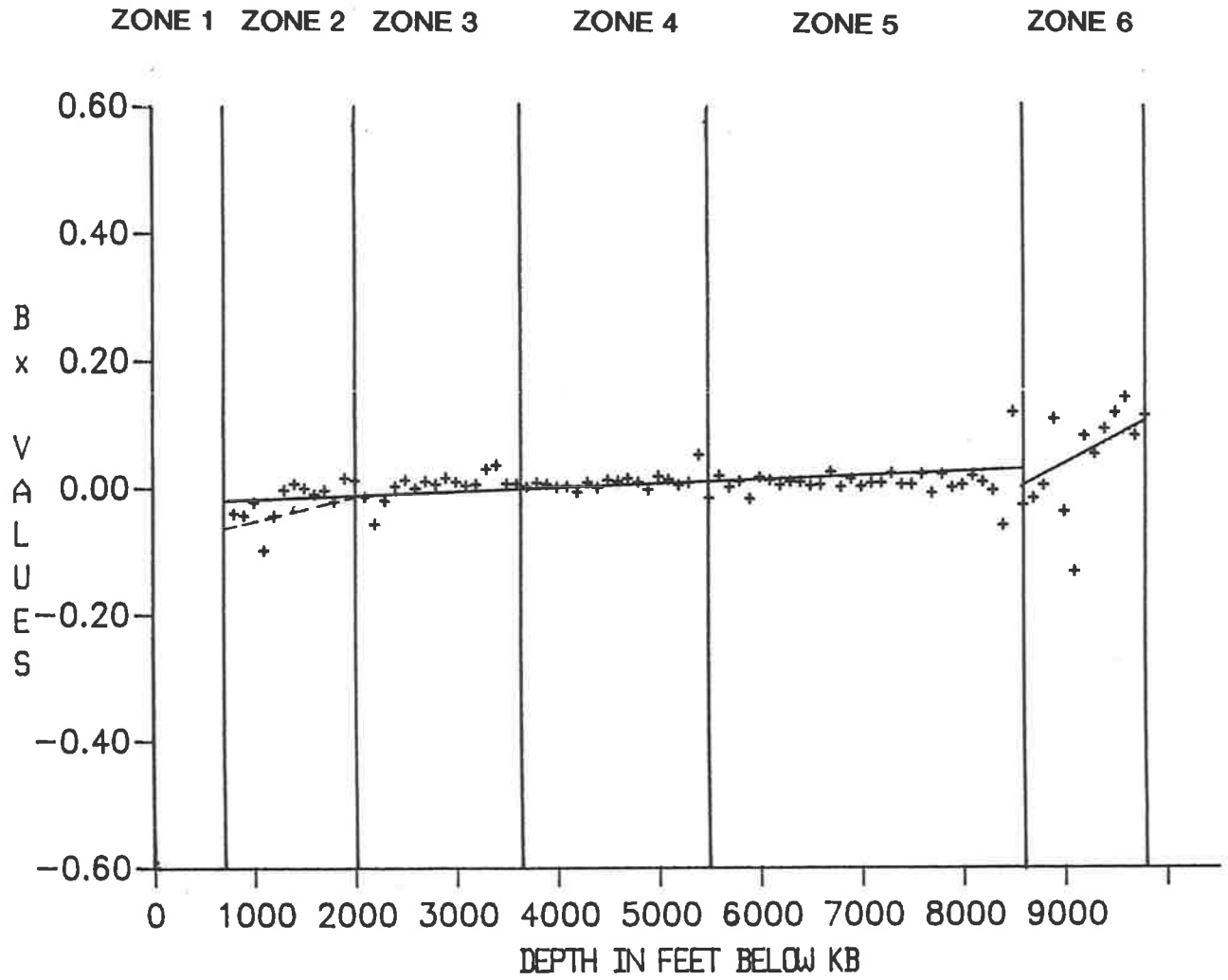

Tirrawarra #22, synthetic VSP with multiples; cumulative attenuation between 10-40 Hz

Fig. 28

rate of attenuation. The line of best fit to the data below 8600 feet is 8.3×10^{-5} dB/Hz/ft. The negative values are the result of interference to the downgoing first arrival.

Table 3 shows the apparent interval attenuation and Q values due to multiple activity, computed for each zone from the k_X data and the interval velocities calculated for each zone. The k_X value for Zone 1 is an extrapolated value.

Zone	Depth Interval in feet below KB	k_X dB Hz/ft	v_X ft/s	α_X dB/wavelength	Q
1	0 - 700	6.5×10^{-6}	6015*	0.0391	698
2	700 - 2000	6.5×10^{-6}	6500	0.0423	645
3	2000 - 3650	6.5×10^{-6}	7780	0.0506	540
4	3650 - 5500	6.5×10^{-6}	8685	0.0565	483
5	5500 - 8600	6.5×10^{-6}	13060	0.0849	322
6	8600 - 9800	8.3×10^{-5}	11540	0.8578	28.5

Table 3. Tirrawarra #22 attenuation values for the synthetic VSP with multiples between 10-40 Hz. (*In the absence of log data this value is derived from the VSP first arrival at 700 feet.)

Considering Zone 6, the k_X value indicates that multiples will cause a signal of 10 Hz to be reduced in amplitude by 1 dB after propagating through the 1200 ft interval, whilst a signal of 40 Hz will be reduced by 4 dB over the same interval. The amplitude reduction for a 10 Hz signal propagating through Zones 1 to 5 ranges between .05 and .2 dB.

The model, with multiples included, has been used for a more detailed testing of the spectral ratio programmes. Figures 29a - 29e are the results of the tests, and the following is observed from these results.

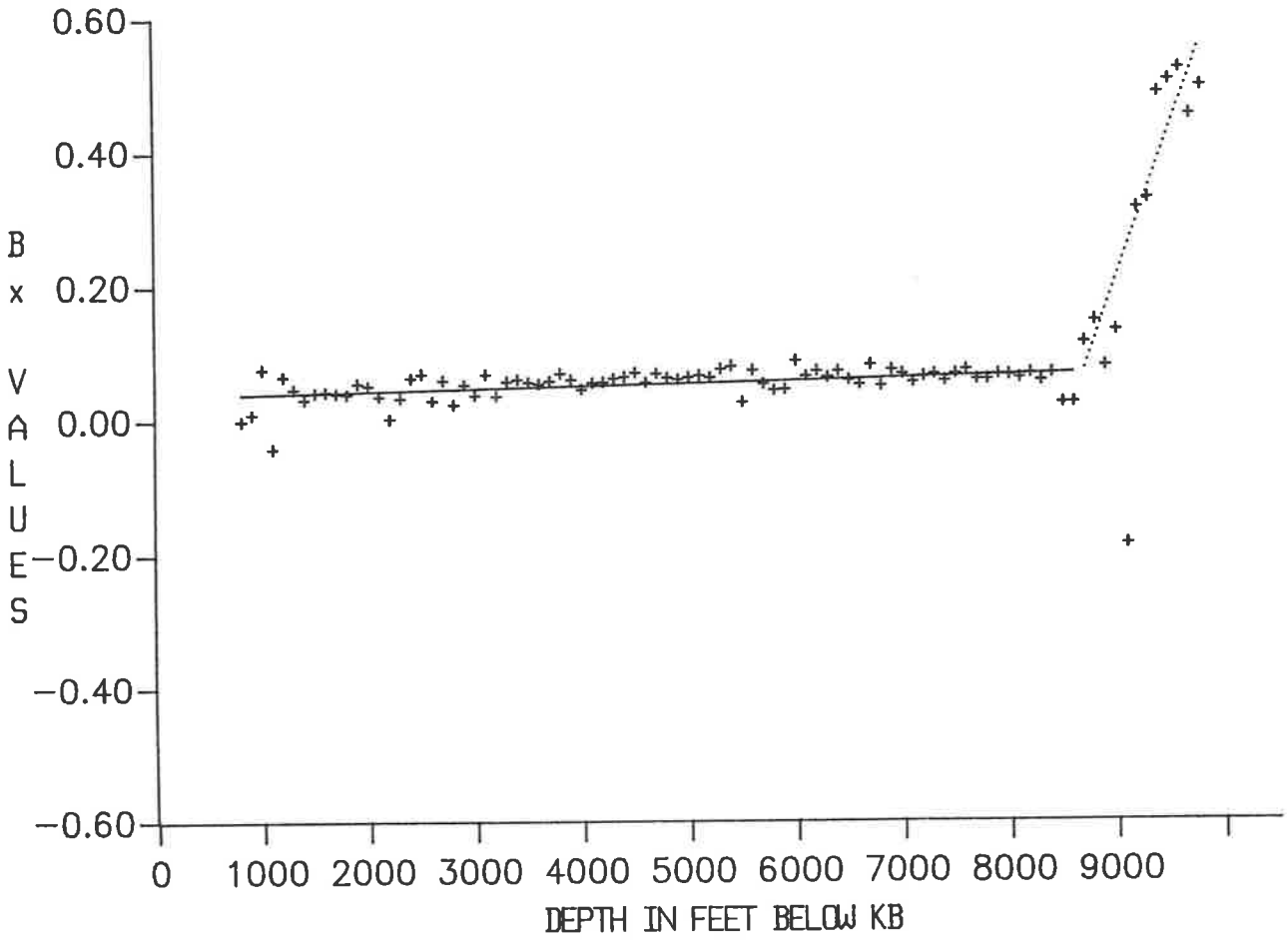

Tirrawarra #22, synthetic VSP with multiples; cumulative attenuation between 10-60 Hz with trace 1 as reference

Fig. 29a

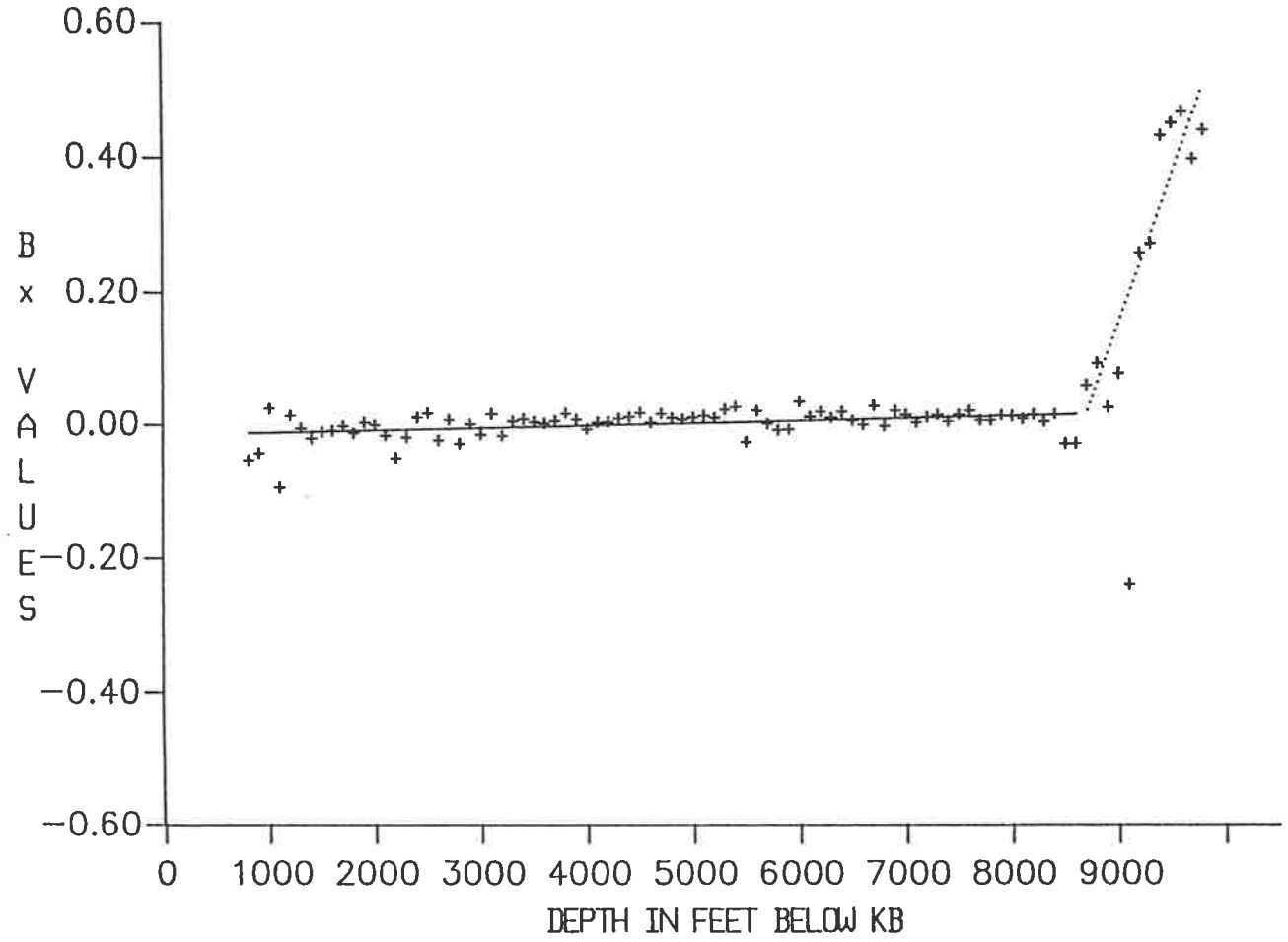

Tirrawarra #22, synthetic VSP with multiples; cumulative attenuation between 10-60 Hz with trace 13 as reference

Fig. 29b

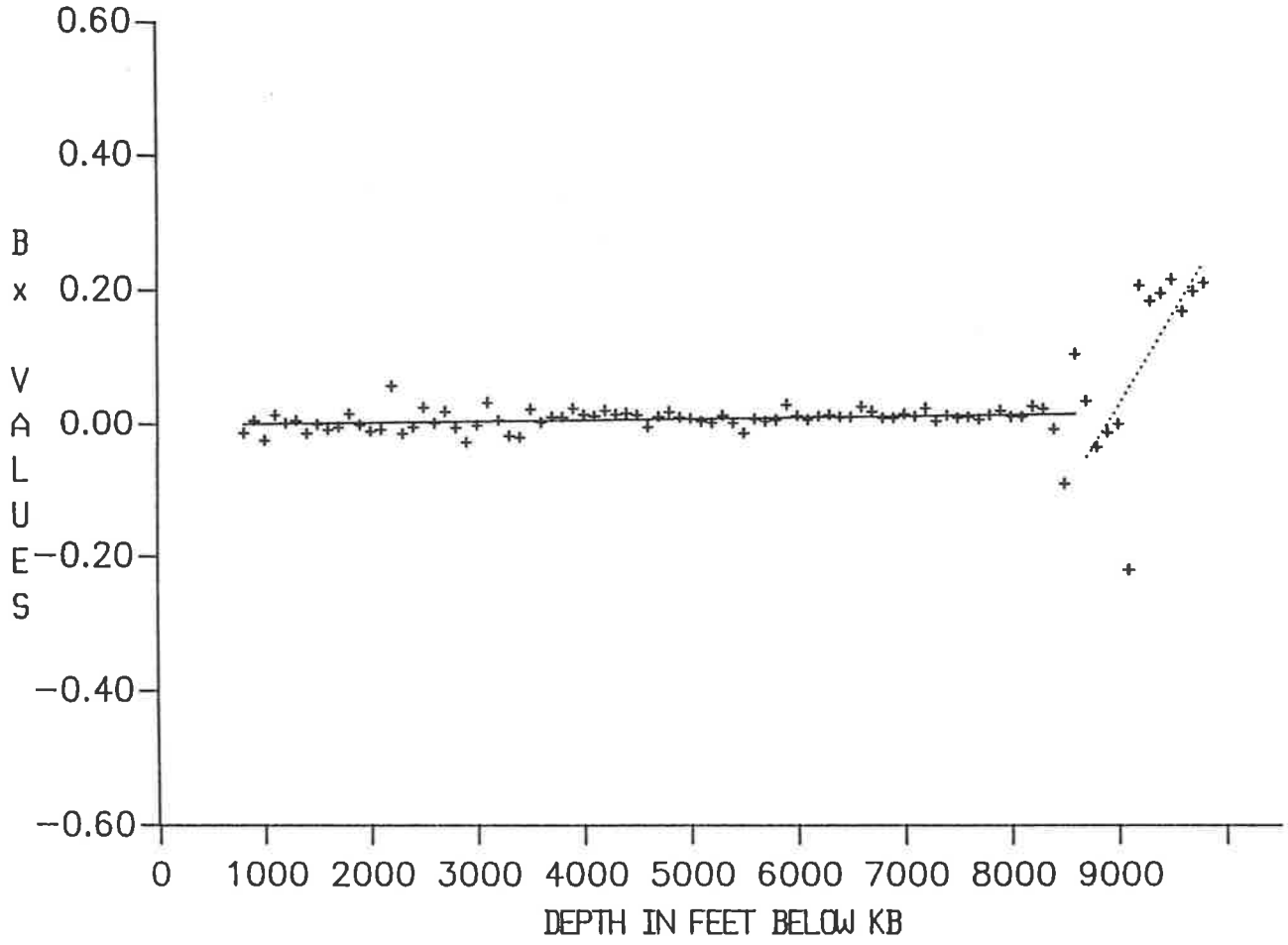

Tirrawarra #22, synthetic VSP with multiples; cumulative attenuation between 10-80 Hz with trace 8 as reference

Fig. 29c

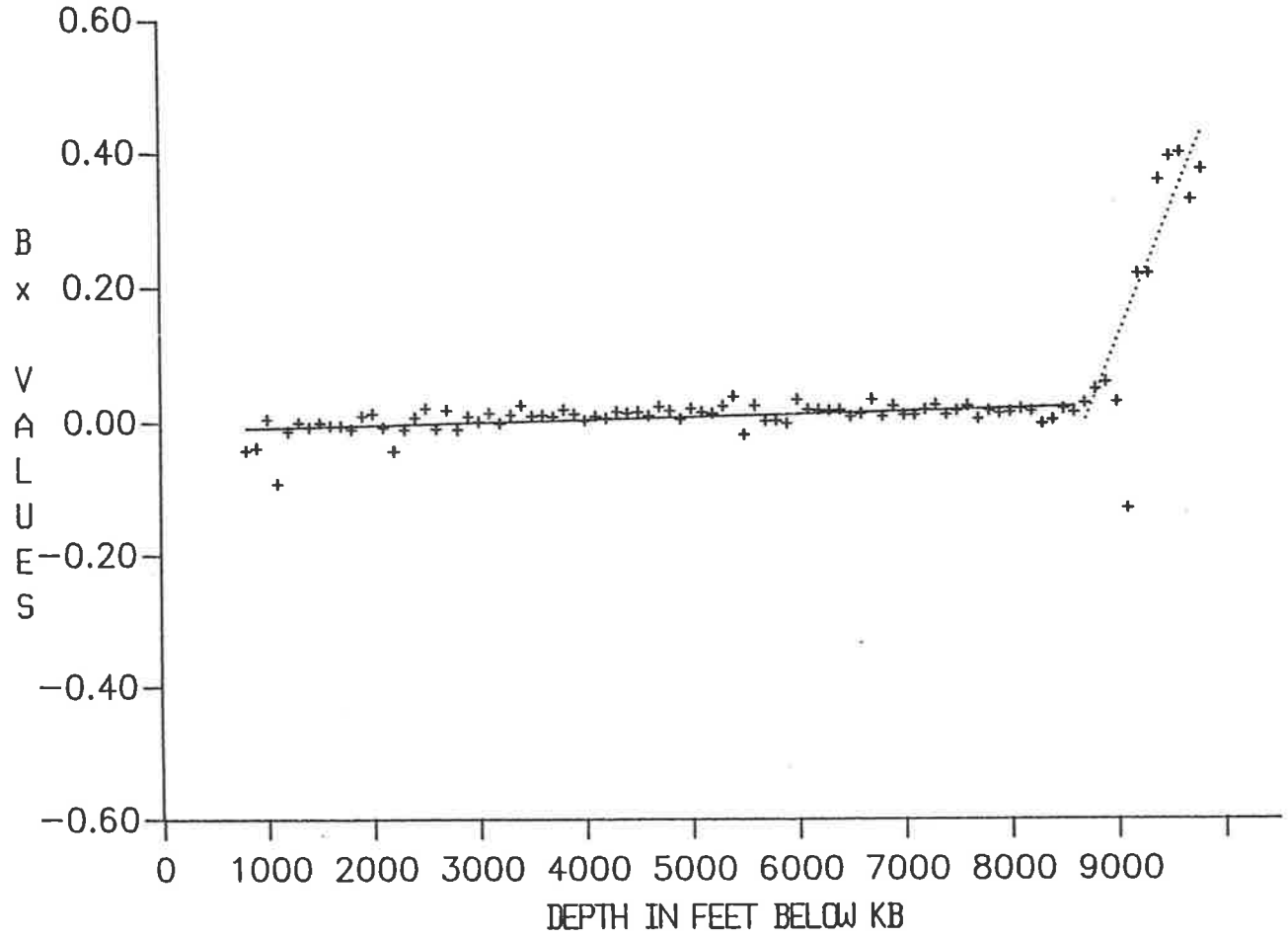

Tirrawarra #22, synthetic VSP with multiples; cumulative attenuation between 5-60 Hz with trace 8 as reference

Fig. 29d

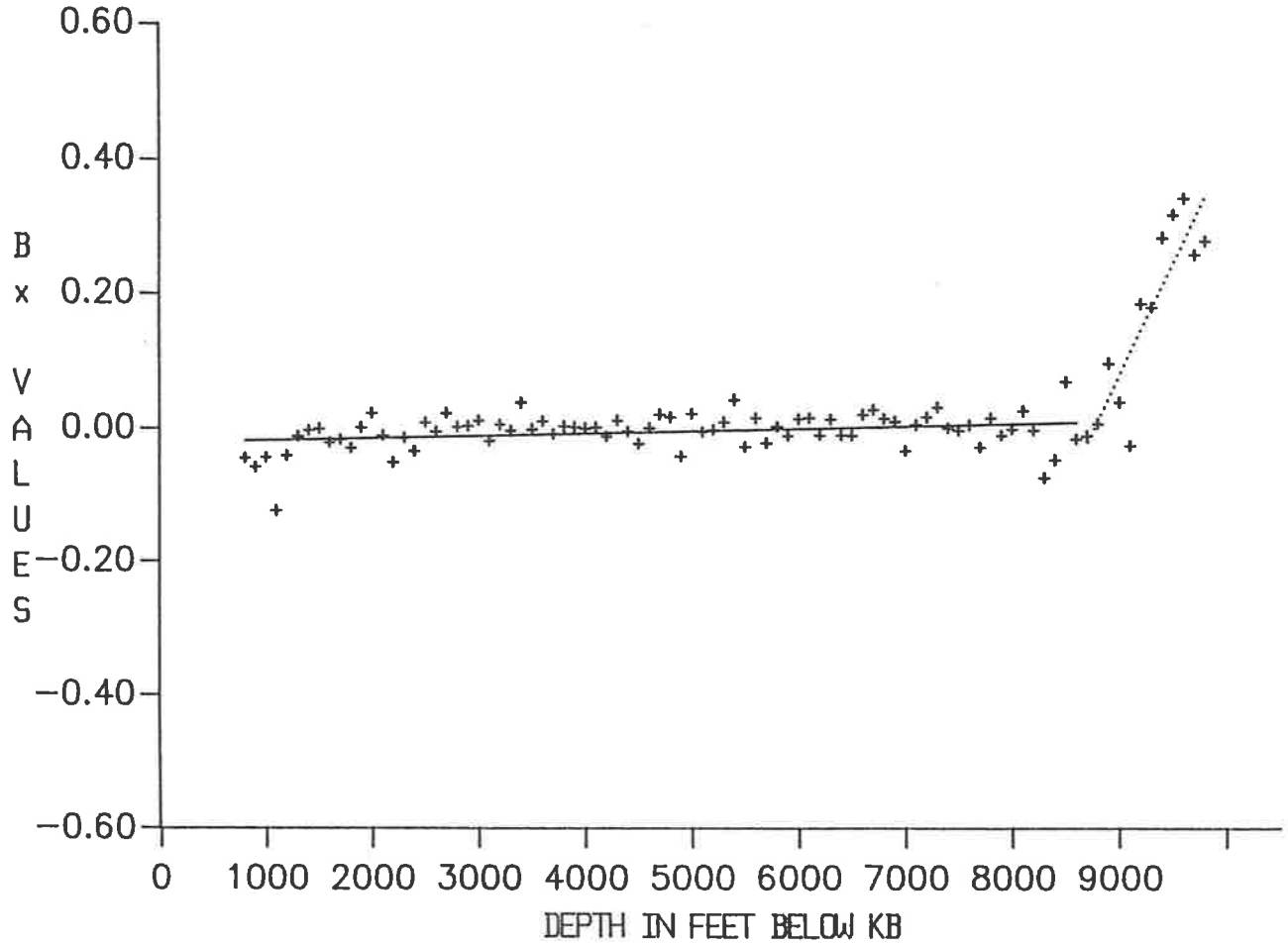

Tirrawarra #22, synthetic VSP with multiples; cumulative attenuation between 1-60 Hz with trace 8 as reference

Fig. 29e

(i) Over a suitable frequency range, the reference trace used does not affect the slope of the cumulative attenuation. It does however alter the actual B_X value.

(ii) The frequency range over which the analysis is performed affects the B_X values and the slope of cumulative attenuation. The results of the analysis over frequencies of 10-80 Hz, deliberately chosen to include frequencies above the usable range, are shown in Figure 29c. Too high a frequency cut off has distorted the slope of least square fit to the data, due to high frequencies in both the reference trace and the analysed trace having very small amplitudes.

(iii) Increasing the low end of the frequency range has little affect on either the B_X values or the slope of cumulative attenuation. The relative increase in the low frequency spectra, observed by Schoenberger and Levin (1974, 1978) as a result of multiples, is not apparent even below 10 Hz.

6.3 Watson #1 Synthetic VSP with Multiples

Using the model described in the previous chapter, a VSP with all order multiples was generated. The result is illustrated in Figure 30. A series of downgoing multiples is evident approximately 300 ms after the first arrival. Spectral ratio analysis of the data was performed using trace 5 at 1000 feet as the reference, and in an identical fashion to the model without multiples. The cumulative attenuation values are plotted in Figure 31.

The B_X values show a similar scatter to the analysis without multiples. However, attenuation is apparent in the model with multiples. The values fall into 2 zones having different gradients. Above 1600 feet the slope of the best fit line is 4.7×10^{-5} dB/Hz/ft, and below 1600 feet the slope is 4.7×10^{-6} dB/Hz/ft.

As for the Tirrawarra model, the Watson model was divided into zones based on sonic log character. Figure 32 illustrates the correlation of the zones between the two models.

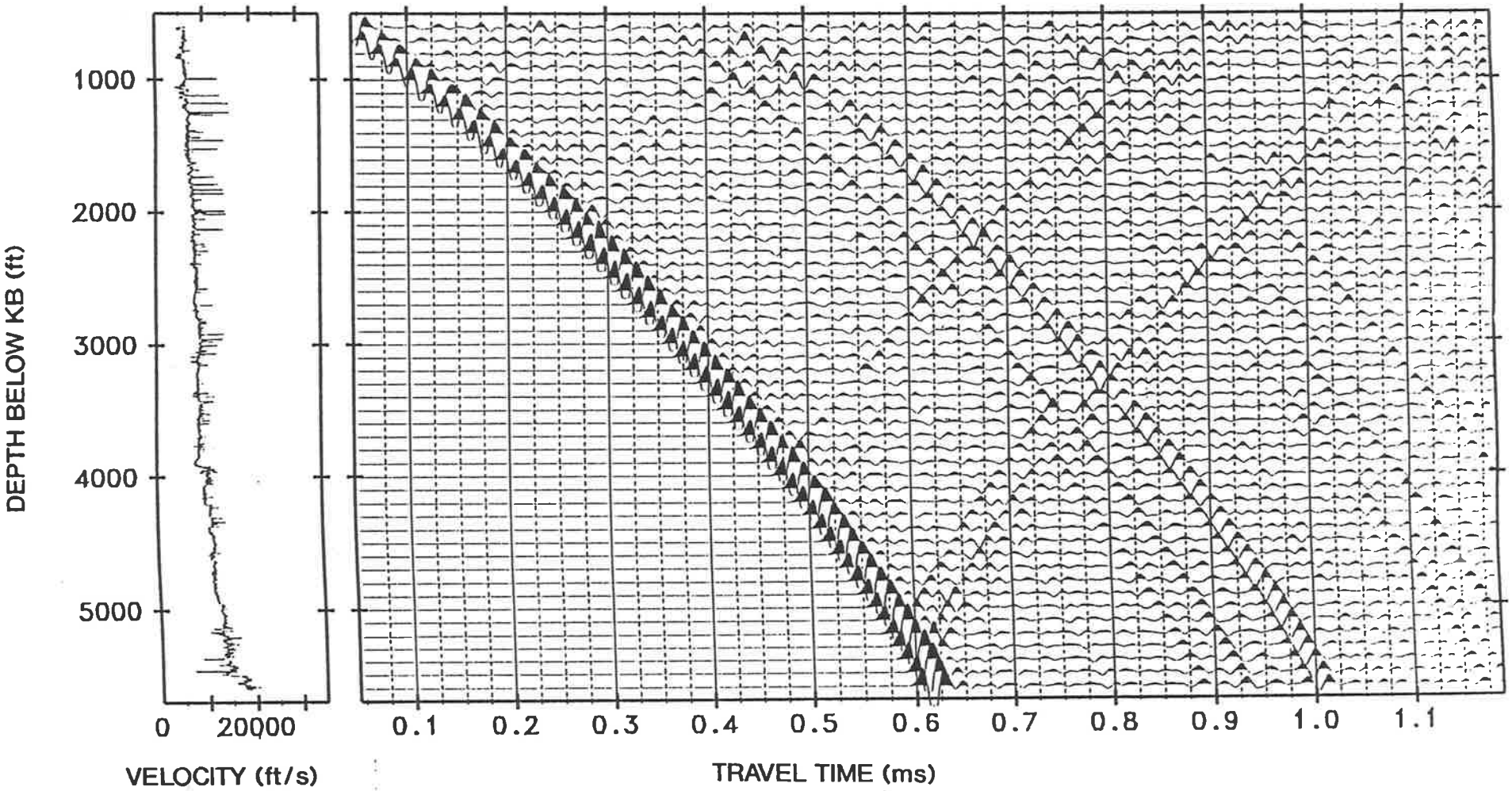

Watson #1, synthetic VSP with multiples

Fig. 30

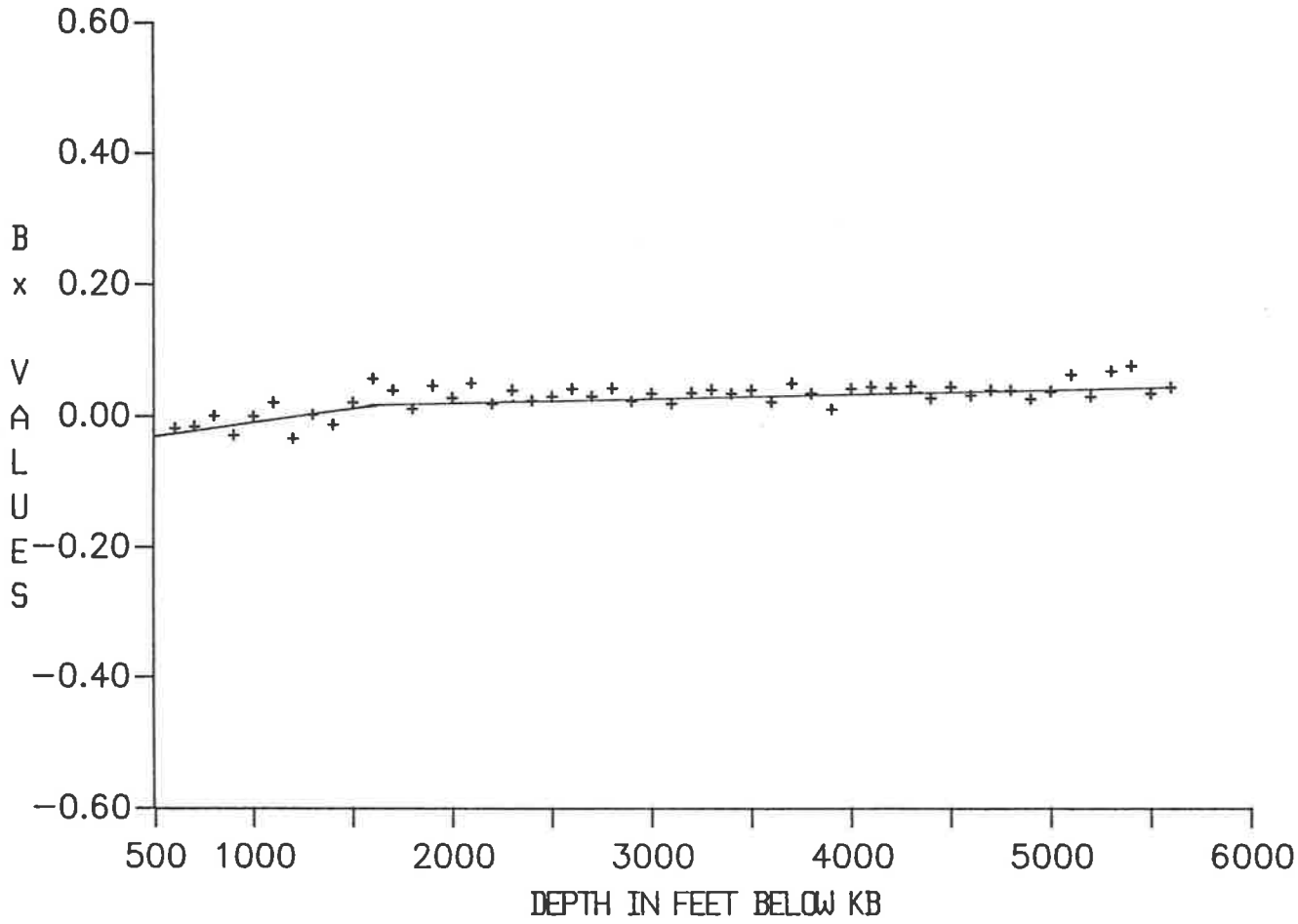

Watson #1, synthetic VSP with multiples; cumulative attenuation between 10-70 Hz

Fig. 31

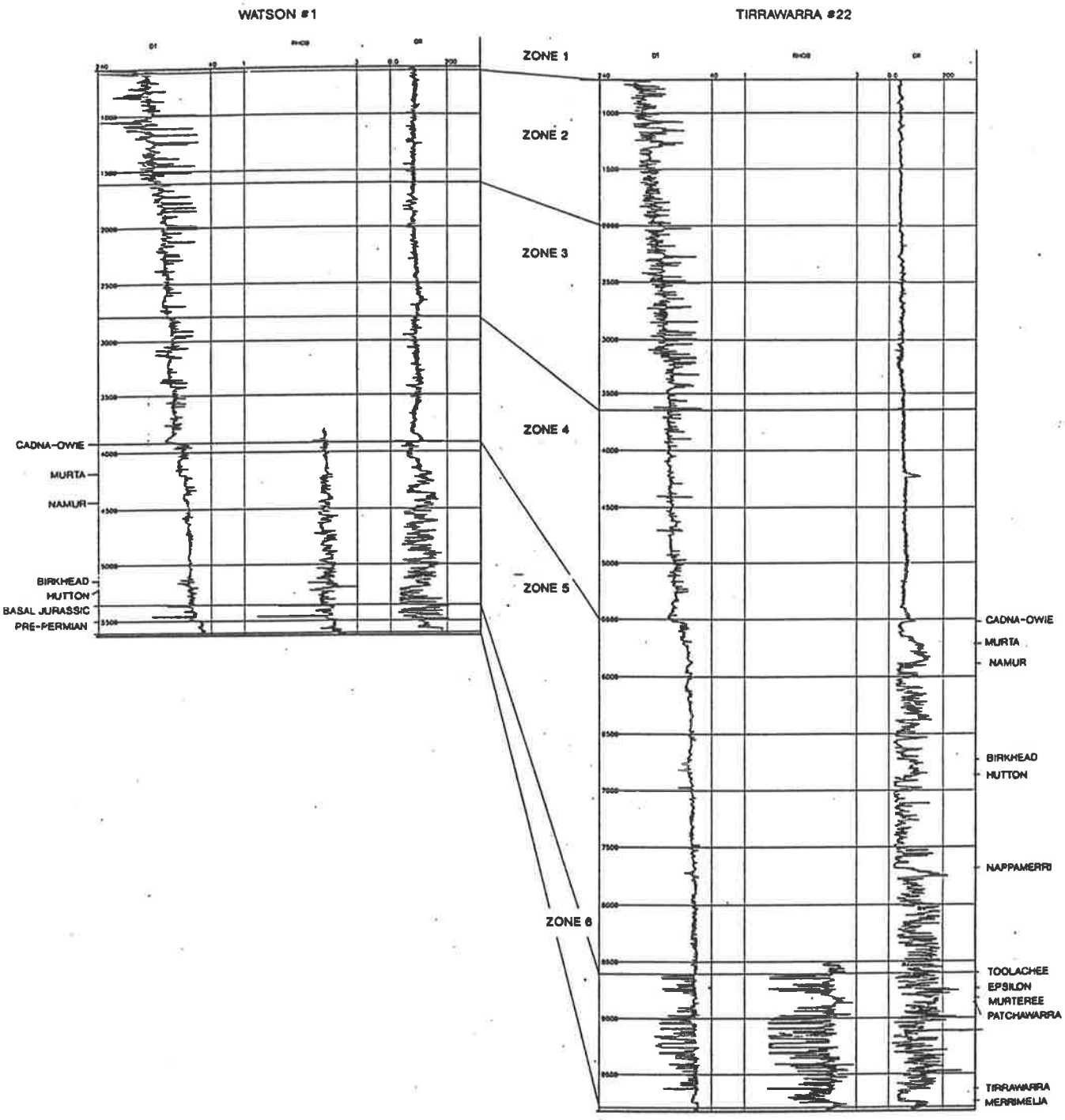

Watson #1 and Tirrawarra #22, acoustic zone correlation

Fig. 32

Major formation tops have also been annotated. Using interval velocities obtained from the input sonic model, the estimates of apparent attenuation due to multiples are as follows;

Zone	Depth Interval in feet below KB	k_x dB Hz/ft	V_x ft/s	α_x dB/wavelength	Q
1	0 - 600	N/A			
2	600 - 1600	4.7×10^{-5}	6680	.3140	87
3	1600 - 2796	4.7×10^{-6}	8360	.0393	695
4	2796 - 3920	4.7×10^{-6}	9525	.0448	610
5	3920 - 5360	4.7×10^{-6}	12310	.0579	472
6	5360 - 5600	4.7×10^{-6}	15000	.0705	387

Table 4. Watson #1, attenuation values for the synthetic VSP with multiples between 10-70 Hz.

The attenuation rate for Zone 2 is high relative to the other zones. Within this zone, there is a cyclic series of low velocities, separated by thin high velocity layers. The model shows that significant intrabed multiples are generated in this zone. The models for Watson #1 and Tirrawarra #22 have similar lithologies over zone 2. However, there is an order of magnitude difference between the estimates of apparent attenuation for the two wells. This highlights the sensitivity of Q values to the slope of the line of best fit drawn through the B_x values. Inspection of Zone 2 in Figures 28 and 31 show that the interpreted slope is controlled by the data points at Watson #1, but that the data exhibits significant scatter at Tirrawarra #22. An alternative interpretation of the Tirrawarra #22 data, (dashed line in Figure 28) gives an estimate of attenuation similar to that determined for Watson #1.

Another possible contribution to the difference in apparent Q in Zone 2 between the two wells is the different sample intervals (0.5 ms in Watson #1 and 1 ms in Tirrawarra #22). Schoenberger and Levin, (1978), showed that decreasing the sampling intervals tends to

increase the apparent attenuation. However, tests on Watson #1 showed no significant difference between the attenuation estimates made from VSP data computed at 0.5 and 1ms sample intervals.

Zones 3 to 6, have the same k_X value. However, as the interval velocity changes over the zones, the values of α_X and Q vary with depth. Zone 6 does not have the cyclic coal sequence of the Tirrawarra model, and the k_X value does not change from the zones above. The k_X values determined over zones 3-5 are similar when the two wells are compared.

CHAPTER 7

ATTENUATION ESTIMATES FROM VSP DATA

7.1 Introduction

The preceeding chapters describe the use of spectral ratio analysis to derive attenuation values, caused by intrabed multiples, from synthetic VSP data. In order to determine the intrinsic attenuation of a propagating seismic signal, it is necessary to apply the same analysis to the real VSP data sets recorded in the wells Watson #1 and Tirrawarra #22. These VSPs, recorded by different contracting companies, and with different acquisition parameters, allow for comparisons in the application of the spectral ratio technique.

An in-situ measurement of attenuation is an important though not straightforward task. Prior to the analysis, the data has to be edited to remove 'noisy' and unwanted levels. In the analysis itself, critical parameters such as the length of the analysis window and the frequency range to be used, must be established by testing. Because of these factors, it would be very difficult to develop a fully automated processing sequence for VSP editing and attenuation analysis.

The recording of a signature phone in both the Watson and Tirrawarra surveys enables attenuation estimates based on a single downhole reference trace to be compared with those made using signature data for each level.

The observed attenuation values derived from the VSPs comprise both intrinsic and apparent attenuation. Having derived estimates for the apparent attenuation from the synthetic data, the intrinsic component can be estimated from the observed attenuation.

7.2 Watson #1 VSP Acquistion Parameters

This VSP, recorded on 17 December, 1985, by Velocity Data Pty. Ltd., formed part of an overall test to evaluate the acquisition and processing of a zero offset VSP and a walkway VSP (Rango and Fitzgerald, 1986).

The source used was a GSI TR4 FORCE 3 vibrator, which generated an 8 second, 9-95 Hz linear sweep with a 50% amplitude taper and a 0.3 second cosine taper.

The signal at the various levels was recorded by a 90 mm Veldata Camlock wall-lock geophone with high temperature detectors. Each shot was also monitored by an inline array of 12 GS 20D 10 Hz geophones laid out on the surface, a disposable slimline geophone at the bottom of a 75 ft hole, and a signature geophone located at 328 ft KB in the well. Figure 33 shows the field configuration.

The VSP levels were separated by equal time intervals of 6 ms, corresponding to depth intervals of between 33 and 80 feet. 108 levels were acquired between 5500 and 155 feet below KB. A list of these depths is given in Appendix 1. The recording filters were set at 8-90 Hz and the sample rate was 2 ms.

The data received from SANTOS Limited consisted of the observer's logs and a SEG-Y format magnetic tape with four channels of zero phase correlated data recorded as follows:

Channel 1: Well wall-lock geophone
Channel 2: 12 surface geophones
Channel 3: Slimline downhole geophone
Channel 4: Signature geophone

Figure 34, shows the VSP levels, logging runs and casing for Watson #1.

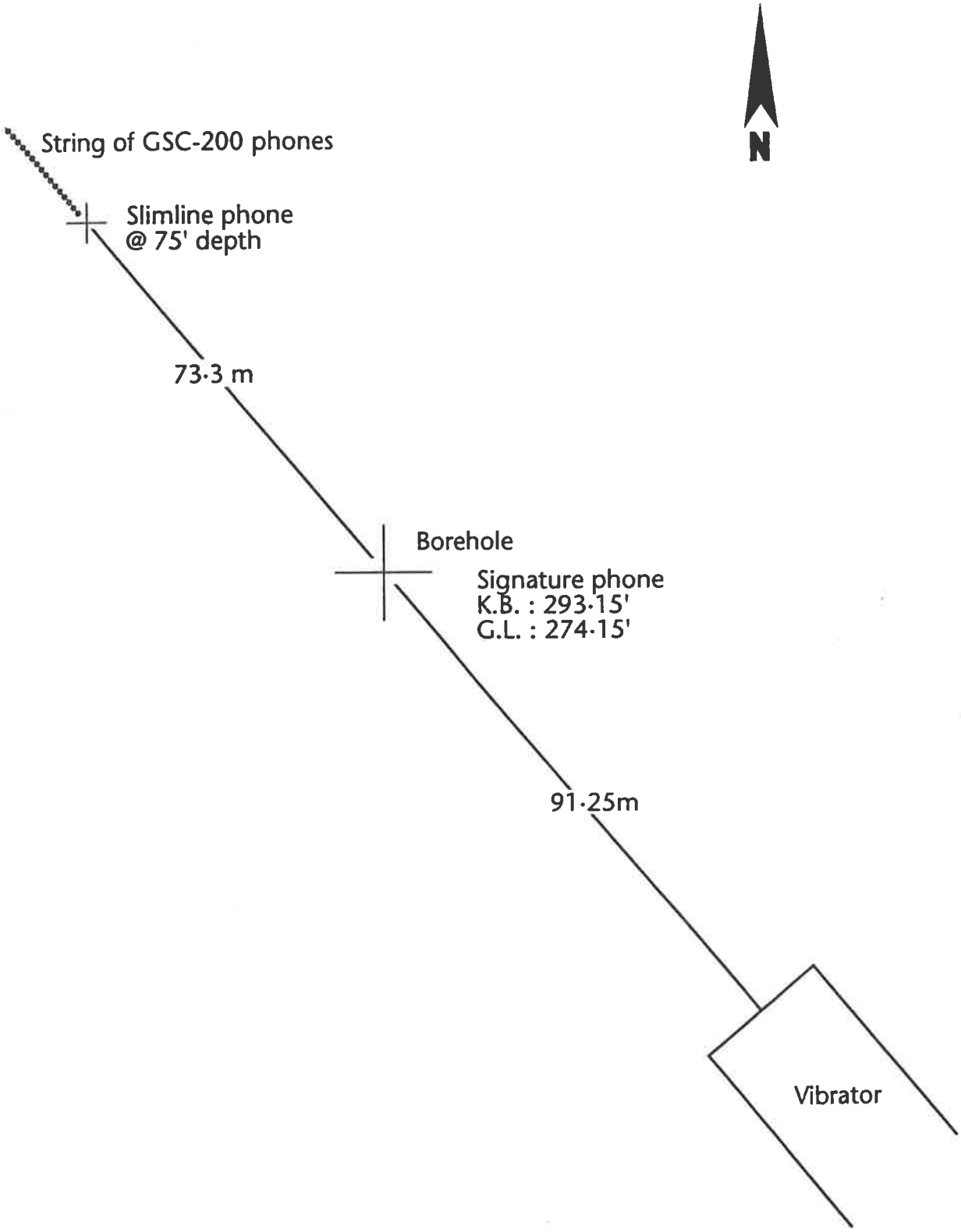

Watson 1, VSP acquisition parameters

Fig. 33

WATSON 1

VSP WELL SUMMARY

Lat. : 28° 05' 28·77" S.
Long. : 142° 04' 47·02" E.
Seismic : LINE 84-SZS
Spudded : 06/12/1985 K.B. : 293·15'

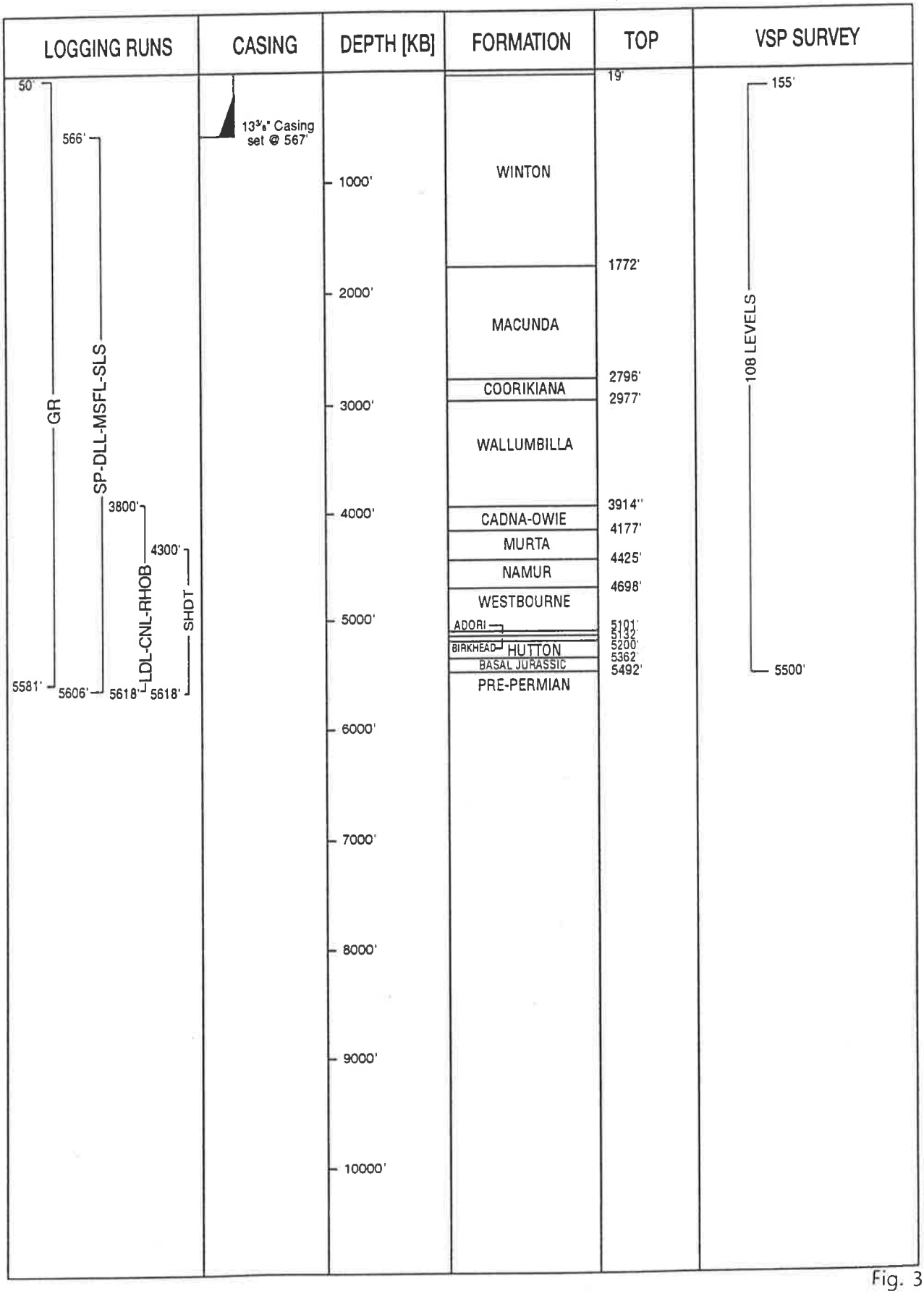

Fig. 34

7.3 Watson #1 VSP Data Preparation

Of the 108 levels recorded, 103 could be read from tape and are displayed in Figure 35. Preliminary editing of the 103 levels to remove recordings distorted by noise, in close proximity to one another (less than 5 feet) and recorded twice at the same depth, reduced this number to 93. Depths removed included all those recorded in surface casing (to 566 feet below KB) which, based on a study by Siebert (1986), show questionable first arrival amplitudes. For all levels above 3545 ft KB, the recording gain for the downhole geophone was reduced by 50%, and a compensation to account for this was applied to the data.

For each downhole geophone recording, the data from the corresponding signature phone was read from tape. A visual inspection of the signature phone traces (not displayed) was made to assess the repeatability of the Vibroseis signal.

Further editing of the downhole geophone data was carried out following inspection of amplitude spectra computed over a window containing the first arrival for each depth. Several of the spectra are distorted, possibly the result of borehole noise, cable slip or instrument noise. 87 levels remained after this final editing. The downhole geophone traces are displayed in Figure 36 after alignment at 700 ms, and the corresponding signature phone traces are displayed in Figure 37 after alignment at 500 ms.

7.4 Watson #1 VSP Spectral Ratio Analysis

The signature geophone allowed excellent monitoring of the source signal input to the ground. The vibrator source remained stationary throughout the survey, however some change in the input to the ground might be expected, due to the compaction of the earth beneath the baseplate following repeated vibration. The edited signature geophone traces, displayed in Figure 37, suggest that the input signals are all very similar.

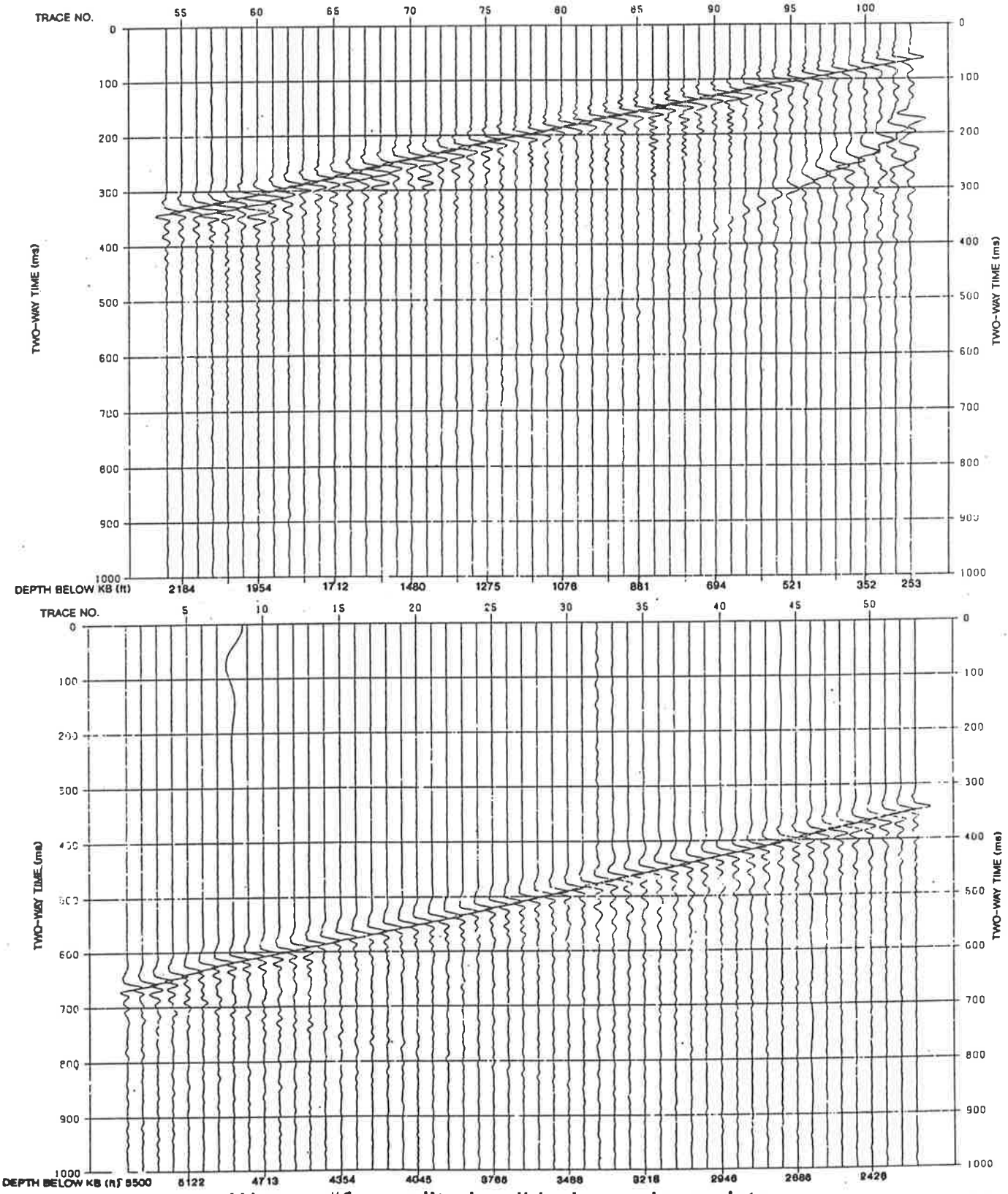

Watson #1, unedited wall-lock geophone data

Fig. 35

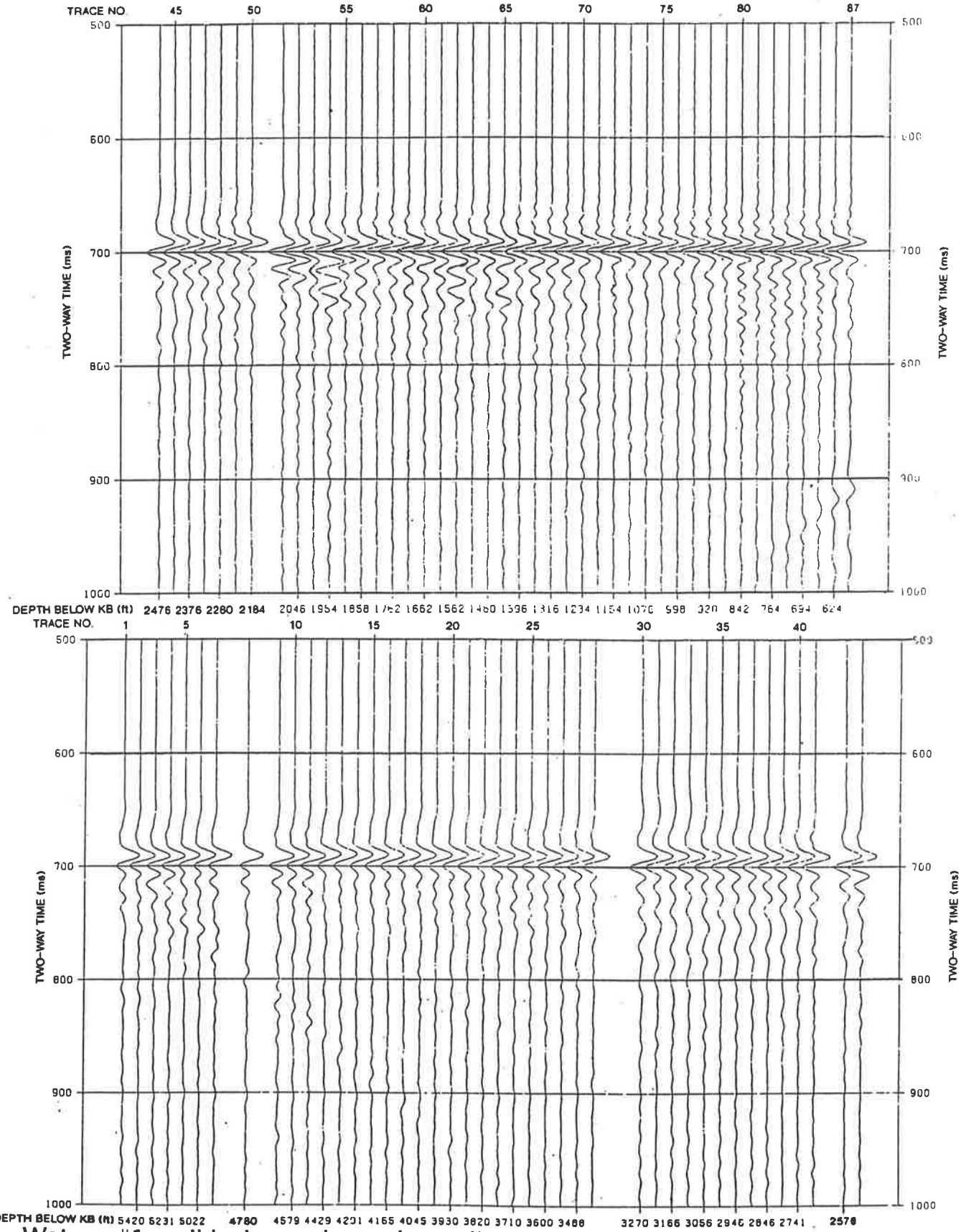

Watson #1, wall-lock geophone data edited and aligned at 700 ms

Fig. 36

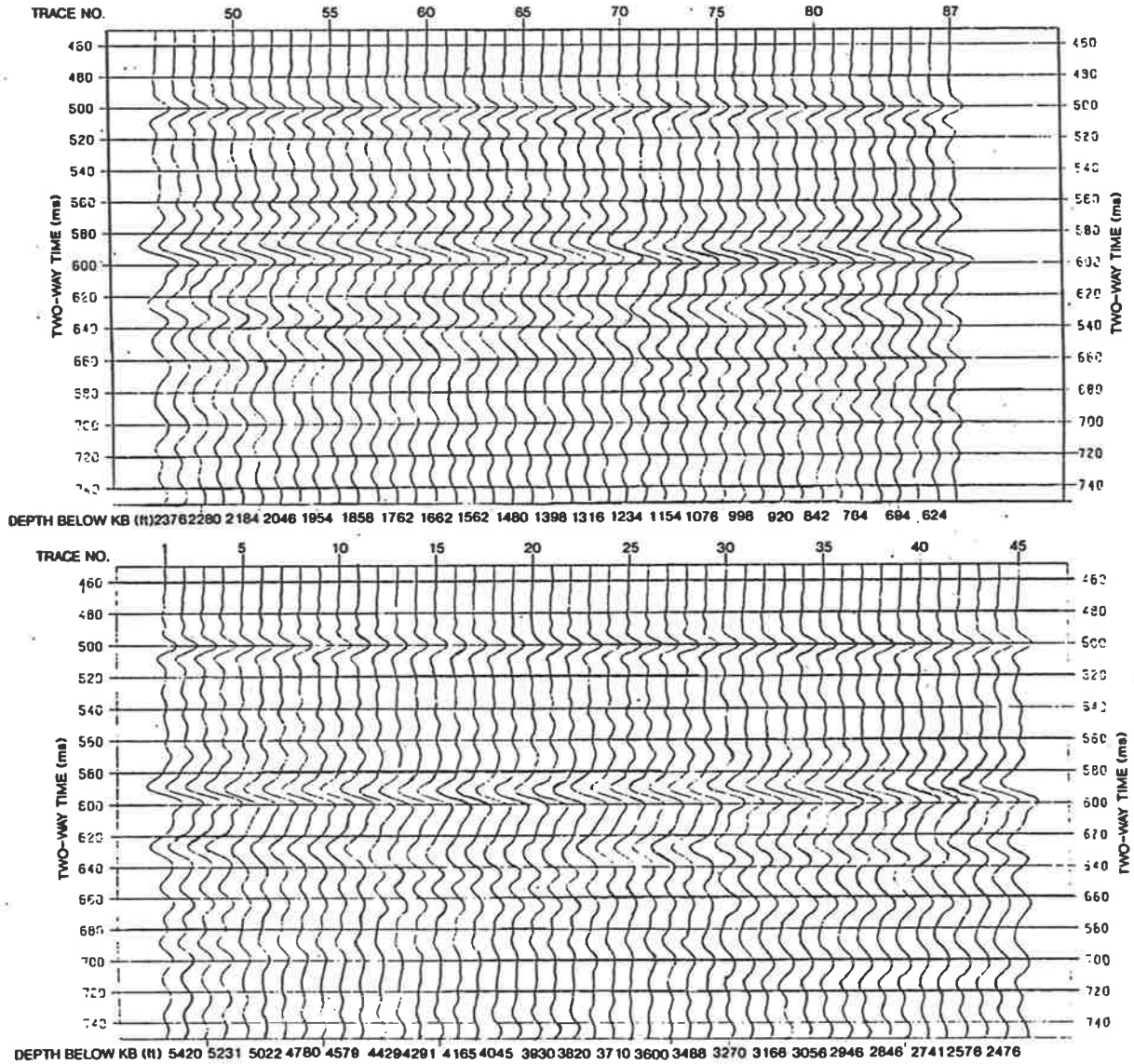

Watson #1, signature phone data edited and aligned at 500 ms

Fig. 37

To further test this similarity, amplitude spectra were computed for the first arrivals on the signature phone traces. Inspection of Figure 37 suggested that the data window for this computation could end at 530 ms. The resulting spectra are displayed in Figure 38. All traces show frequency content between 5 and 95 Hz, with the maximum amplitude between 25 and 50 Hz. Some variations in the spectra are apparent.

The amplitude spectra between 5 and 90 Hz were input to the spectral ratio analysis, using the signature trace recorded at the 589 feet level as a reference. As expected, there is some variation in the input signal. It appears from Figure 38 that as the survey progressed, the amplitude spectra varied, which may be a direct result of near surface compaction. The spectra suggest that if surface compaction is having an effect, it is gradual and progressive throughout the survey. As illustrated previously, the selection of the reference trace will not affect the result of the above analysis. Figure 39 is a plot of the B_X values for each of the 87 signature recordings against depth. This plot highlights the differences between the traces. Figure 40 shows the result of confining the analysis to frequencies between 5 and 70 Hz. Similar trends are apparent in both plots.

It is necessary to determine whether the scatter in the B_X values falls within the range of ± 0.035 about the average determined from the synthetic data. If it does, then the signal input to the ground will be accepted as being identical for all Vibrator sweeps. If it is outside this range then the signal is changing to an extent that will not be masked by the scatter inherent to the analysis. From Figures 39 and 40 it is evident that the input signal does show significant change.

The recording of the signature geophone, apart from providing a continuous monitor on the input signal, allows for a refinement in the spectral ratio technique. The analysis performed on the synthetic data makes the assumption that the input signal is identical for every level and a single downhole trace can be used as the reference trace to determine the amplitude ratios. If the input signal is varying however, then the amplitude ratios determined in this way will be contaminated by the effects of the source variation. If, instead, the

Watson #1, amplitude spectra of the first arrivals from the edited signature phone data

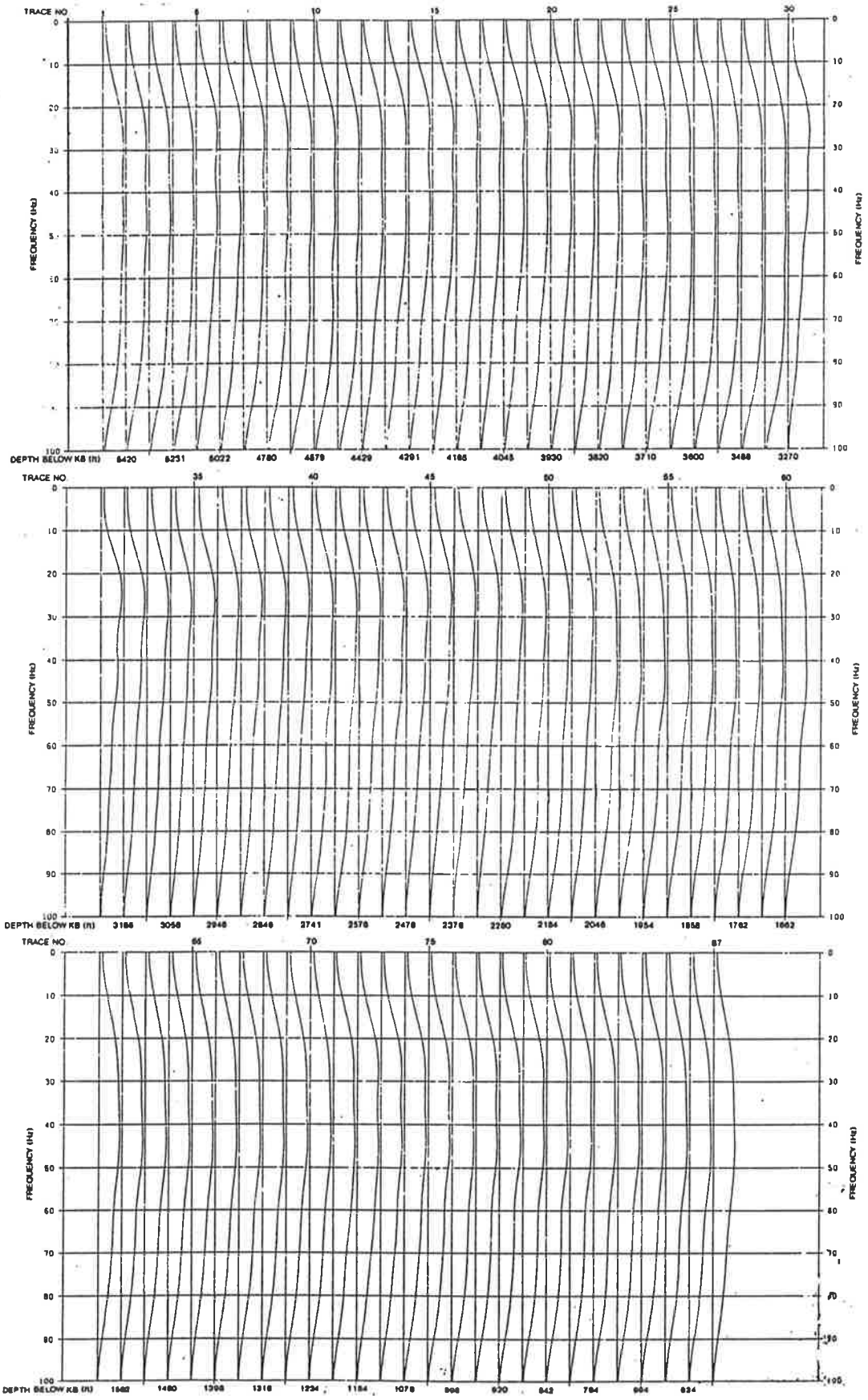

Fig. 38

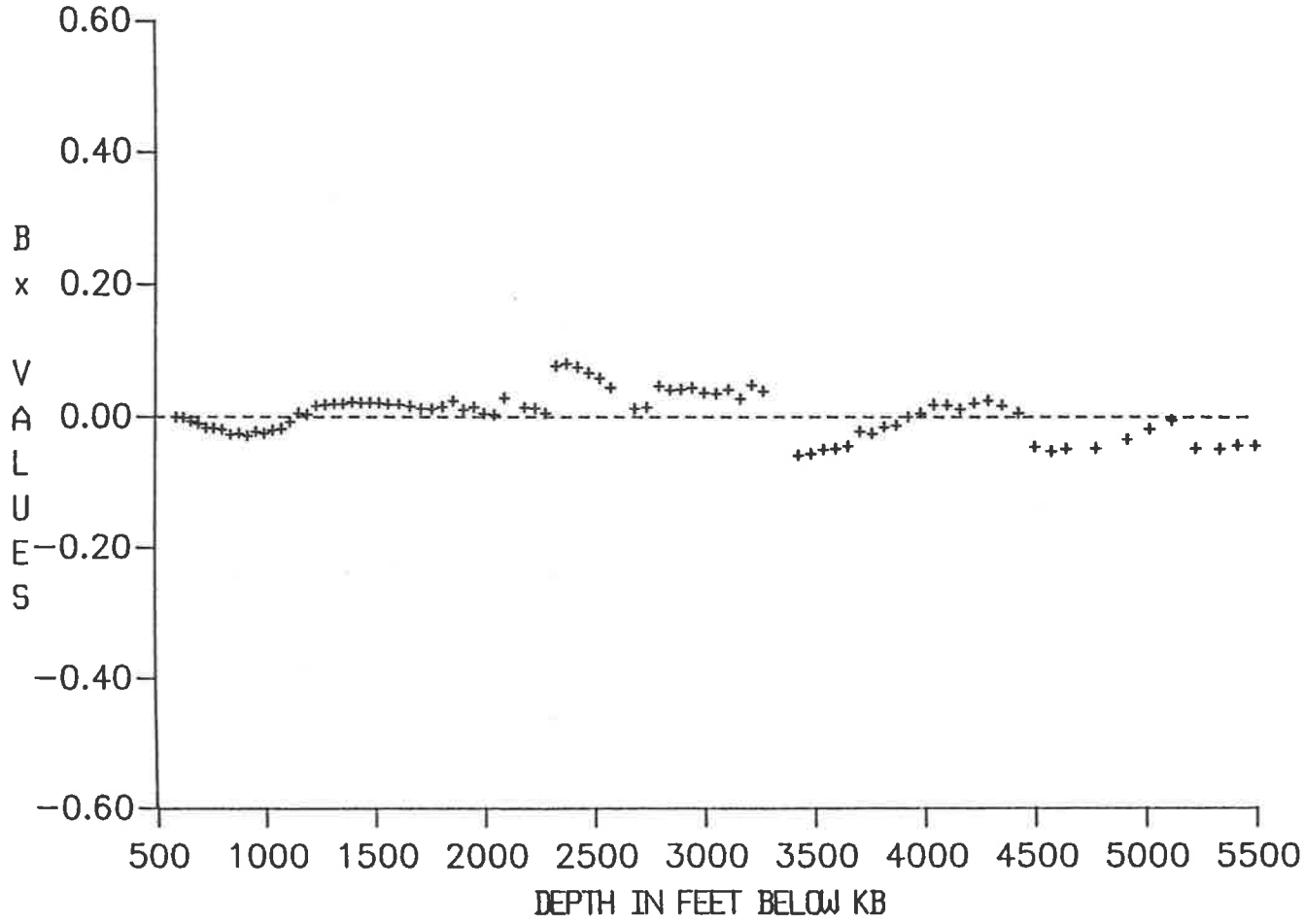

Watson #1, signature phone; amplitude ratios between 5-90 Hz with the reference at 589 feet

Fig. 39

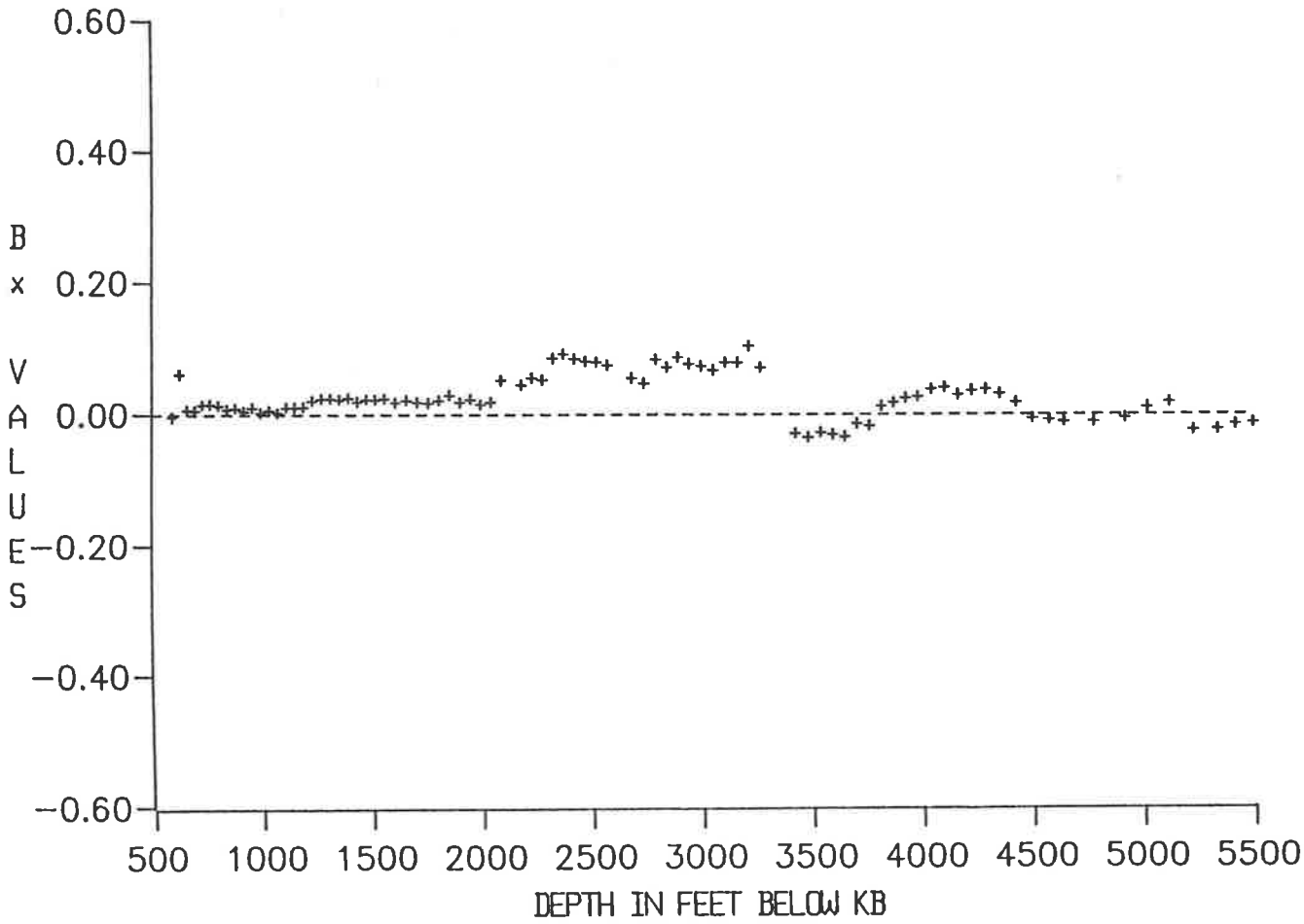

Watson #1, signature phone; cumulative attenuation between 5-70 Hz with the reference at 589 feet

Fig. 40

corresponding signature phone trace is used as the reference for each downhole trace, the reference and downhole traces do result from the same shot and the assumption of a constant source signal is no longer required. Although the signature geophone and the borehole geophone are not of the same type, do not have the same response, and are recorded with different instrument gains, this should not present a problem, as it is the cumulative attenuation slope, and not the actual B_X values, that are required. If the source were to remain constant then spectral ratio analysis using either method would give identical slopes (within experimental error).

For spectral ratio analysis it is necessary to determine a window length for the first arrivals at the downhole geophone. This is a somewhat subjective process, and was approached in this study by trial and careful analysis. Too wide a window risks increasing the amount of interference from upgoing waves, whilst if the window is too narrow, it may not include the complete arrival. Spectral ratio trials with first arrival window lengths between 30 and 150 ms suggested that a short window length results in a large scatter in the B_X values. As the window length increases the amplitude ratios become smoother. Careful examination of large scale plots of the first 200 ms of live data, in conjunction with the spectral-ratio trials, led to the selection of a window length of 65 ms with a 15 ms cosine ramp. The amplitude spectra determined are displayed in Figure 41.

Spectral ratios were calculated between the downhole geophone spectra and the corresponding signature geophone spectra for frequencies between 5 and 90 Hz. The results are displayed in Figure 42. The ratios show a consistent but gradual increase in attenuation with depth. The plots for some levels contain marked fluctuations from a smooth trend for frequencies below about 15 to 20 Hz. In many cases (e.g. traces 30 to 40, corresponding to depths between 3720 and 2741 ft), these anomalies are clearly due to irregularities in the spectrum of the downhole geophone signal (Figure 41), possibly a result of poor coupling or tool slip. Many of the levels, particularly at depths greater than 2500 ft (trace numbers less than 43), show an increase in the slope of the spectral-ratio values at frequencies above 70 to 80 Hz. Within the intervening bandwidth, the ratios generally have a smooth, linear

Watson #1; wall-lock geophone; amplitude spectra of the first arrivals

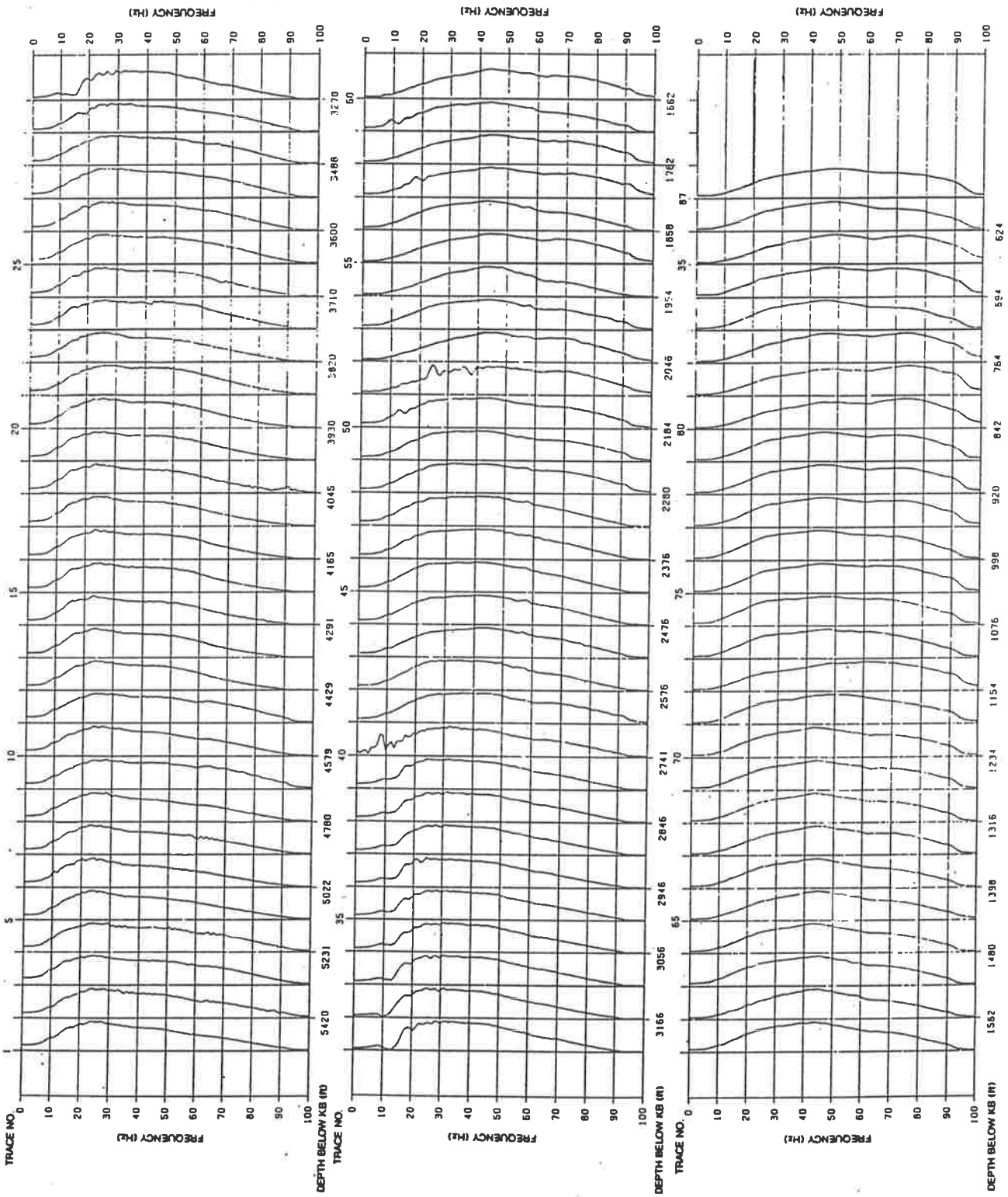

Fig. 41

Watson #1, wall-lock geophone; amplitude ratios between 5-90 Hz using the corresponding signature phone as a reference

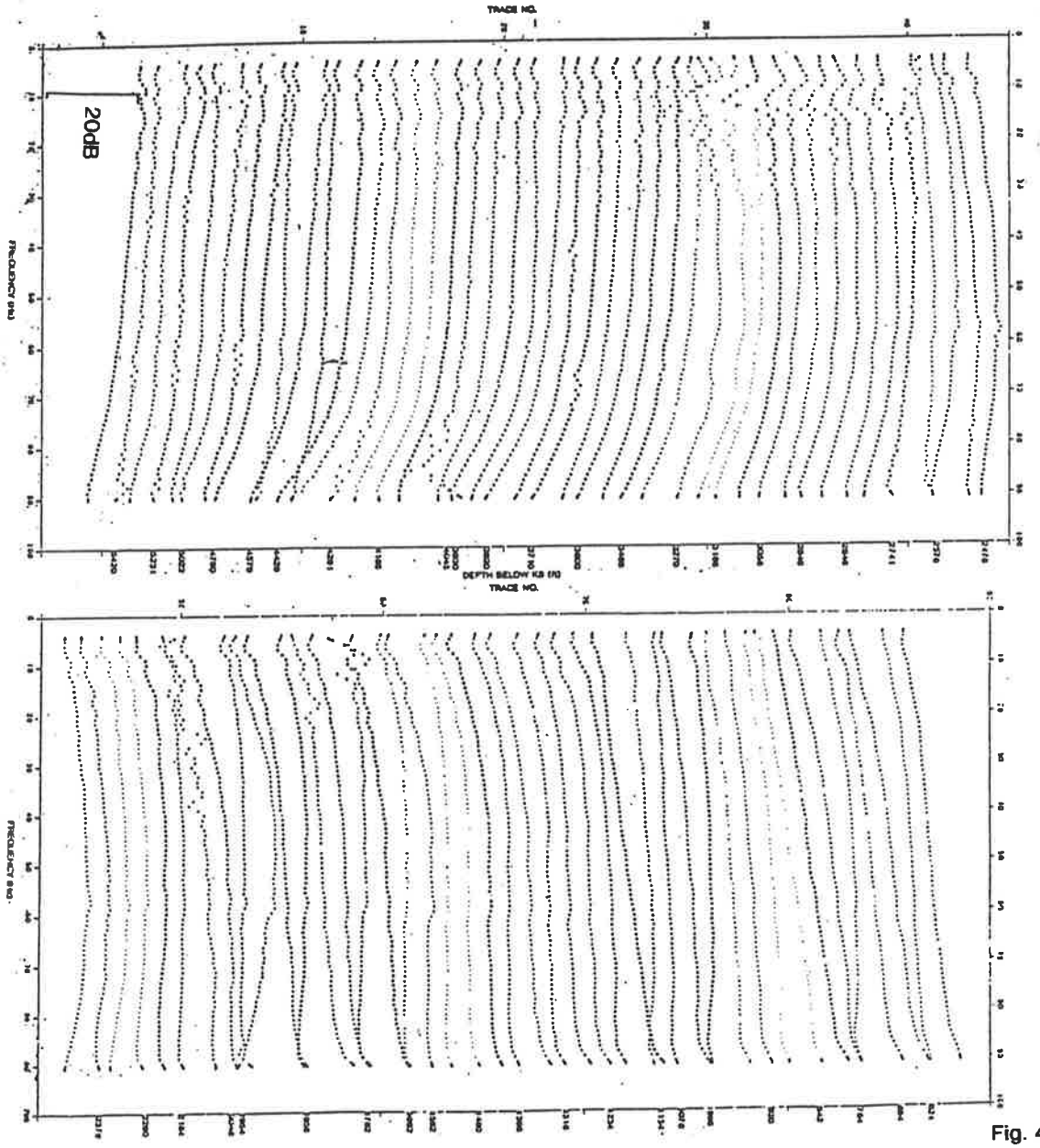

Fig. 42

appearance. Since this bandwidth is typical of seismic data recorded in the study area, it appears that the constant-Q model is a reasonable approximation for such data.

Least square lines of best fit were computed, and the slopes measured to give the cumulative attenuation, B_X, as a function of depth. The B_X values generated by fitting the whole bandwidth (5 to 90 Hz) are shown in Figure 43. This indicates a steady increase in cumulative attenuation to about 3300 ft, with only a minor increase below this depth. There is a significant amount of scatter in the data, particularly at depths shallower than 2000 ft.

B_X values were recomputed by fitting straight lines to the data using a series of different bandwidths to test the sensitivity of the cumulative attenuation to the non-linearities in the spectral-ratios at both high and low frequencies noted above. The results are plotted in Figures 44 to 50. All the plots show very similar trends and scatter, suggesting that the attenuation estimates are not very sensitive to the bandwidth used in the analysis, at least over the range of frequencies tested. There is a minor decrease in the total cumulative attenuation computed from top to bottom of the well as the bandwidth is reduced (compare Figures 43 and 48). There are also some significant changes in the B_X values over the interval between 2700 and 3300 ft as the low frequency cut off is increased (compare Figures 43 and 46). These levels were noted previously as having significant low frequency fluctuations, which appear to affect the least squares fitting process if they are retained in the analysis.

On the basis of these tests, it was decided to use the B_X values calculated over the frequency range between 15 and 80 Hz for attenuation estimates (Figure 51). Three separate rates of attenuation are identified from the B_X data as follows, where the definition of the boundaries has been made on the basis of variations in lithology;

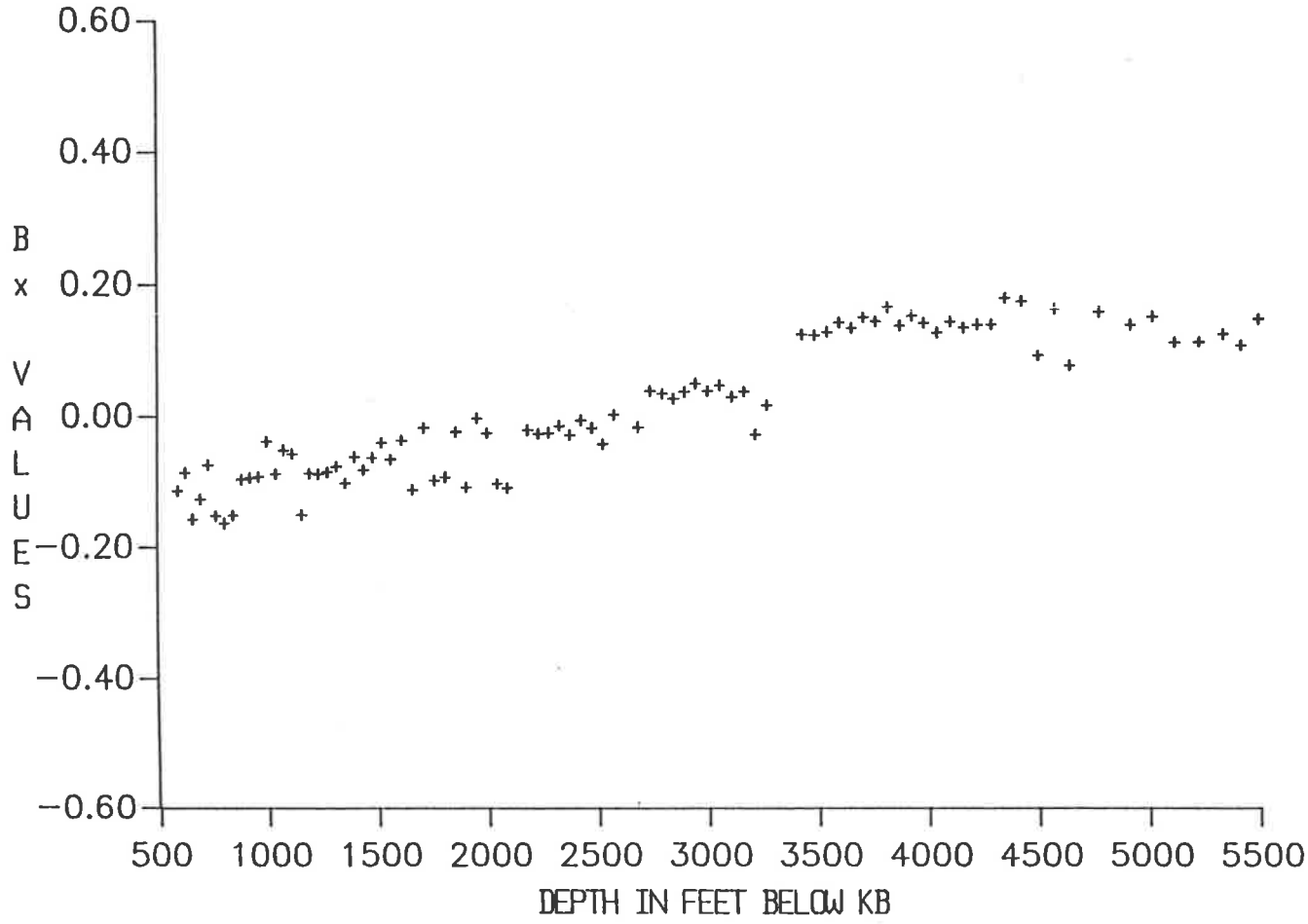

Watson #1, wall-lock geophone; cumulative attenuation between 5-90 Hz using the corresponding signature phone as a reference

Fig. 43

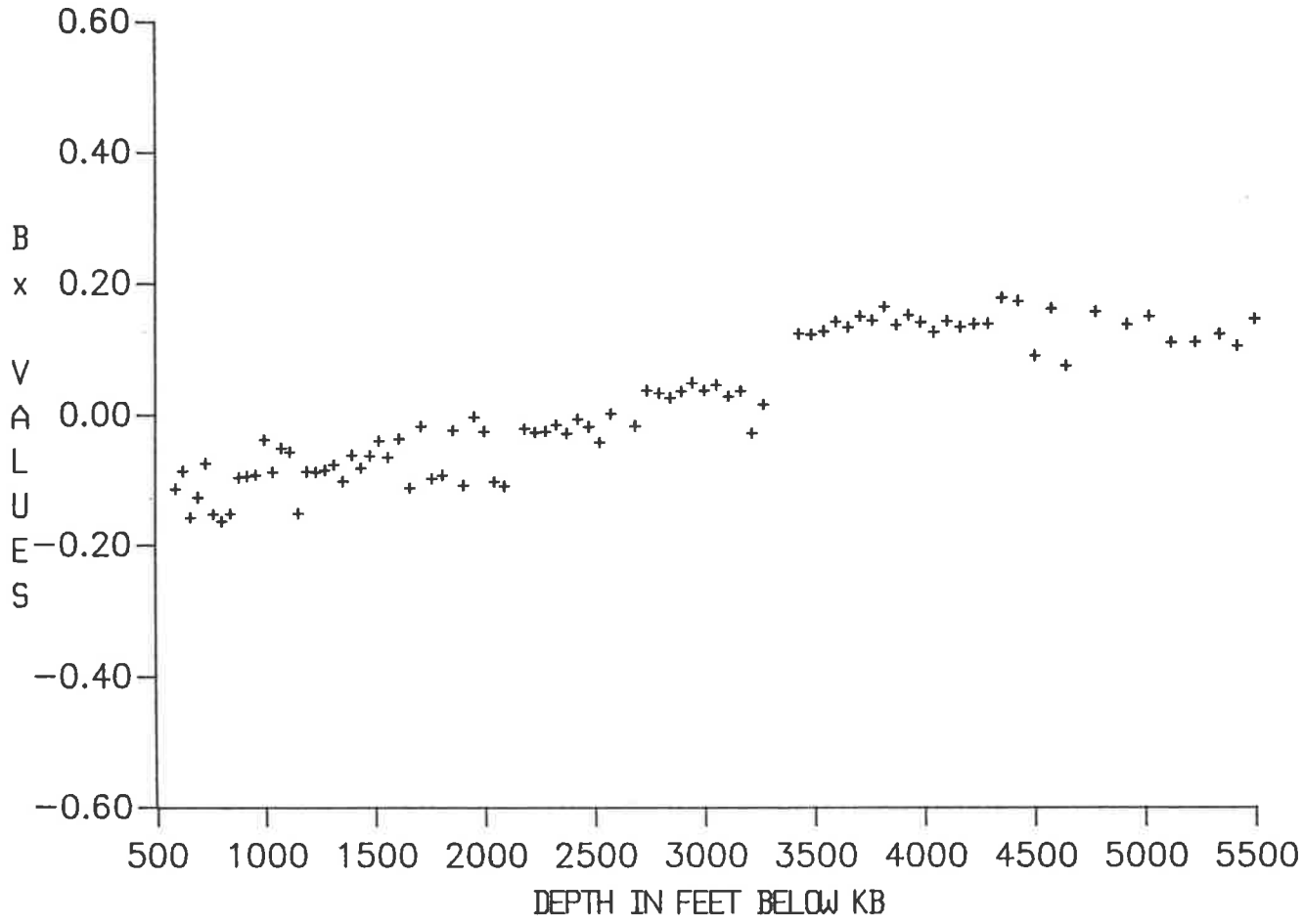

Watson #1, wall-lock geophone/signature phone; cumulative attenuation between 10-90 Hz

Fig. 44

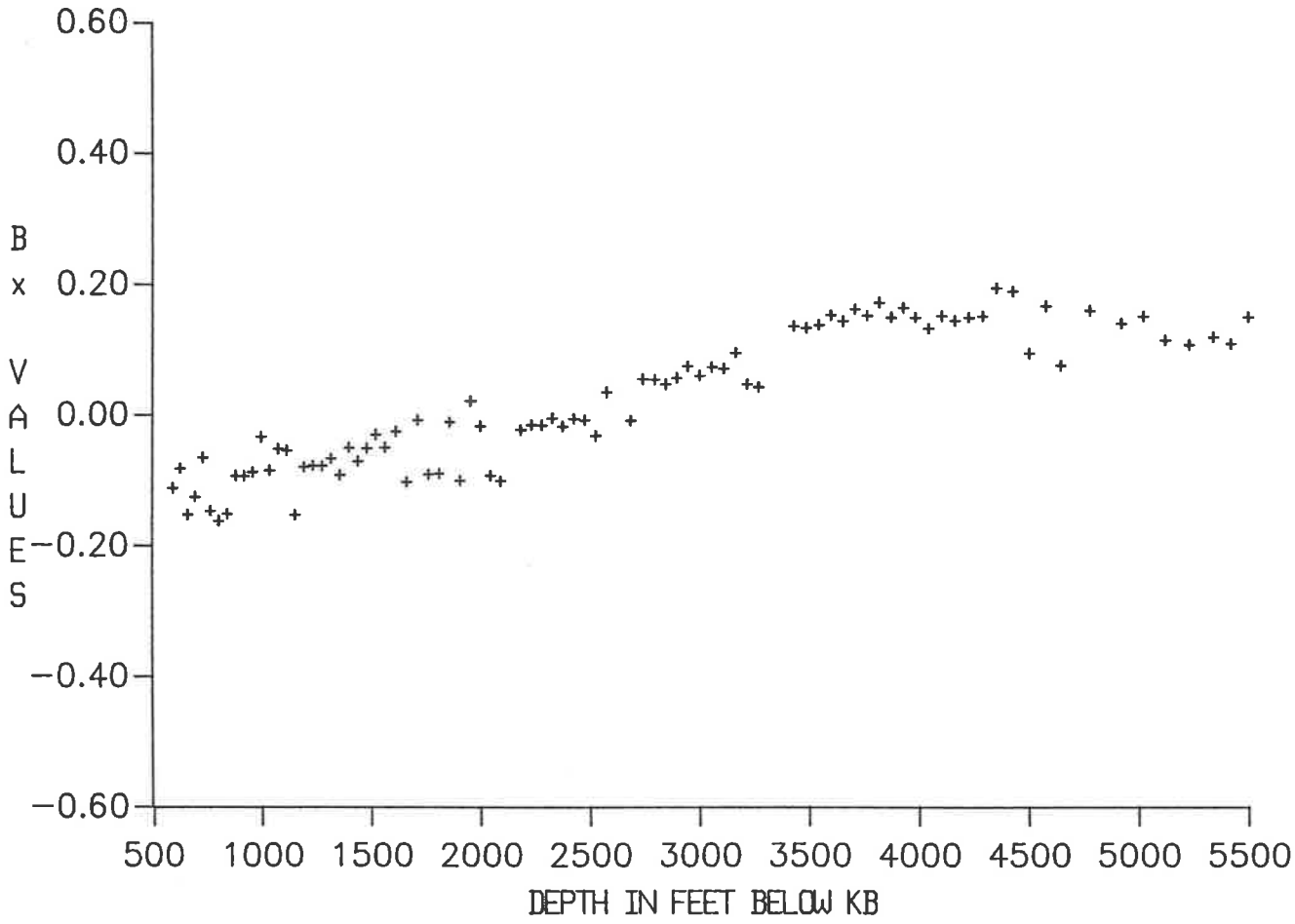

Watson #1, wall-lock geophone/signature phone; cumulative attenuation between 15-90 Hz

Fig. 45

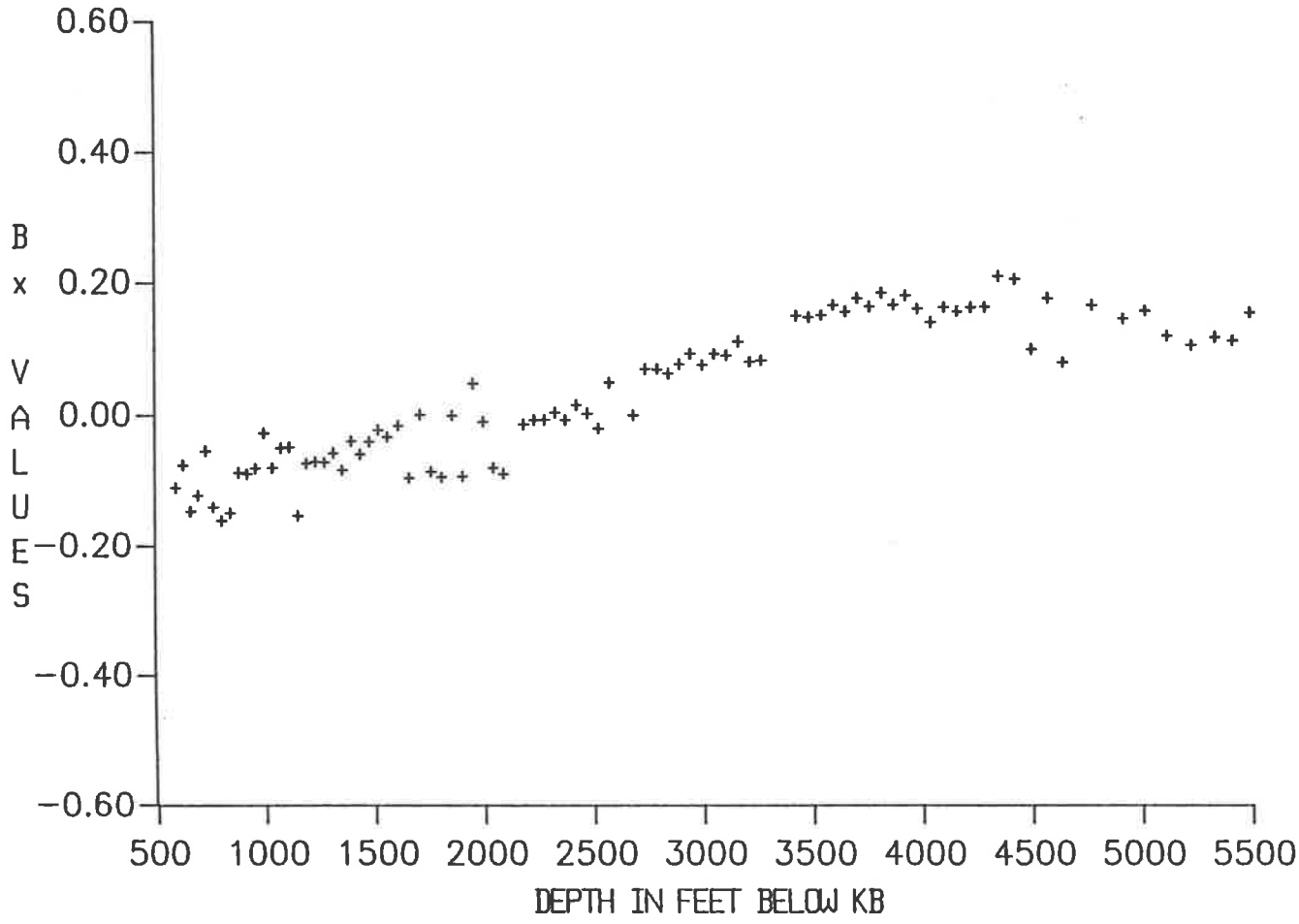

Watson #1, wall-lock geophone/signature phone; cumulative attenuation between 20-90 Hz

Fig. 46

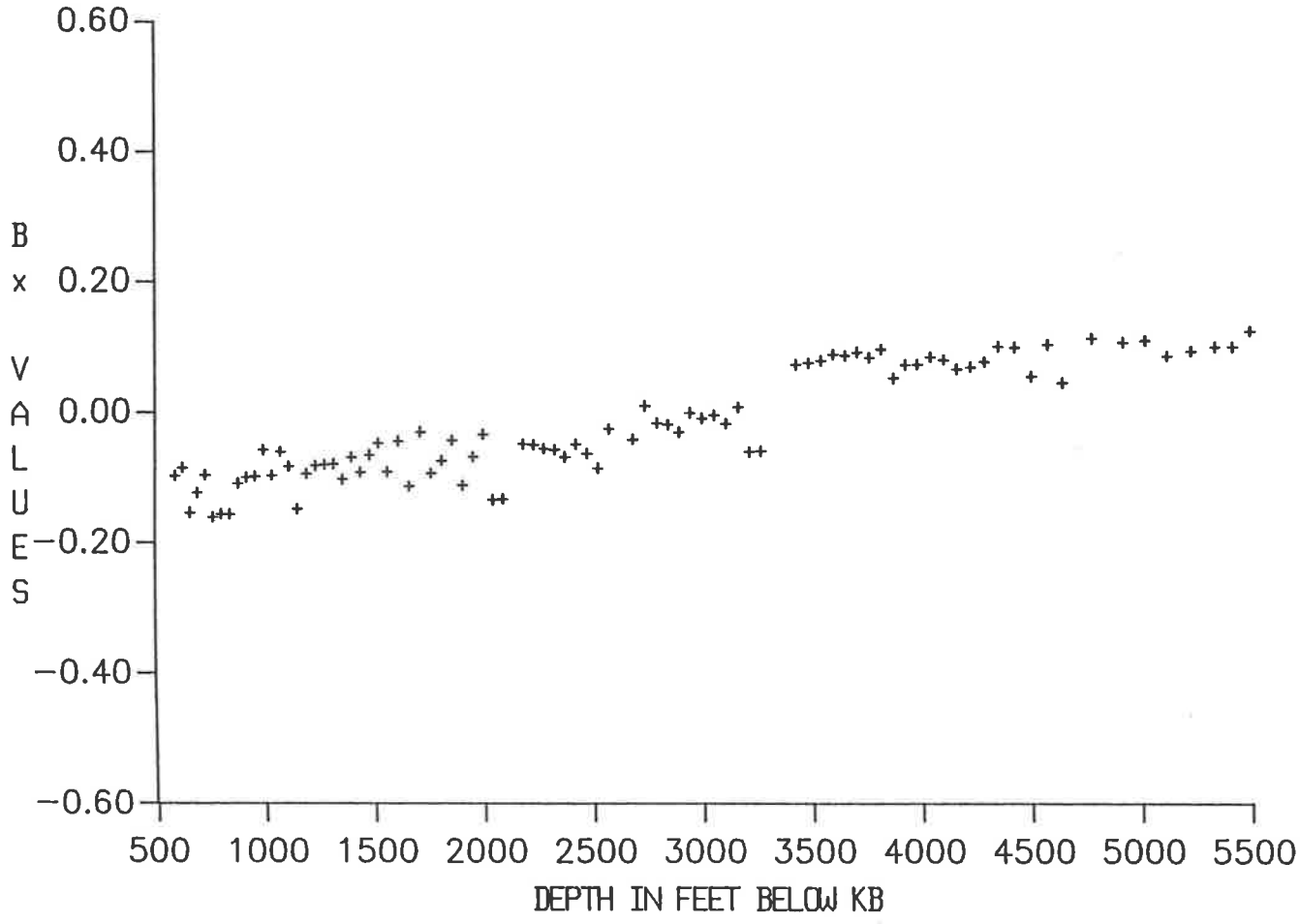

Watson #1, wall-lock geophone/signature phone; cumulative attenuation between 15-70 Hz

Fig. 47

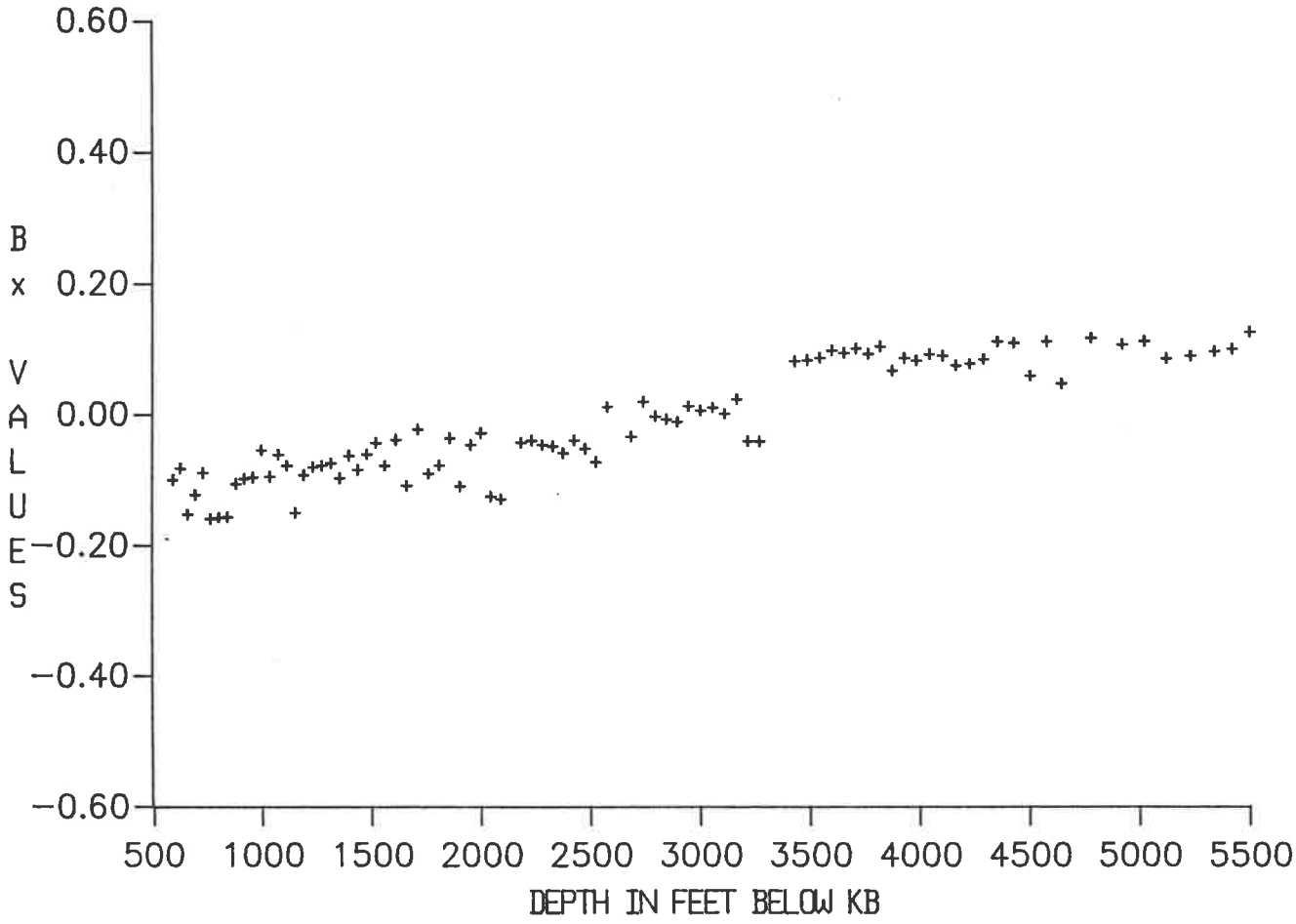

Watson #1, wall-lock geophone/signature phone; cumulative attenuation between 15-75 Hz

Fig. 48

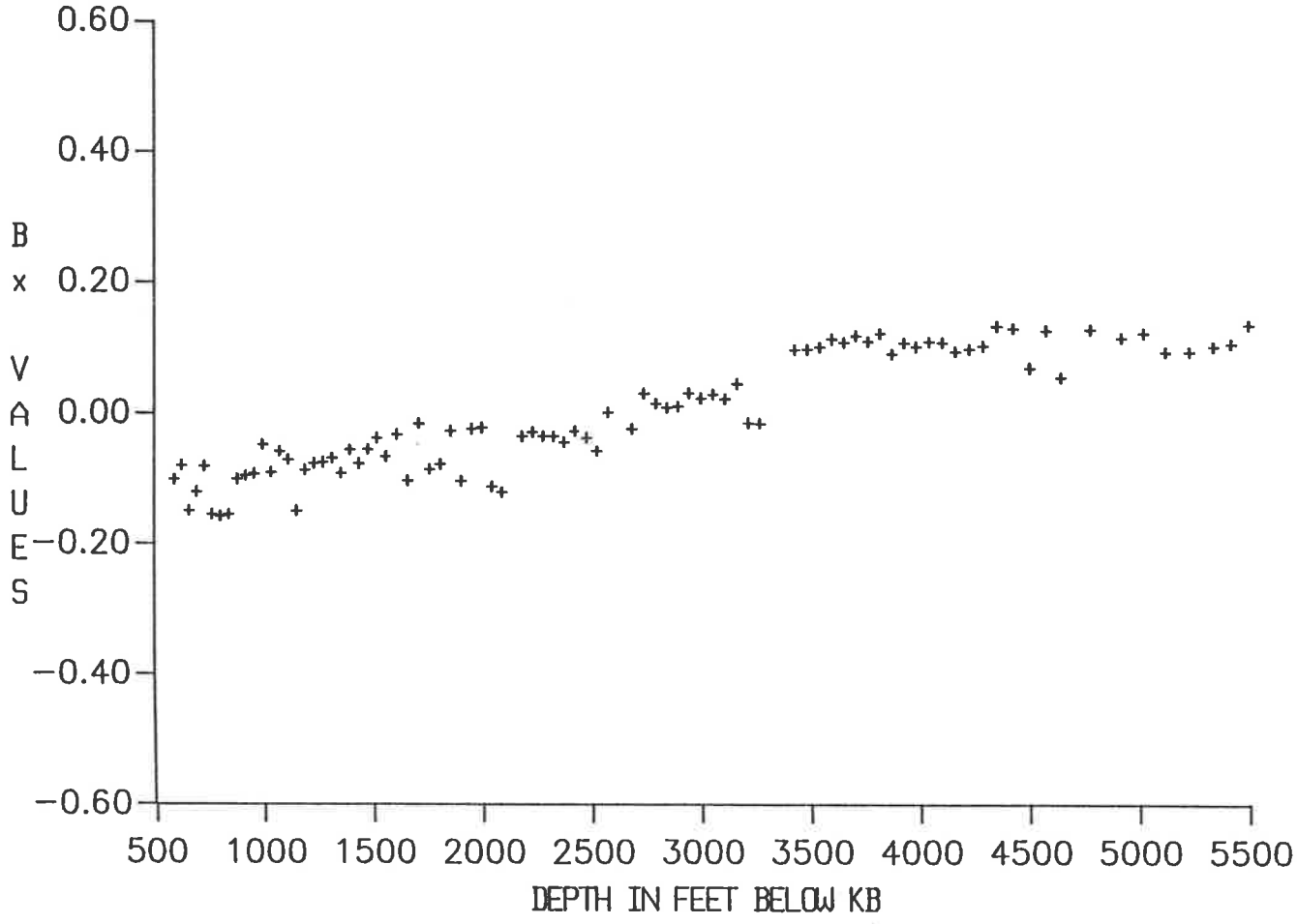

Watson #1, wall-lock geophone/signature phone; cumulative attenuation between 15-80 Hz

Fig. 49

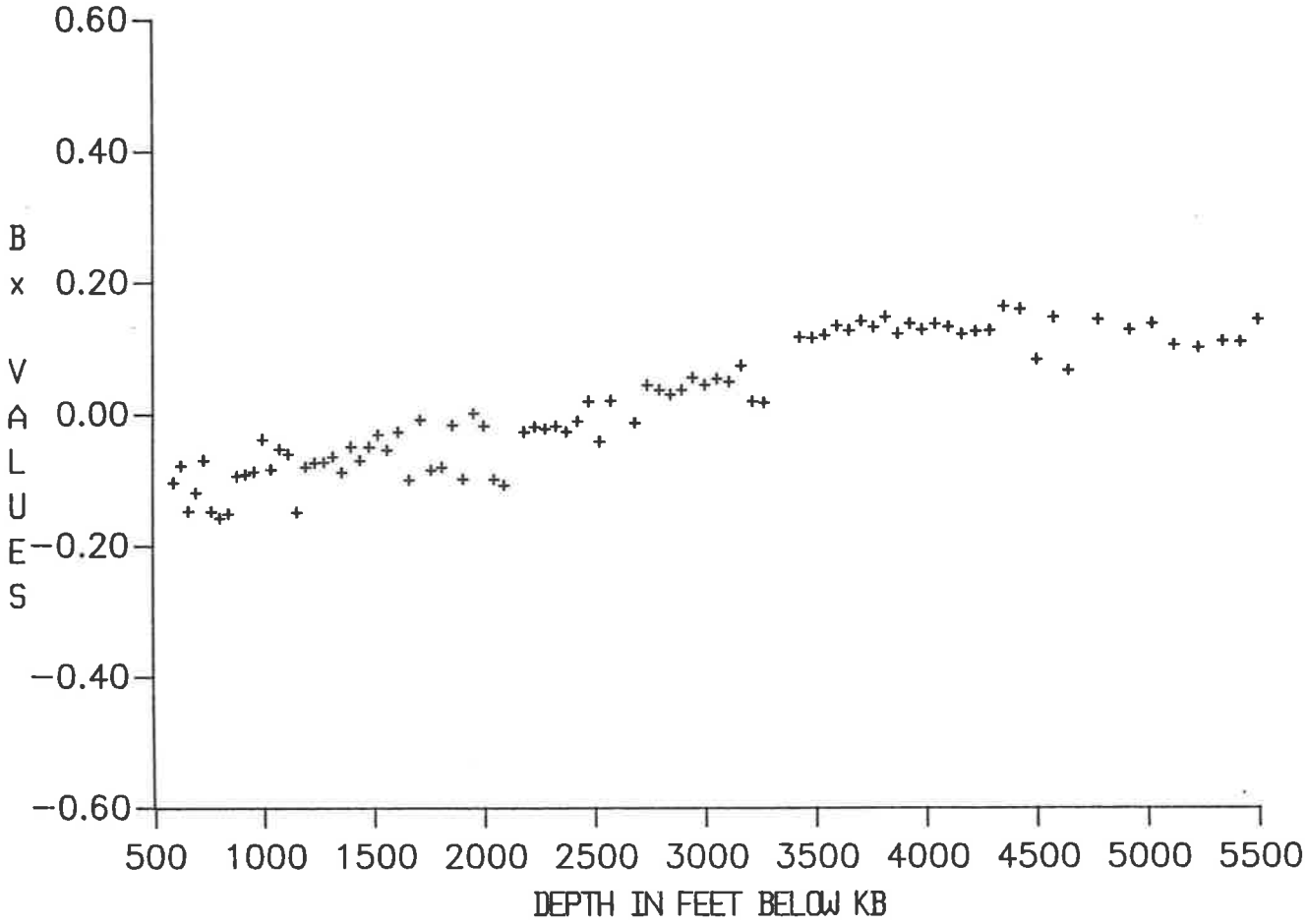

Watson #1, wall-lock geophone/signature phone; cumulative attenuation between 15-85 Hz

Fig. 50

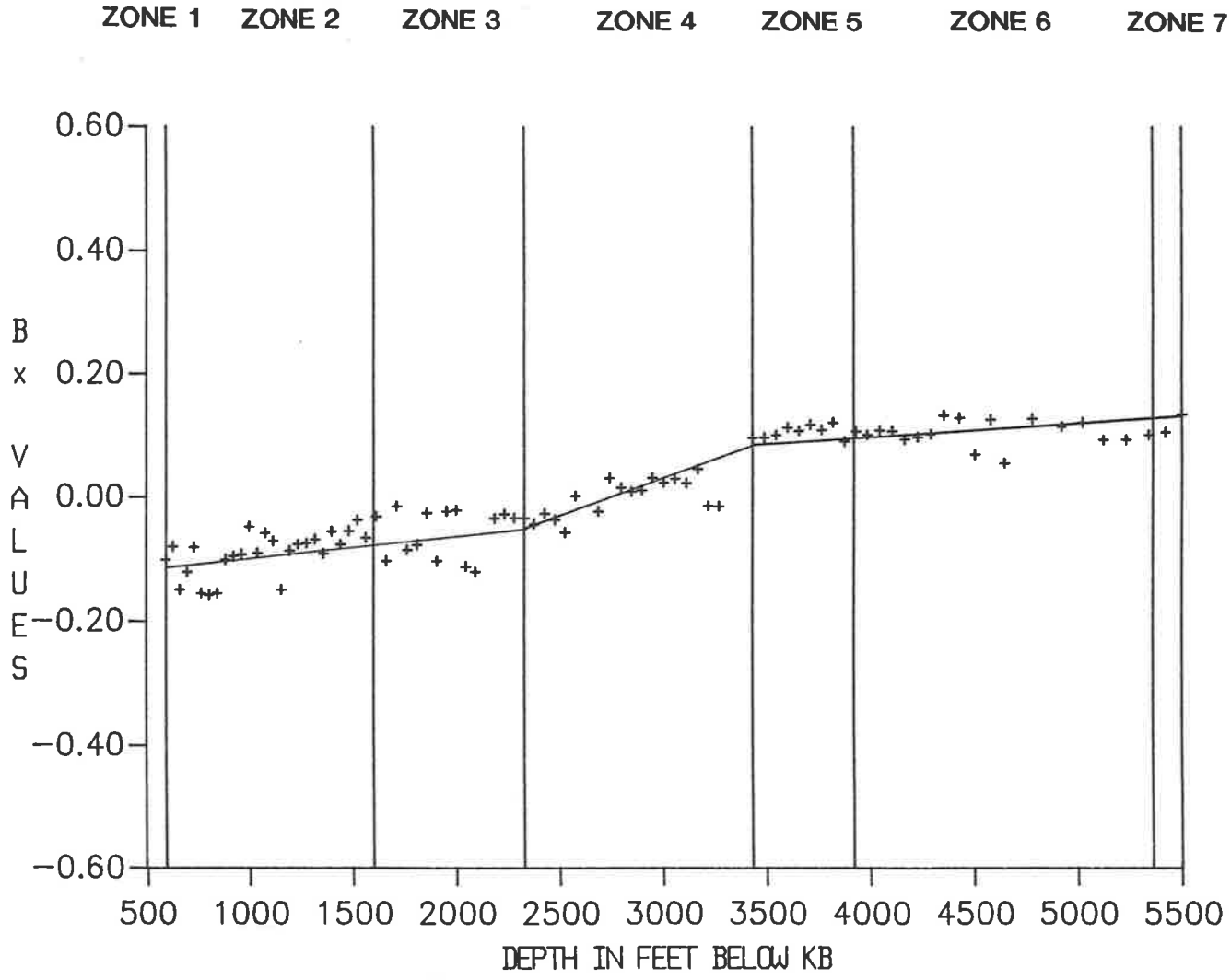

Watson #1, wall-lock geophone/signature phone; cumulative attenuation between 15-80 Hz with interpreted slopes annotated

Fig. 51

Depth in feet below KB	k_x dB/Hz/ft	V_x ft/s	α_x dB/wavelength	Q
589 - 2328	5.7×10^{-5}	7340	0.4814	65
2328 - 3431	1.3×10^{-4}	8540	1.1102	25
3431 - 5500	1.8×10^{-5}	11230	0.2021	135

Table 5, Observed attenuation values from geophone/signature phone data.

Between 3431 and 2328 ft (traces 29-47) the rate of attenuation is high. There is no indication of a similar rate of attenuation in the model data and it is therefore attributed to the lithology, which consists of a 500 ft massive siltstone commencing at 2324 ft followed by a series of interbedded sandstone and siltstone with some carbonaceous streaks.

The sensitivity of the analysis to the definition of depth intervals is illustrated by a reinterpretation of the data in Figure 51,

Depth in feet below KB	k_x dB/Hz/ft	V_x ft/s	α_x dB/wavelength	Q
589 - 3431	8.5×10^{-5}	7760	0.6596	41
3431 - 5500	1.8×10^{-5}	11230	0.2021	135

Table 6, Reinterpretation of B_x data in Table 5.

Over the range 589-3431 ft the total attenuation is identical for both tables. The interval attenuation over the same depth range varies markedly between the tables. As concluded by Hauge (1981), the depth interval definition is critical to the analysis, and the scatter in the B_x data limits it to fairly gross intervals.

The analysis of the model data with multiples in Chapter 6.3 shows that a portion of the observed attenuation may be attributed to multiple activity. This can be subtracted from the

observed attenuation to determine the intrinsic attenuation. Subdividing the well to combine the zones observed in the model and depth intervals in the real data gives 7 zones. Table 7 gives the attenuation estimates for each zone. The apparent interval attenuation contributes between 4% and 82% of the observed α_x.

Zone	Depth Interval in feet below KB	Attenuation (dB/wavelength) Observed	Apparent	Intrinsic	Q (Intrinsic)
1	0 - 589	Information unavailable			
2	589 - 1600	0.3808	0.3140(82%)	0.0668	409
3	1600 - 2328	0.4626	0.0381(8%)	0.4245	64
4	2328 - 3431	1.1102	0.0401(4%)	1.0701	26
5	3431 - 3920	0.1572	0.0410(26%)	0.1162	235
6	3920 - 5360	0.2216	0.0579(26%)	0.1637	167
7	5360 - TD	0.2700	0.0705(26%)	0.1995	137

Table 7 Watson #1 intrinsic attenuation estimates using multiple references. The percentage figures indicate the percentage of the observed attenuation accounted for by the apparent attenuation.

The apparent and observed attenuation estimates were computed over different bandwidths. Matching these, by recomputing the observed attenuation estimates over the bandwidth 10-70 Hz, had no effect as any changes in k_x were small enough to be masked by the scatter in the data.

The above estimates take into account the variation of the signal input into the ground. As many VSPs are recorded without a signature geophone monitoring the input, attenuation

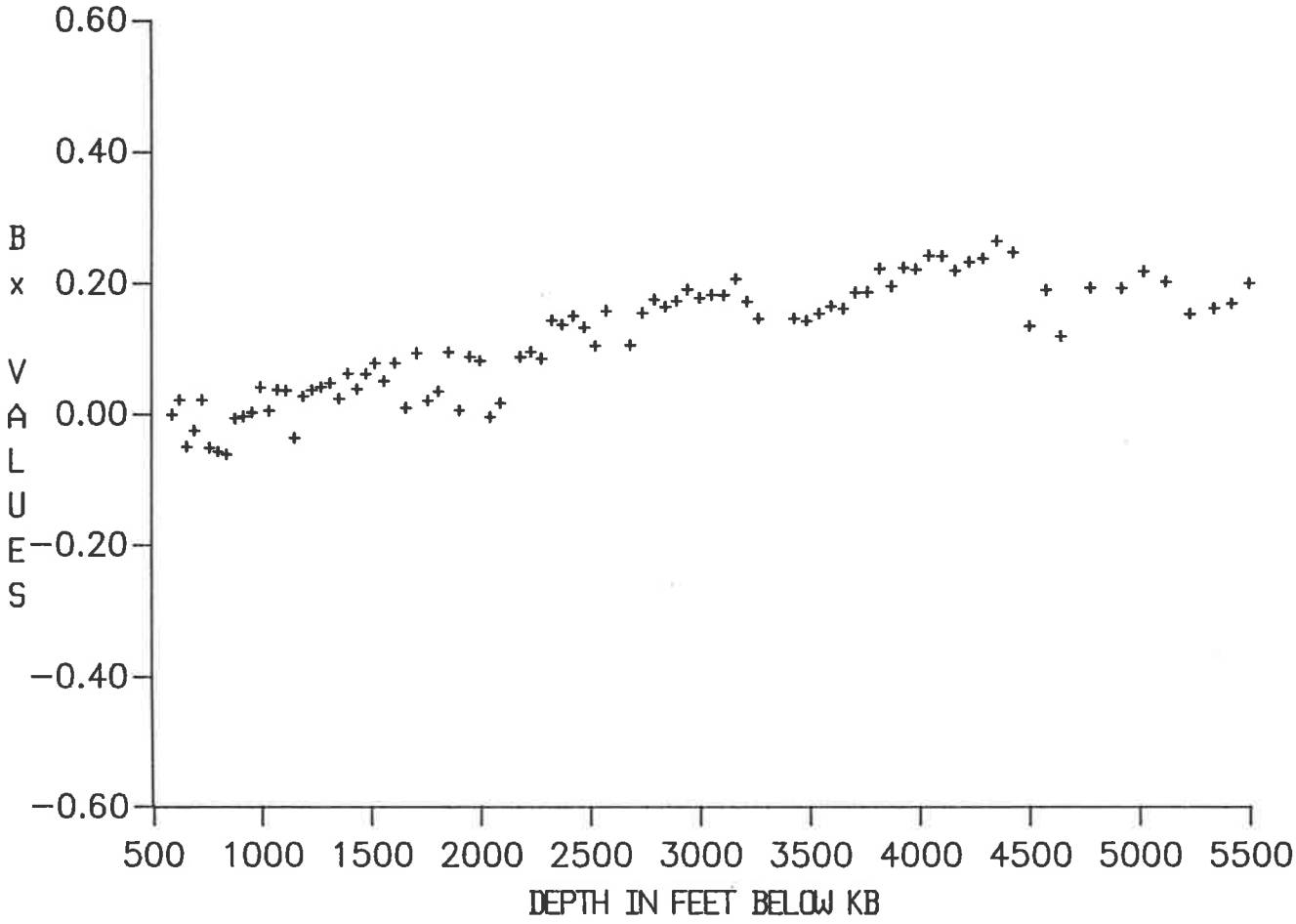

Watson #1, wall-lock geophone; cumulative attenuation between 15-80 Hz with the reference at 589 feet

Fig. 52

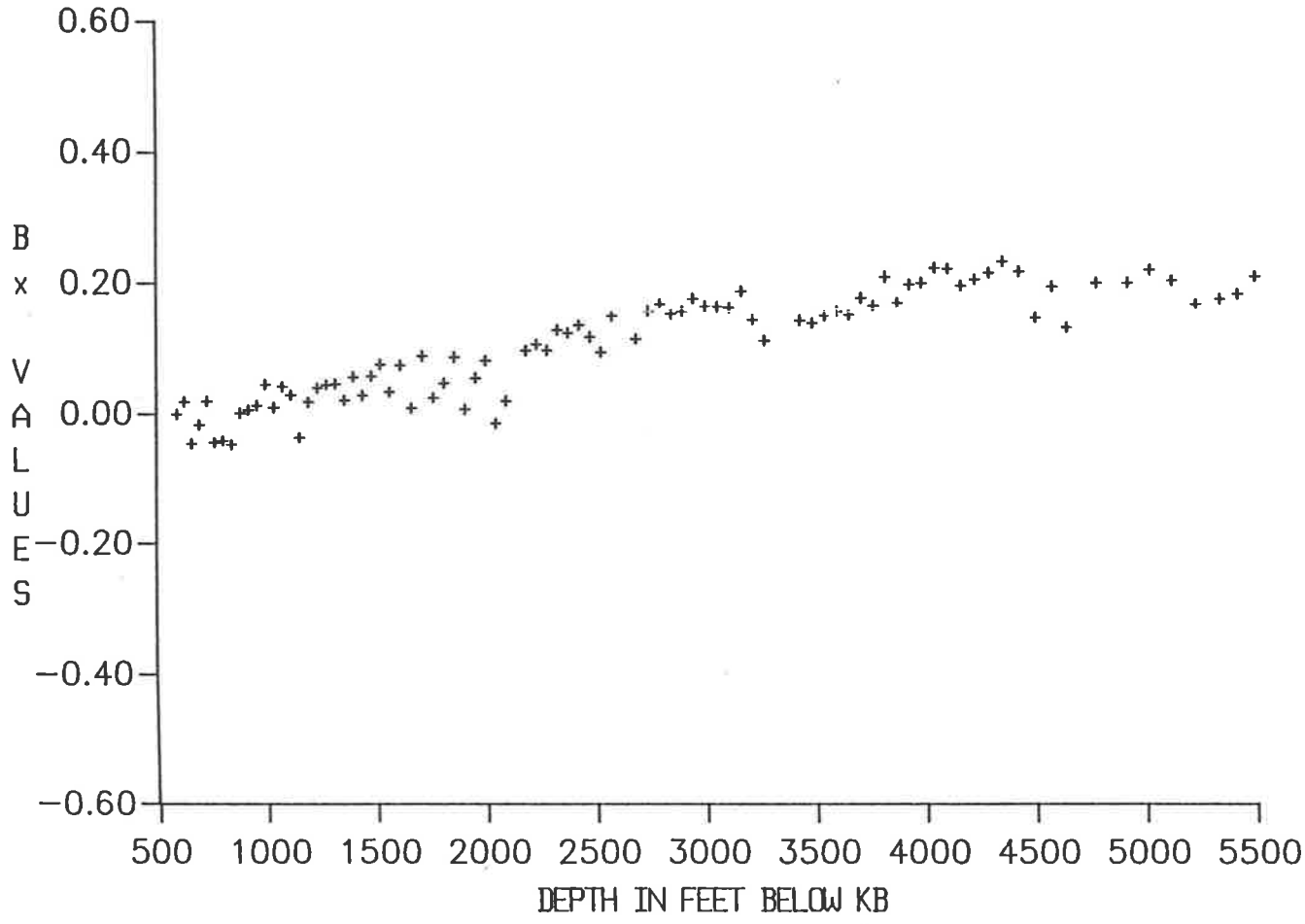

Watson #1, wall-lock geophone; cumulative attenuation between 15-70 Hz with the reference at 589 feet

Fig. 53

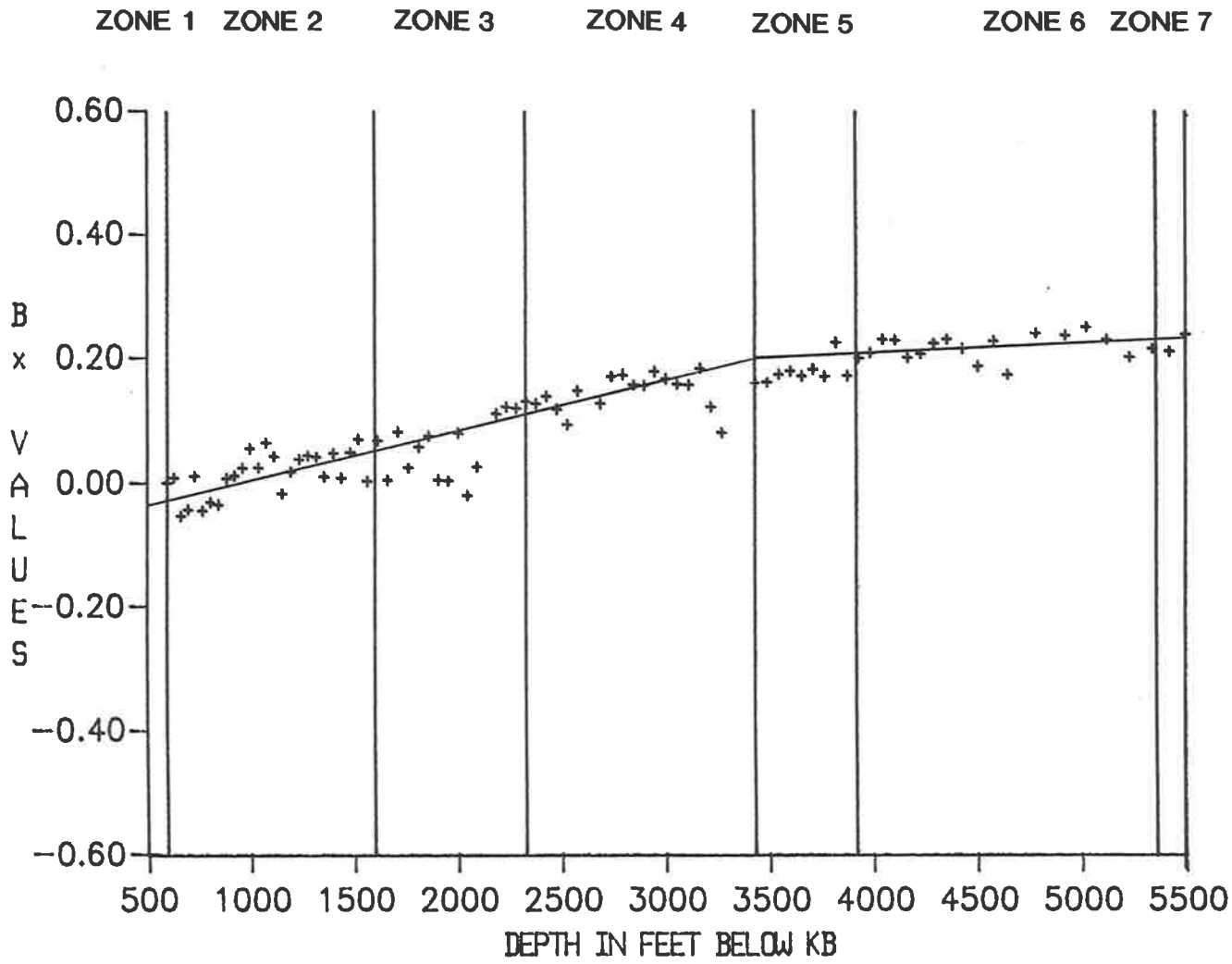

Watson #1, wall-lock geophone; cumulative attenuation between 15-60 Hz with the reference at 589 feet

Fig. 54

estimates using a single reference trace were made using the Watson #1 data, for comparison with those computed using a signature geophone.

Using the trace at 589 feet as the reference trace, spectral ratio analysis was carried out between 15 and 80 Hz. The amplitude ratios show an increase in slope with depth. From 3431 to 2686 feet (trace 29 - 41) the low frequency end of the ratios shows some anomalous values, as noted for the signature phone analysis. The B_X values determined from the least squares fit to the amplitude ratios between 15 and 80 Hz are displayed in Figure 52. The scatter for the single reference trace is much greater than that seen using the signature geophone, particularly below 3500 feet. By reducing the high frequency end of the least squares analysis to 70 Hz (Figure 53), and 60 Hz (Figure 54) the scatter is reduced, allowing an easier interpretation. Two linear segments can be discerned in the data set, which, upon further analysis, give the results shown in Table 8 below.

Zone	Depth Interval in feet below KB	k_X dB/Hz/ft	Attenuation (dB/wavelength) Observed	Intrinsic	Q (Intrinsic)
1	0 - 589	Information unavailable			
2	589 - 1600	8.2×10^{-5}	0.5478	0.2338	117
3	1600 - 2328	8.2×10^{-5}	0.6655	0.6274	44
4	2328 - 3431	8.2×10^{-5}	0.7003	0.6602	41
5	3431 - 3920	1.5×10^{-5}	0.1310	0.0900	303
6	3920 - 5360	1.5×10^{-5}	0.1847	0.1268	215
7	5360 - TD	1.5×10^{-5}	0.2250	0.1545	177

Table 8: Watson #1 intrinsic attenuation estimates using a single reference trace from 589 feet.

Taking into account the scatter in the data, Q values determined using the two methods of analysis are in reasonable agreement over zones 3 to 7. There is a large difference over

Zone 2, which is attributed to the interpretation of the cumulative attenuation data. For the multiple reference analysis three slopes have been fitted to the data, for the single reference only two. If for the multiple reference analysis two slopes had been fitted, Table 6, then the Q estimates would be in much closer agreement.

On the basis of the above results it is difficult to determine which of the Q estimates is the most reasonable. If the first arrival at the signature geophone was known to be multiple free it would be the obvious selection, but this is not the case.

7.5 Tirrawarra #22 VSP Acquisition Parameters

This VSP, in conjunction with a checkshot survey, was recorded on 16 September, 1982, by Seismograph Service Limited.

The source used was an 80 cu. inch airgun, operating at 1800 psi in the mudpit. The downhole detector was a GHC-100 high temperature geophone, and the shot was monitored by a hydrophone suspended 2 ft above the airgun. Figure 55 shows the field configuration.

The VSP levels were separated by equal depth intervals of 100 feet. 107 levels, comprising 257 individual shot records, were acquired between 9800 and 500 feet below KB. A list of these depths is given in Appendix 1. The recording filter for the downhole geophone was set with a high cut of 55 Hz. The sample rate was 2 ms.

The data received from SANTOS Limited consisted of the observer's logs and a SEG-Y format magnetic tape with 3 channels of data recorded as follows:

Channel 1: Parity trace

Channel 2: Gun hydrophone

Channel 3: Well geophone trace

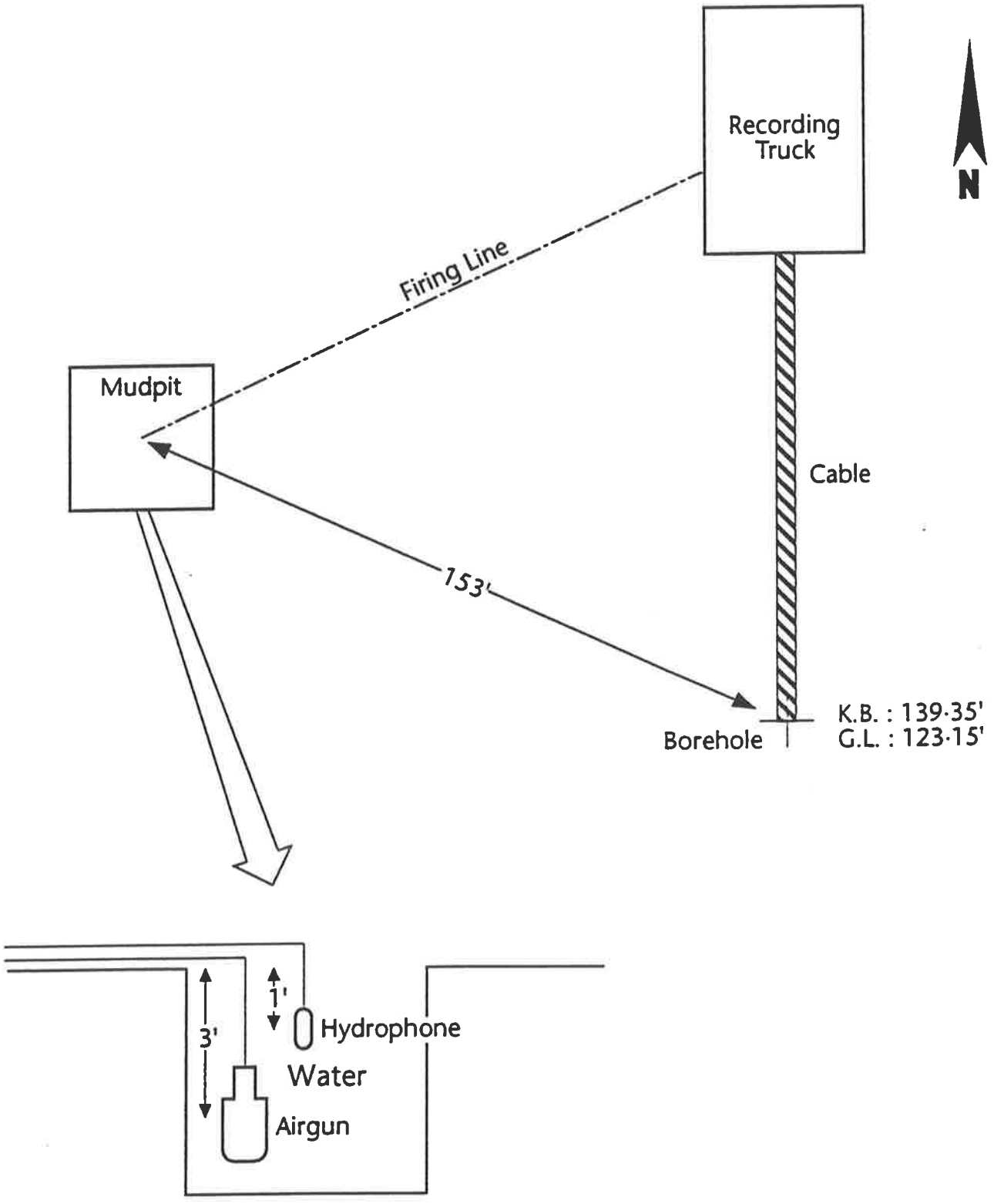

Tirrawarra 22, VSP acquisition parameters

Fig. 55

TIRRAWARRA 22

VSP WELL SUMMARY

Lat. : 27° 38' 07·40" S.
Long. : 140° 07' 13·01" E.
Seismic : LINE 80-T7
Spudded : 20/08/1982 K.B. : 139·35'

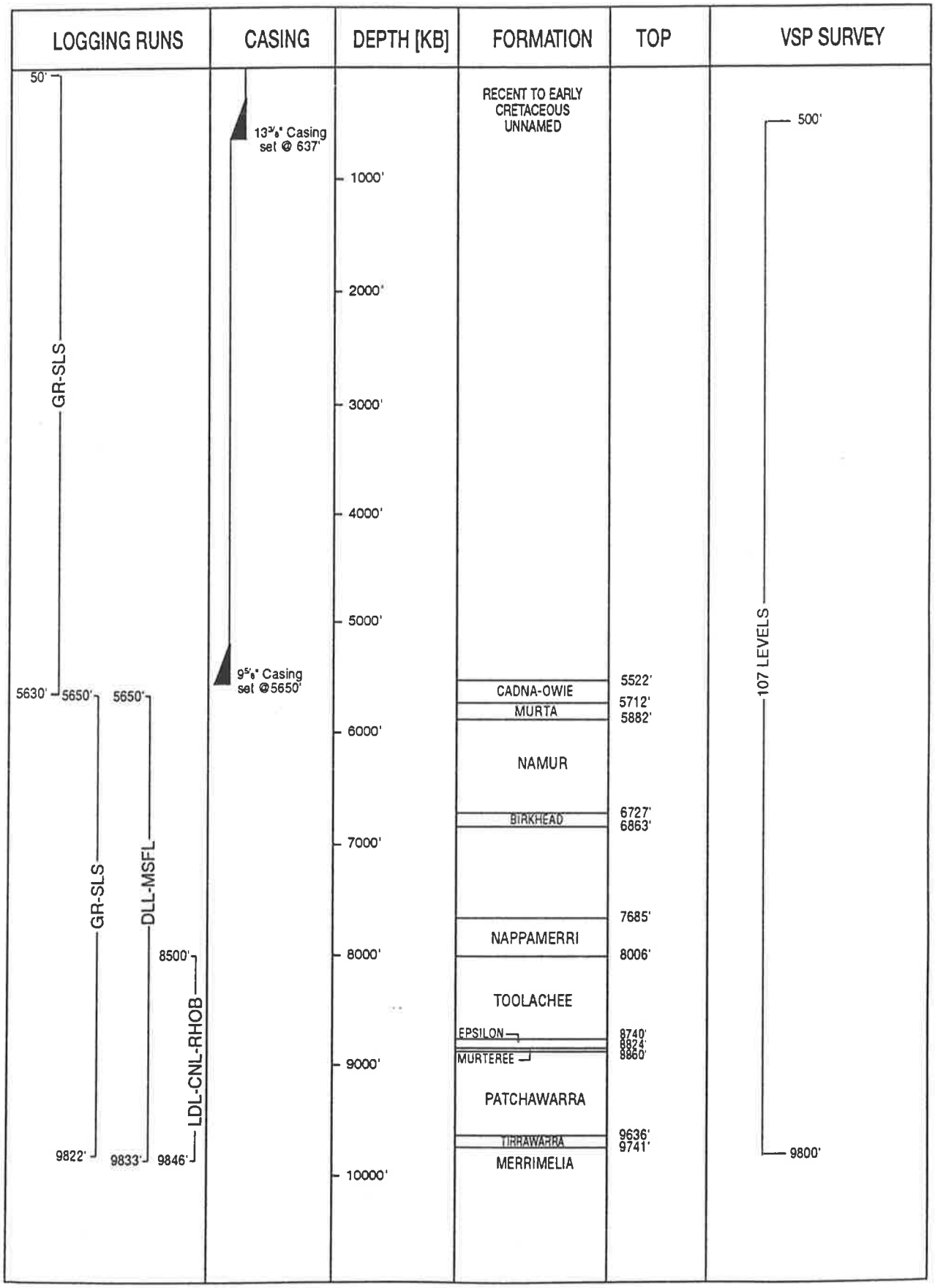

Fig. 56

Figure 56, shows the VSP levels, logging runs and casing for Tirrawarra #22.

7.6 Tirrawarra #22 VSP Data Preparation

Editing of the 257 traces to remove those not recorded as part of the VSP or badly distorted by noise, reduced this number to 167. The first two seconds of this data are displayed in Figure 57, in which the traces have been normalised for display purposes. Bursts of high frequency noise can be seen on several traces, with the deeper levels being particularly badly affected. The caliper log in the deep zone of the borehole does not indicate washout, which may have explained the noise as due to poor coupling. The appearance of this noise, through many traces, both before and after the first arrival, along with its cyclicity, suggests that it may be due to electrical pick-up, perhaps from a rig generator. There does not appear to be any cross feed on the hydrophone traces.

Prior to further editing, stacking of the records to improve the signal to noise ratio was carried out. The result of this was inconclusive with respect to the first arrivals. To avoid any possible distortion in the first arrivals, as a result of stacking, a decision was made to select an unstacked trace from each level for spectral ratio analysis.

Following an inspection of the 167 geophone traces and the corresponding amplitude spectra computed over a window containing the first arrivals for each depth (not displayed), it was necessary to edit the data further. Three depth intervals, 1000 to 1700, 2700 to 3200, and 5600 to 5900 feet are particularly noisy. It is difficult to explain the cause of this noise given the information available. Of the 91 VSP levels originally recorded, 68 remained after this final editing. For each geophone trace selected the corresponding hydrophone signal was read from tape.

Geophone and hydrophone first arrivals were aligned at 1000 ms, and displayed as Figure 58 (a) and (b) respectively. The hydrophone signature appears to be fairly consistent with little noise. Filters to reduce the noise component of the geophone traces were not

Tirrawarra #22, unedited geophone data

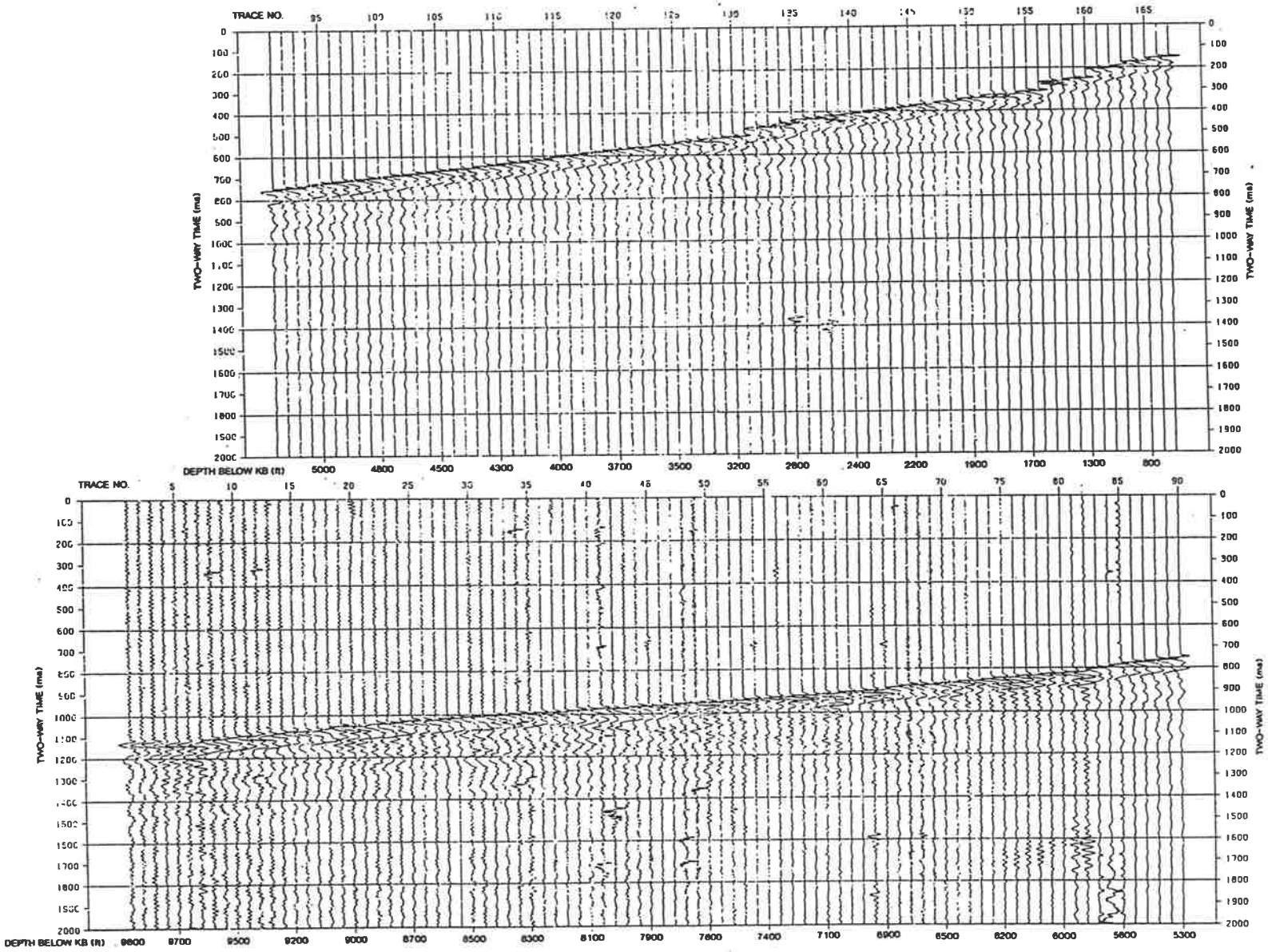

Fig. 57

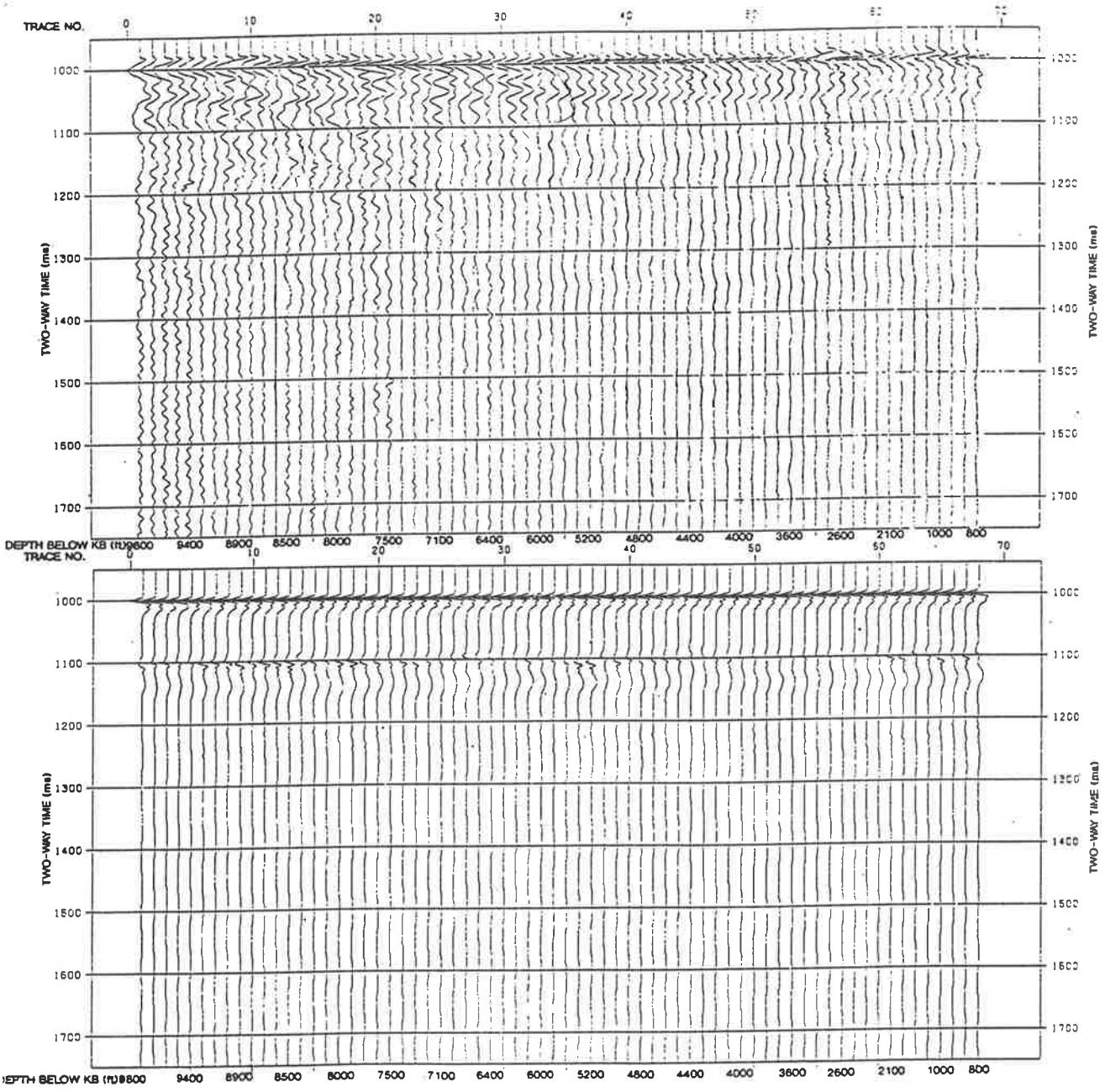

Tirrawarra #22, edited geophone data aligned at 1000ms Fig. 58a

Hydrophone data aligned at 1000ms Fig. 58b

considered for this study, since any filtering would affect the first arrival, and the attenuation is very dependent on small changes in pulse shape. A broadening of the first arrival is seen on the deeper traces, possibly due to short-period multiples as described previously.

7.7 Tirrawarra #22 VSP Spectral Ratio Analysis

The gun hydrophone allowed excellent monitoring of the source signal, but did not monitor the actual signal input to the ground. Although no mention is made on the observer's log, in the author's experience, using an airgun in a pit filled with water can present problems. The airgun occasionally becomes buried in the sediment at the bottom of the pit, and the ports through which the air discharges may become partially or fully blocked. The water level in the pit may change due to evaporation, and in soft sediments the walls of the pit may collapse. One or a combination of the above may occur, so altering the airgun signal. However, the edited gun hydrophone traces, displayed in Figure 58b suggest that the source signal remained reasonably constant throughout the survey.

Amplitude spectra were computed for the first arrivals on the gun hydrophone traces. Inspection of Figure 58b suggested that the data window for this computation could end at 1040 ms. The resulting spectra are displayed in Figure 59. The traces show the source to be wide band with the maximum amplitude occurring at 25 Hz after a rapid increase from low frequency. The spectra are very smooth.

Spectral ratio analysis was performed on the gun hydrophone data for frequencies between 5 and 70 Hz. The hydrophone trace recorded for the 700 ft geophone level (trace 68) was used as the reference trace. The B_X values are displayed in Figure 60. Comparison with the degree of scatter in the analysis of synthetic data suggests that the source signature does not quite remain constant, within the accuracy of the data, since 12 of the 68 B_X values fall just outside the range of ± 0.035 of the average. The airgun source operates on the discharge of compressed air, which for this survey was provided from gas bottles. The pressure gauge for the airgun was set at 1800 psi but fluctuations in pressure have been observed to occur in

Tirrawarra #22, hydrophone; amplitude spectra of the first arrivals

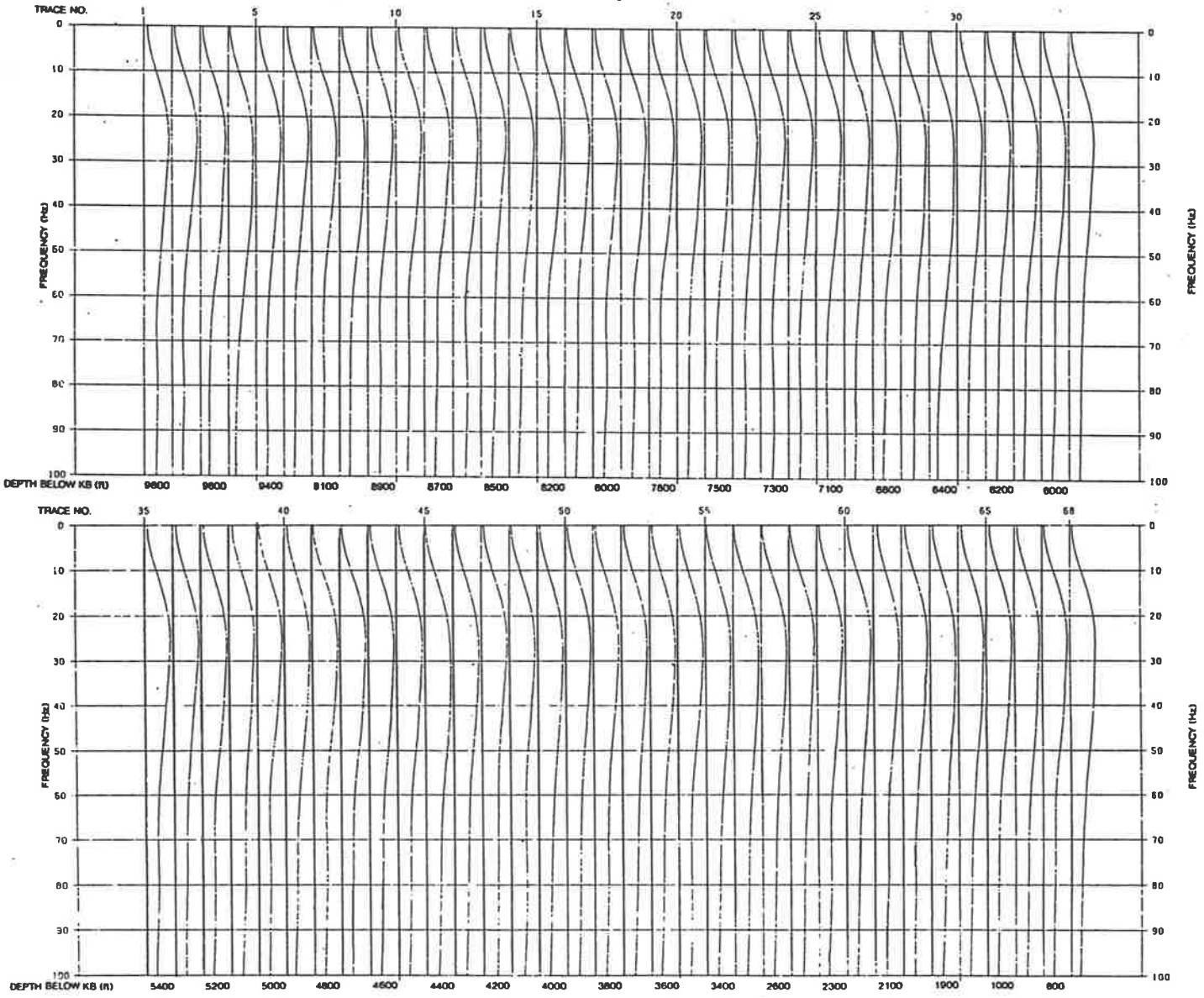

Fig. 59

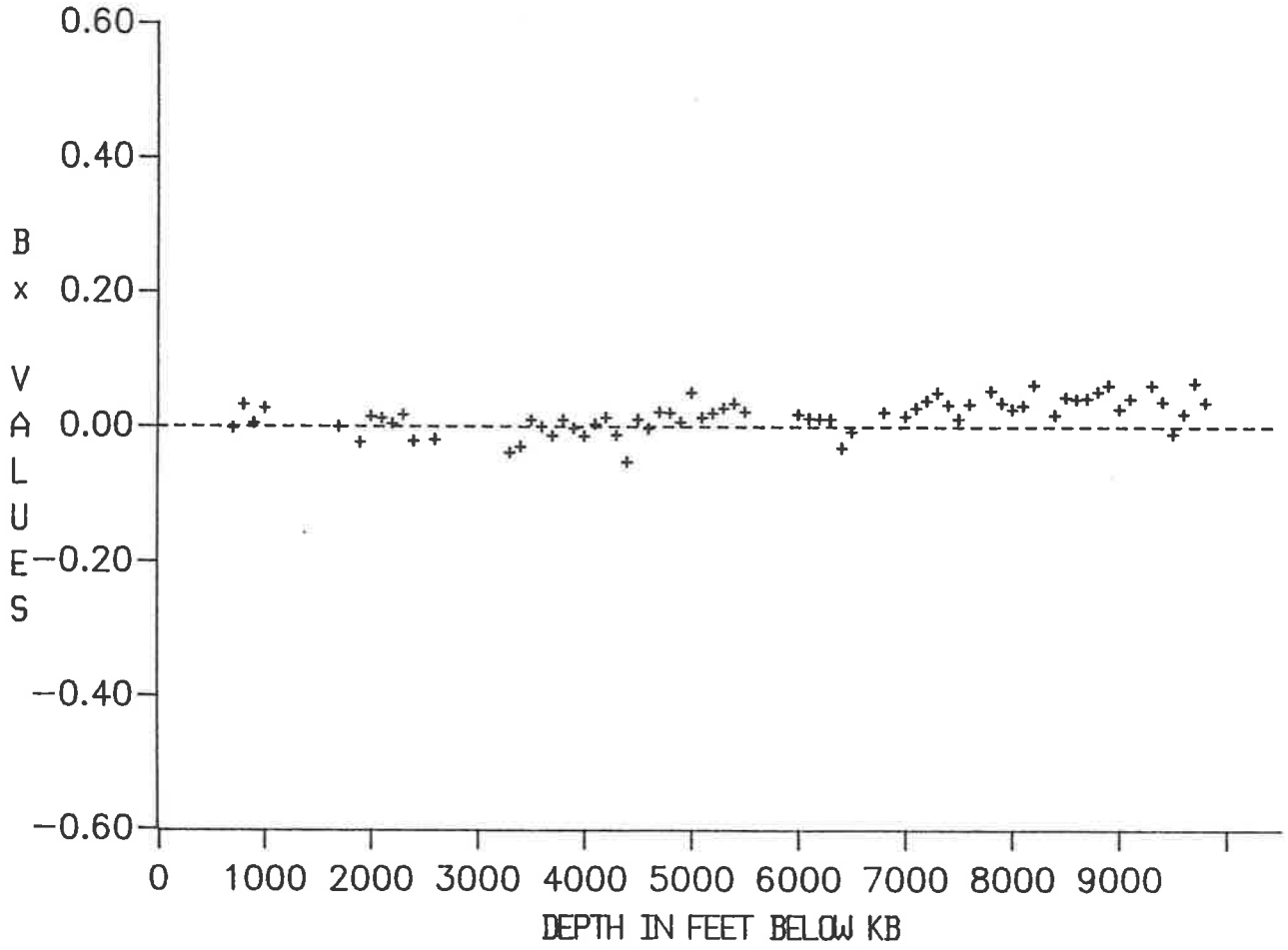

Tirrawarra #22, hydrophone; cumulative attenuation between 5-70 Hz with the reference at 700 feet

Fig. 60

Tirrawarra #22, well geophone; amplitude spectra of the first arrivals

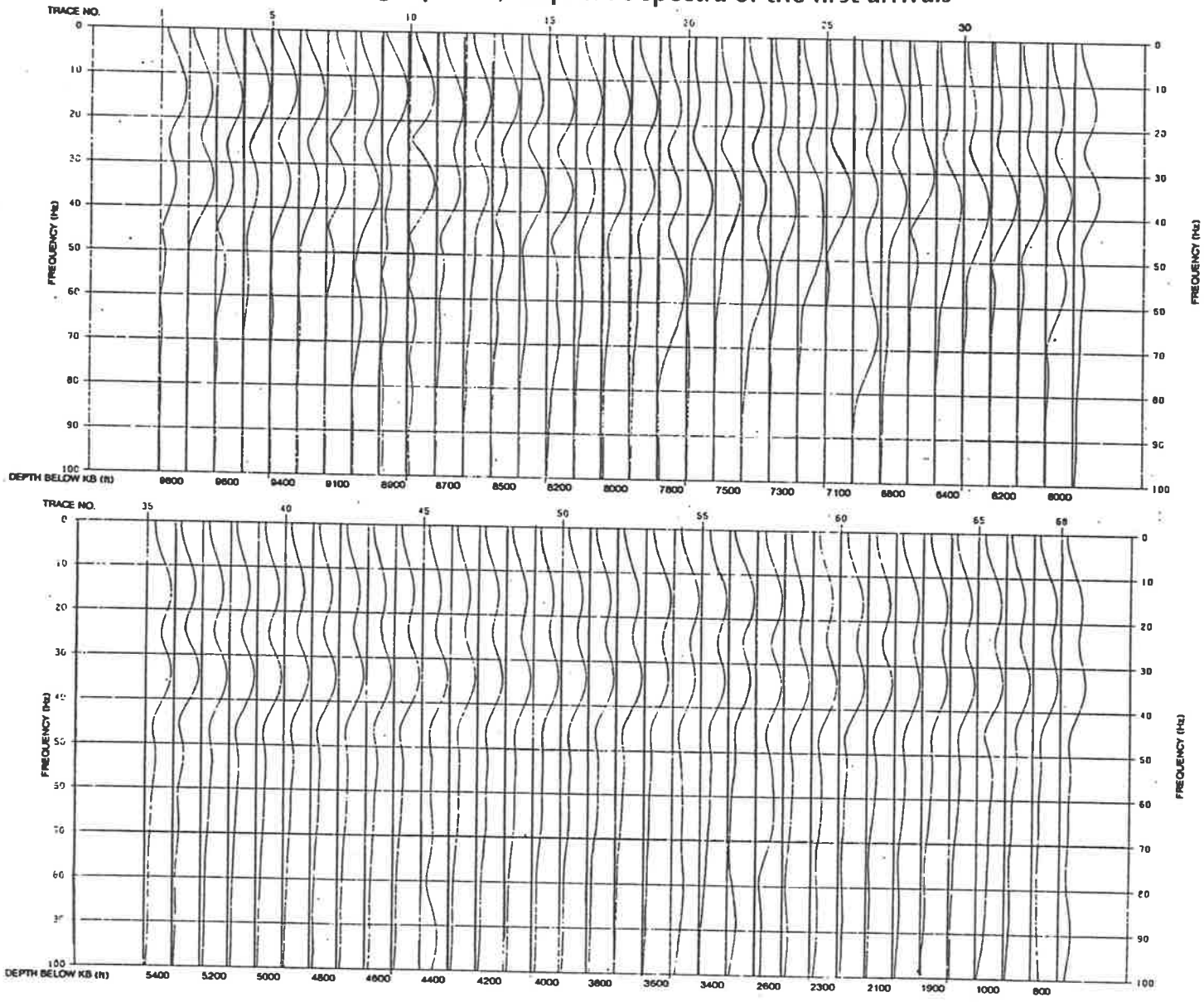

Fig. 61

similar surveys. This, or any of the previously discussed factors, may be the reason for the slight variation in the source signal.

Expanding the display of the downhole geophone arrivals aligned at 1000 ms allowed an estimate of the first arrival length to be made. Including data out to 1035 ms gave a first arrival length of 60 ms. The amplitude spectra computed over this window are displayed in Figure 61. The plots show similar trends, apart from the levels at 8900, 7800, 7400 and 6500 ft (corresponding to traces 9, 19, 22 and 28). In general, the spectra show amplitude peaks at both 15 and 35 Hz with very flat spectra at frequencies higher than approximately 50 Hz. The amplitude peak at 35Hz is unexpected as it is not present on the gun hydrophone amplitude spectra. It is consistent over the entire depth range and therefore, unlikely to be a result of either lithology or tool slip. It may be due to "ghosting" of the downgoing wavelet. This would be present on all downgoing geophone traces, while not apparent on the hydrophone trace.

Spectral ratios were calculated between the downhole geophone spectra and the corresponding gun hydrophone spectra over a frequency range of 10 to 60 Hz displayed in Figure 62. The ratios do not exhibit the linear trends expected but are distorted by the 35 Hz peak and 25 Hz and 45 Hz notches observed on the downhole geophone spectra. Between 10 to 25 Hz, and 35 to 45 Hz the ratios show a consistent and gradual increase in slope with depth. Above 45 Hz the ratios are inconsistent in their trends. The plots for some levels show fluctuations from the trends corresponding to irregularities in the downhole geophone amplitude spectra (traces 9, 10, 13, 19, 22, 23, 24, 28, 29 and 33, corresponding to observations at 8900, 8800, 8500, 7800, 7400, 7300, 7200, 6800, 6400 and 6000 feet). The application of a 55 Hz high cut filter to the downhole geophone suggests that noise (mechanical or electrical) was observed during recording.

As a comparison with the multiple reference spectral ratio analysis, amplitude ratios were calculated using as a single reference the geophone trace from 800 ft (trace 67). The amplitude ratios between 10-60 Hz are displayed in Figure 63. They show trends similar to

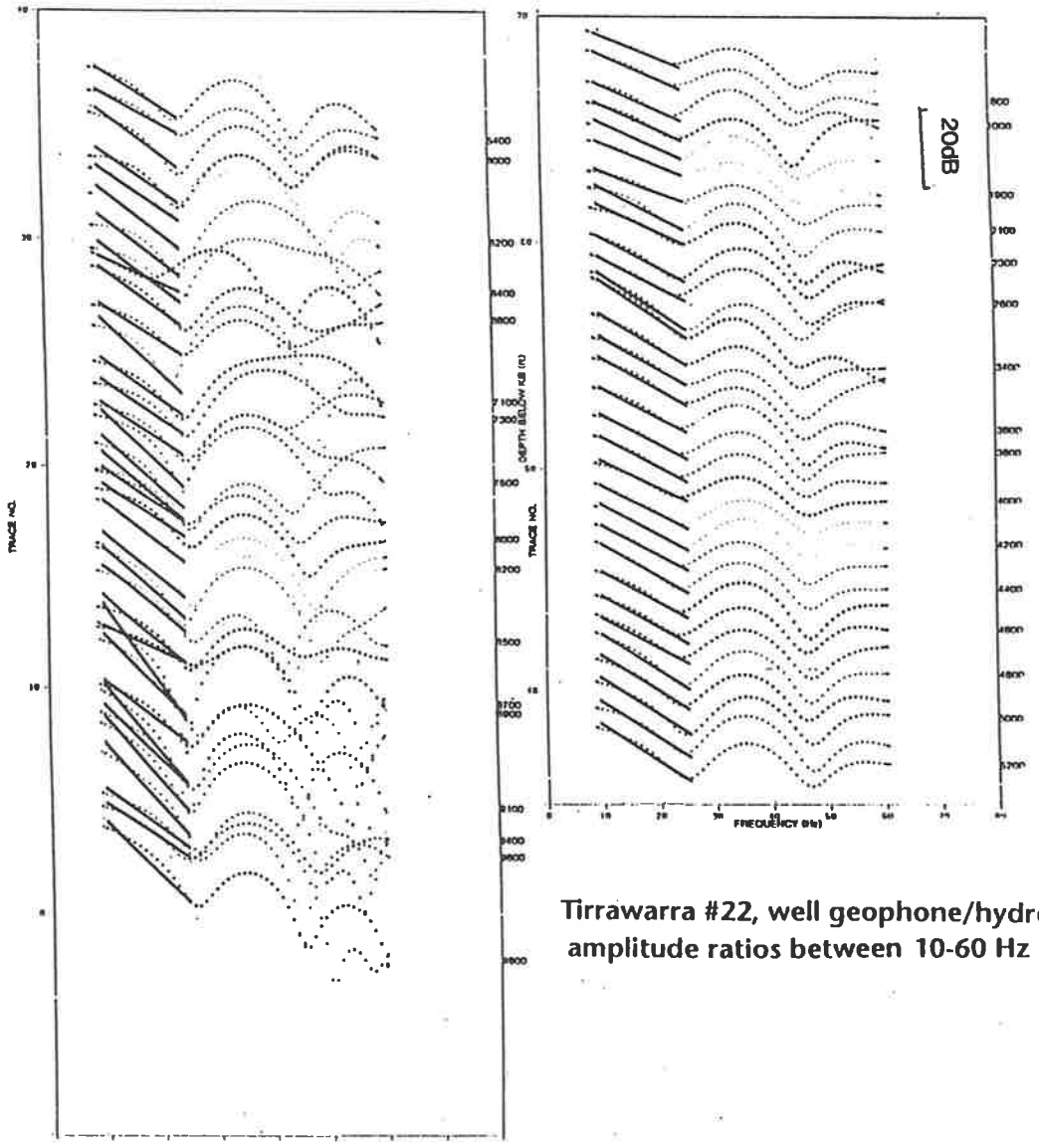

Tirrawarra #22, well geophone/hydrophone; amplitude ratios between 10-60 Hz

Fig. 62

Tirrawarra #22, well geophone/reference trace at 800 ft (trace 67)
amplitude ratios between 10-60 Hz

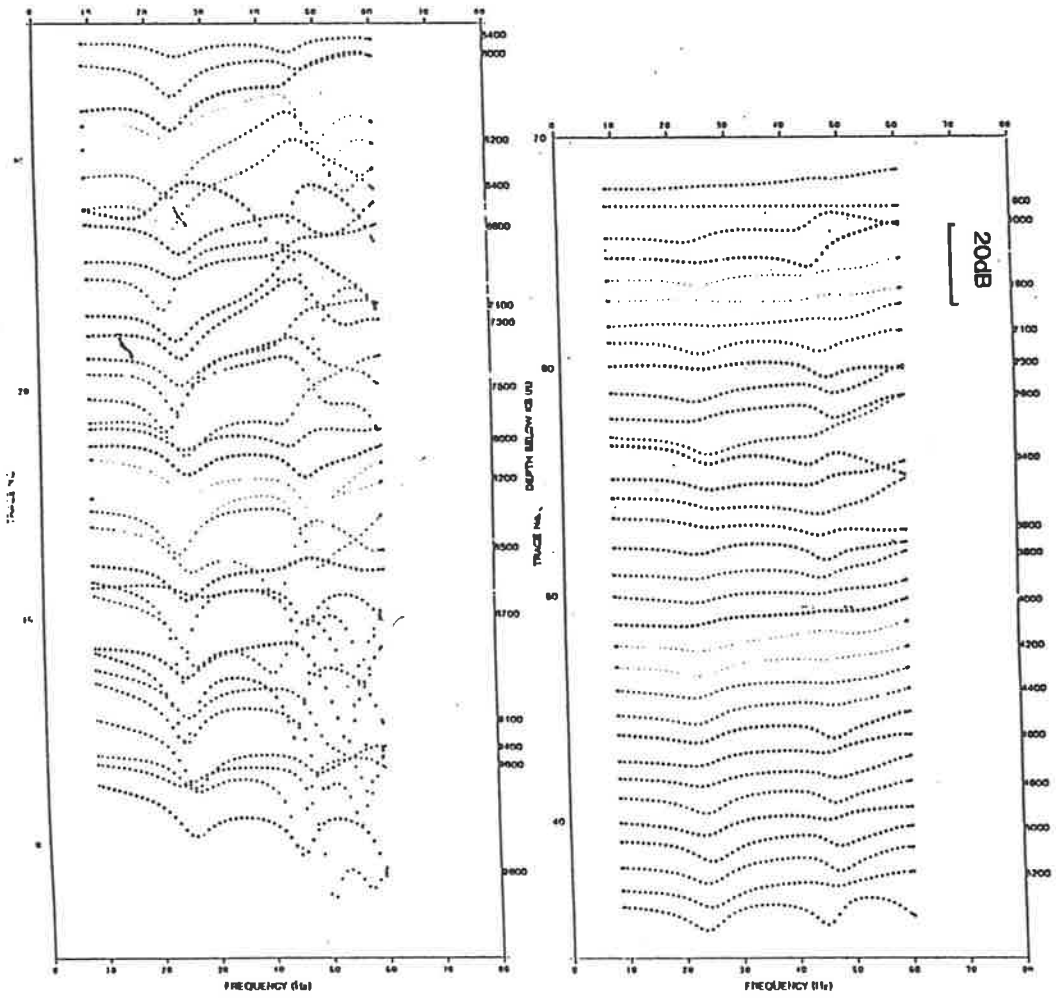

Fig. 63

those observed for the multiple reference analysis. The notching at 25 Hz and 45 Hz is reduced relative to that observed in the spectral ratios calculated using the hydrophone trace on the reference, particularly for depths less than 6000 ft. This is no doubt due to the notching also being present in the reference trace, so that its effect tends to be diminished in the ratio data.

The amplitude ratios suggest that outside of a 10-25 Hz bandwidth, either a constant Q assumption is incorrect for this data, or the downgoing signal was contaminated. The evidence, both in the literature and this study, is supportive of the constant Q model. "Ghosting" of the downgoing wavelet may have contaminated the downgoing signal, which upon analysis, gives the results observed. Isolating the cause of the observed notch may have led to filtering to remove its effect. However, this was not possible with the available data.

Further analysis of the Tirrawarra #22 data set was not undertaken as realistic B_X values could not be obtained from the notch affected amplitude data.

7.8 Spectral Ratio Analysis in Cased Boreholes

A limited amount of information is available concerning the effects of casing and its bonding on signal attenuation. Observations by van Sandt and Levin (1963), and Hardage (1983) suggest that there is no significant difference in the shape of a seismic wavelet recorded in open hole when compared to that recorded through a well cemented single casing string. Recordings through multiple strings are rarely successful due to one or more of the strings not bonding with the formation.

Tirrawarra #22 has surface casing to a depth of 650 ft below KB, and at the time of the VSP survey, a single casing string to a depth of 5650 ft below KB. The propagation velocity of the first arrival over the cased interval ranges between 6000 ft/s and 9000 ft/s, which is characteristic of the formation velocities, and not of the steel casing (17000 ft/s). Steel casing has a very high Q value and does not attenuate the seismic signal. The medium between the

casing and the formations does not appear to have any appreciable effect on the seismic signal, and therefore if the rates of intrinsic attenuation could have been determined for the cased interval of Tirrawarra #22 it is believed they would be representative of the lithology.

Without access to, and analysis of, more VSP data recorded under both cased and uncased conditions, the above observations are not conclusive.

CHAPTER 8

DISCUSSION AND CONCLUSIONS

8.1 Introduction.

Intrinsic attenuation is the anelastic loss of energy, through conversion to heat, from a propagating seismic wavelet. The method of analysis used to determine this parameter was the spectral ratio technique. This is one of several recognized methods and is generally accepted to give reliable results. A processing route involving the spectral ratio method was devised and used to construct cumulative attenuation curves for two VSPs recorded in the Cooper and Eromaga Basins. Rates of attenuation were determined from these curves. The observed attenuation is the sum of the intrinsic attenuation, due to lithology, and the apparent attenuation resulting from short-period multiple activity.

The use of synthetic VSP data, constructed from log data, both with and without multiples provides a method to determine the apparent attenuation.

Quantifying attenuation has the potential to improve the results from conventional surface seismic recording via the optimization of in-field recording parameters and inverse-Q filtering during processing.

8.2 VSP Acquisition For Attenuation Measurements

Processing of the VSP data sets for Watson #1 and Tirrawarra #22 has highlighted several of the conditions that such data should satisfy to maximize the accuracy of attenuation estimates.

i) The source signature must be repeatable and the input to the ground adequately monitored, preferably by a fixed downhole monitor. Using the downhole signature phone to record multiple reference traces allows the removal of source and coupling variations from the spectral ratio analysis of the geophone data.

ii) The source must have a reasonable frequency bandwidth. Cultural noise, for example generator, traffic and rig noises, should be eliminated if possible.

iii) The VSP should be recorded with sufficient levels over the zones of interest and to within as close to the earth's surface as is possible. A check on coupling of the downhole geophone to the borehole must be made at all levels, to eliminate tool slippage. An examination of the caliper log, if available, should be made prior to the survey to locate zones where oversize hole conditions may cause difficulties in clamping the geophone.

iv) VSP levels can be recorded through single casing strings provided they are adequately cemented to the formations.

8.3 Use of the Spectral Ratio Method to Compute Attenuation

Determining attenuation from VSP data using the spectral ratio method assumes Q to be independent of frequency, which apart from a slight dependence due to dispersion, is generally accepted. Experimental evidence to support the constant-Q model, at least over the range of frequencies encountered in seismic measurements, is extensively documented in the literature. The technique also assumes the formations surrounding the borehole are homogeneous, that the VSP data is free from noise, interference and mode conversion.

Criticism of the method is that selection of both the first time break window and the frequency bandwidth over which to perform the analysis is highly subjective. Ideally the time window should encompass an interval representative of the source signature and free from

reflected energy, while the frequency bandwidth should be that of the source signature. In reality the first arrival changes in frequency content and becomes broader with increasing depth.

It is recommended that the first break time window be determined from a visual inspection of all the geophone traces, displayed on expanded scales, with either the minimum or maximum amplitude of the first breaks aligned. Comparison of the traces should enable definition of a window that encompasses the energy of the first arrival and has a signature that remains similar in shape with increasing depth.

A least squares fit to the amplitude ratios for the spectral ratio analysis should be made only after inspection of the data with respect to frequency. Hauge (1981) made several runs with the spectral ratio method using different frequency ranges and reference depths before selecting the parameters that he considered gave the best results.

Cumulative attenuation plots, generated from the spectral ratio analysis of model data, indicate a point scatter that is inherent in this method. The model VSP results provide a lower limit on the scatter likely to be encountered in the real data.

8.4 Estimating Multiple Attenuation Effects

The estimates of attenuation determined from VSP data are composed of the intrinsic attenuation due to lithology, and the apparent attenuation resulting from short-period multiple reflections. Schoenberger and Levin (1974, 1978) showed that in 33 wells, from all over the world, the apparent attenuation ranged from 0.01 to 0.22 dB/wavelength, while Hauge (1981) determined contributions of up to 52% of the observed attenuation.

The apparent attenuation can be estimated using the spectral ratio method applied to synthetic VSP data generated from sonic and density logs. In this work the estimates were

made from data containing multiples of all orders, and may be affected by the sample rate of the model (1 ms).

Estimates of the apparent attenuation for the two wells studied range from 0.0381 to 0.9578 dB/wavelength. The greatest contribution is found over the Permian section of the Tirrawarra #22 well, which is dominated by a cyclic sequence of coals, sands and shales that generate a very strong short-period multiple train.

8.5 Attenuation Measurements and Lithology

Direct measurements that allow an understanding of the region around a borehole are of great importance to both hydrocarbon and mineral exploration. Laboratory research has shown that attenuation is related to other important rock properties, but accurate in-situ measurements of attenuation are required for these correlations to be useful. The results from the analysis of Watson #1 illustrate that intrinsic attenuation can be calculated using the direct arrivals in VSP data. The values for intrinsic attenuation range between 0.0668 to 1.0701 dB/wavelength in this well. From the scatter seen in the cumulative attenuation plots, it is evident that the vertical resolution of attenuation measurements is no better than several hundred feet, confirming the conclusion of Hauge (1981).

Mari (1989) developed a Q log using attributes of the VSP first arrivals and showed that a correlation between a known reservoir and a decreased Q value could be made. The average thickness of this reservoir is 150 feet with 590 feet of shale cap rock. The reservoir and cap rock had Q values of 20 and 50 respectively. Using the rates of intrinsic attenuation and the interval velocities determined from the VSP first arrivals, a Q log was constructed for Watson #1 and this is displayed in Figure 64. Most of the variation in the Q log reflects the changes in interval velocities, which is in turn controlled by the depth sampling for the VSP. The variation does show some correlation with the sonic log however, a correlation cannot be made between the 17 foot thick reservoir within the Hutton formation and a change in Q. Based on this result it is difficult to envisage using this type of analysis to define rock

WATSON 1

K.B. 293.15 FEET ATP 259 P
T.D. 5627 FEET NACCOWLAH

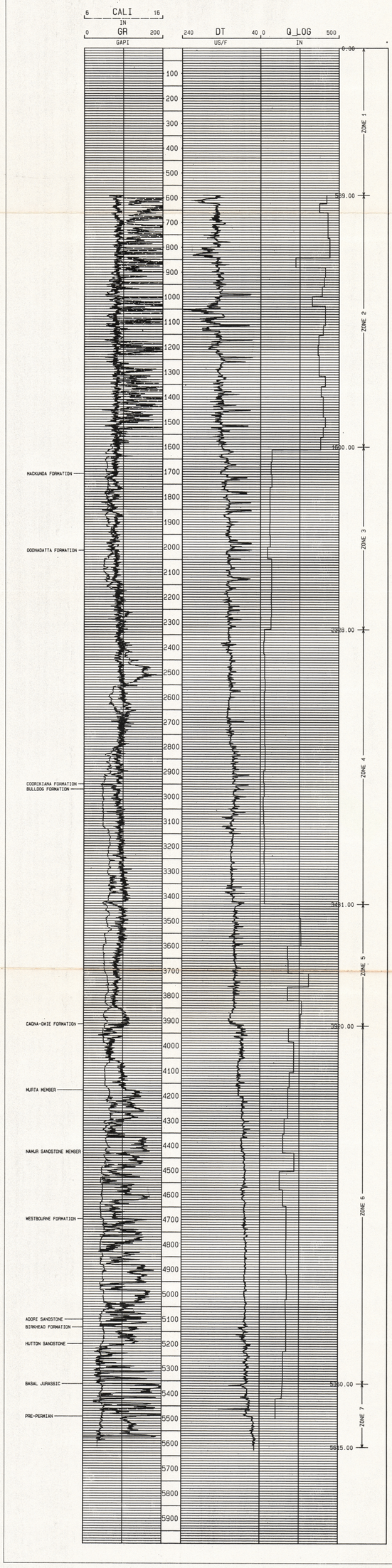

Watson #1, Q log

Fig. 64

properties over typical reservoirs in the Cooper and Eromanga Basins because of their limited vertical extent.

Both of the VSPs studied were recorded several years ago, and with modern borehole geophones a reduction in the amount of scatter for the real data is a possibility. The use of multi-level geophones could remove some of the problems involved in acquisition and the availability of a repeatable seismic source with a bandwidth of several hundred hertz may allow resolution over a smaller interval. However, as demonstrated by the noise-free model data, the basic problem is that the attenuation effects over short intervals are generally small and highly susceptible to distortion by reflections from interfaces close to the receiver.

8.6 Attenuation and Seismic Acquisition

The aim of surface seismic acquisition and processing is to present an image of the earth. In the ideal case, each reflecting interface would be represented on a seismic trace by a spike; however, in reality, this is unachievable. The actual result is a band limited response, generally of mixed phase, with limited resolution both vertically and horizontally. The measurement of a parameter that quantifies the changing nature of the frequency spectrum of the propagating seismic pulse, and at the same time allows for possible improvements in acquisition and processing techniques, may benefit exploration.

Several of the known Cooper Basin reservoirs are found below the Early-Permian Coal sequences, that, in the Tirrawarra #22 analysis, gave rise to a very large apparent attenuation. The results from the model VSP data suggest that the response from the Permian formations is highly attenuated for frequencies above about 40 Hz, almost entirely as a result of short-period multiple activity.

Conventional processing attempts to rectify the amplitude decay caused by spherical divergence and attenuation through the application of an AGC-type of scaling, and the frequency-dependent losses by deconvolution. However with a measure of the attenuation

that the propagating wavelet undergoes it is possible that the processing route could be altered to a correction for spherical divergence and then the application of an inverse-Q filter derived from VSP data. Gelius (1987) used such a scheme on seismic data across a shallow gas reservoir (1.6 s two way time) in the North Sea, and suggested that the method improves the resolution, especially in the reservoir zone. The inverse-Q filter is a time variant operator derived from the apparent attenuation data.

For the purposes of correlating surface seismic with synthetic data, the synthetic seismogram should be processed with the application of the apparent Q attenuation. Gelius (1987) concluded that synthetics with attenuation applied show a better tie, when the Q can be estimated fairly accurately, than synthetics without attenuation.

The VSP first arrival can be used as a measure of the attenuation that a seismic wavelet undergoes during propagation. By statistically determining wavelets that, on convolution with the downgoing first arrival, generate a spike, a series of wavelets will be generated that can be used to condition the surface seismic prior to deconvolution. Alternatively, an operator to stabilise the surface seismic can be determined using the Q-corrected synthetic trace for the convolution.

For both Watson #1 and Tirrawarra #22, attenuation estimates have not been made for the near surface (ground level to approximately 500 feet), since the shallowest VSP level is below the surface casing shoe. Within this zone, which is traversed twice by the signals recorded in surface seismic, the unconsolidated sediments are likely to exhibit high rates of attenuation. Attenuation estimates for this zone could be made using the downgoing wave that is generated as a multiple from the free-air surface. This requires identifying the multiple in the downgoing wave train and carrying out spectral ratio analysis upon it. Alternatively, a shallow borehole could be used to collect data using either a surface or downhole source in a more elaborate version of the uphole survey commonly used to acquire static information. As it is unusual to log the borehole to surface, only apparent attenuation can be estimated using

the techniques developed here. Dillon (1991) shows that estimates of intrinsic attenuation can be determined from the surface down using VSP data and the energy-flux theorem.

8.7 Future Areas of research using Q-estimates:

1. The application of inverse-Q filters to reflection seismic data in order to improve resolution and interpretation.

2. The use of model data with known Q values, to determine the accuracy of intrinsic Q estimation, and to determine the resolution limits under different conditions.
3. The derivation of Q-estimates for the near surface using both VSP arrivals and uphole data recorded in conjunction with surface seismic.
4. The derivation of Q using full array sonic log data and its comparison with VSP data.
5. An investigation into the effects of casing and its bonding on the VSP first arrival.

These areas would have been interesting to investigate, however due to time restrictions and limited data availability these extra areas of interest have not been explored.

In summary, this study has shown that using the spectral ratio method and VSP data, estimates of intrinsic attenuation for the Cooper and Eromanga Basin can be determined, although the limits of resolution are too large to allow direct correlation with lithology. The observed Q values are parameters that can be used to improve acquisition, processing and interpretation of seismic reflection data, areas that should prove valuable in a known hydrocarbon province.

ACKNOWLEDGEMENTS

I would like to thank the following:

- Andrew Mitchell, my supervisor and tutor, for his endless patience, assistance and encouragement throughout my study.

- SANTOS Limited, for providing me with the data and relevant material.

- Jodie Lavis, for her hours spent typing the many revisions of my thesis.

- finally my wife Jo-anne, without whose support and encouragement all of this would not have been possible.

BIBLIOGRAPHY

1. Attewell, P.B. and Ramana, Y.V., 1966, Wave attenuation and internal friction as functions of frequency in rocks: Geophysics, v. 31, p. 1049-1056.
2. Balch, A.H., Lee, M.W., Miller, J.J., and Ryder, R.T., 1982, The use of vertical seismic profiles in seismic investigations of the earth: Geophysics, v. 47, p. 906-918.
3. Biot, M.A., 1962, Mechanics of deformation and acoustic propagation in porous media: Journal of the Acoustic Society of America, v. 34, p. 1254-1264.
4. Born, W.T., 1941, The attenuation constant of earth materials: Geophysics, v.6, P 132-148
5. Dillon, P.B., Collyer, V.A., 1985, On timing the VSP first arrival: Geophysical Prospecting, v. 33, p. 1174-1194.
6. Dillon, P.B., 1991, Q and upward extension of VSP data through the energy-flux theorem: First Break, v. 9 no 6 p 289-298.
7. Futterman, W.I., 1962, Dispersive body waves: Journal of Geophysical Research, v. 67, p. 5279-5291.
8. Gal'perin, E.I., 1974, Vertical Seismic Profiling: Society of Exploration Geophysicists Special Publication No. 12, 270 pages.
9. Ganley, D.C., Kanasawich, E.R., 1980, Measurement of absorption and dispersion from checkshot surveys: Journal of Geophysical Research, v. 85, p. 5219-5226.

10. Gardner, G.H.F., Wyllie, M.R.J., Droschak, D.M., 1964, Effects of pressure and fluid saturation on the attenuation of elastic waves in sands: Journal of Petroleum Technology, February, p. 189-198.
11. Gelius, L.J., 1987, Inverse Q-filtering. A spectral balancing technique: Geophysical Prospecting, v. 35, p. 656-667.
12. Gladwin, M.T. Stacey, F.D., 1974, Anelastic degradataion of acoustic pulses in rock: Phys. Earth Plan. Int., v.8, p. 332-336.
13. Gordon, R.B., Davis, L.A., 1968, Velocity and attenuation of seismic waves in imperfectly elastic rock: Journal of Geophysical Research, v. 73, p. 3917-3935.
14. Gravestock, D.I., Alexander, E.M., 1986, Porosity and permeability of caprocks in the Eromanga Basin, South Australia: The APEA Journal, v. 26 pt. 1, p. 202-213.
15. Hamilton, E.L., 1972, Compressional - wave attenuation in marine sediments: Geophysics, v. 37, p. 620-646.
16. Hardage, B.A., 1983, Vertical Seismic Profiling, Part A: Principles: Handbook of Geophysical Exploration Vol. 14, Geophysical Press, 450 pages.
17. Hauge, P.S., 1981, Measurements of attenuation from vertical seismic profiles: Geophysics, v. 46, p. 1548-1558.
18. Jackson, D.D., Anderson, D.L., 1970, Physical mechanisms of seismic wave attenuation: Review of Geophysics and Space Physics, v. 8, p. 1-63.
19. Johnston, D.H., Toksoz, M.N., Timur, A., 1979, Attenuation of seismic waves in dry and saturated rocks: II. Mechanisms: Geophysics, v. 44, p. 691-711.
20. Johnston, D.H., Toksoz, M.N. 1981, Seismic wave attenuation: Geophysical Reprint Series, 2, Soc. Explor. Geophys.

21. Jones, T.D. 1986, Pore fluids and frequency dependent wave propagation in rocks: Geophysics, v. 51, p. 1939-1953.

22. Kantsler, A.J., Prudence, T.J.C., Cook, A.C., Zwigulis, M., 1983, Hydrocarbon habitat of the Cooper/Eromanga Basin, Australia: The APEA Journal, v. 23 pt. 1, p. 75-92.

23. Kennett, P., Ireson, R.L., 1977, Vertical seismic profiling - recent advances in techniques for data acquisition, processing and interpretation: Presented at the 47th Annual International Meeting of the Society of Exploration Geophysicists.

24. Kennett, P., Ireson, R.L., Conn, P.J., 1980, Vertical seismic profiles - their applications in exploration geophysics: Geophysical Prospecting, v. 28, p. 676-699.

25. Kennett, P., Ireson, R.L., 1981, The VSP as an interpretation tool for structural and stratigraphic analysis: Paper presented at the 43rd Meeting of the EAEG, Venice, Italy.

26. Kennett, P., Ireson, R.L., 1982, Vertical seismic profiles: EAEG Continuing Education, 184 pages.

27. Kjartansson, E., 1979, Constant-Q wave propagation and attenuation: Journal of Geophysical Research, v.84, p.4737-4748.

28. Klimentos, T., McCann, C., 1990, Relationships between compressional wave attenuation, porosity, clay content and permeability of sandstones: Geophysics, v. 55, p. 998-1014.

29. Knopoff, L., McDonald, G.J.F., 1958, Attenuation of small amplitude stress waves in solid. Review of Modern Physics, v. 30, p. 1178-1192.

30. Kolsky, H., 1955, The propagation of stress pulses in viscoelastic solids: Philosophical Magazine, v.1, p. 693-710.

31. Mari, J.L., 1989, Q-log determination on downgoing wavelets and tube wave analysis in vertical seismic profiles: Geophysical Prospecting, v. 37, p. 257-277.

32. Mavko, G.M., Nur, A., 1975, Melt squirt in the aesthenosphere: Journal of Geophysical Research, v. 81, p. 1444-1448.

33. Mavko, G.M., Nur, A., 1979, Wave attenuation in partially saturated rocks: Geophysics, v. 44, p. 161-178.

34. Mavko, G.M., Kjartansson, E., Winkler, K., 1979, Seismic wave attenuation in rocks: Review of Geophysics and Space Physics, v. 17, p. 1155-1162.

35. Newman, P., 1973, Divergence effects in layered earth: Geophysics, v. 38 p 481-488.

36. McDonal, F.J., Angona, F.A., Mills, R.L., Sengbush, R.L., van Nostrand, R.A., and White, J.E., 1958, Attenution of shear and compressional waves in Pierre shale: Geophysics, v. 23, p. 421-439.

37. Nur, A., Winkler, K., 1980, The role of friction and fluid flow in wave attenuation in rocks (abstract) : Geophysics, v. 45, p. 591-592.

38. O'Connell, R.J., Budiansky, B., 1977, Viscoelastic properties of fluid-saturated cracked solids: Journal of Geophysical Research v. 82, p. 5719-5735.

39. O'Doherty, R.F., Anstey, N.A., 1971, Reflections on amplitudes: Geophysical Prospecting, v, 19, p. 430-458.

40. O'Hara, S.G., 1989, Elastic-wave attenuation in fluid saturated Berea sandstone: Geophysics, v. 54, p. 785-788.

41. Peselnick, L., Outerbridge, W.F., 1961, Internal friction in shear and shear modulus of Solenhofen Limestone over a frequency range of 10^7 cycles per second: Journal of Geophysical Research, v. 66, p. 581-588.

42. Rango, R., Fitzgerald, N., 1986, Internal report on the acquisition and processing of a vertical seismic profile well: Watson #1: Delhi Petroleum Pty Ltd. (unpublished)

43. Ricker, N. 1953, The form and laws of propagation of seismic wavelets: Geophysics v. 18, p. 10-40.

44. Sams, M., Goldberg, D., 1990, the validity of Q estimates from borehole data using spectral-ratios: Geophysics v. 55, p. 97-101.

45. Savage, J.C., 1965, Thermoelastic attenuation of elastic waves by cracks: Journal of Geophysical Research, v. 71, p. 3929-3938.

46. Schoenberger, M., Levin, F.K., 1974, Apparent attenuation due to intrabed multiples: Geophysics, v. 39, p. 278-291.

47. Schoenberger, M., Levin, F.K., 1978, Apparent attenuation due to intrabed multiples, II: Geophysics, v. 43, p. 730-737.

48. Sheriff, R.E., Telford, W.M., Geldart, L.P. and Keys, D.A., 1976, Applied Geophysics: Cambridge University Press, 860 pages.

49. Siebert, M.G., 1986, Vertical seismic profiling: A study of a standard zero-offset survey recorded in the Cooper Basin: Honours thesis, University of Adelaide. (unpublished)

50. Stainsby, S.D., Worthington, M.H., 1985, Q estimation from vertical seismic profile data and anomalous variations in the Central North Sea: Geophysics, v. 50, p. 615-626.

51. Stoll, R.D., 1974, Acoustic waves in saturated sediments: Physics of sound in marine sediments, Plenum Press.

52. Stuart, W.J., 1976, The genesis of Permian and Lower Triassic reservoir sandstones during phases of Southern Cooper Basin development: The APEA Journal, v. 16, pt. 1, p. 37-48.

53. Tarif, P., Bourbie, T., 1987, Experimental comparison between spectral-ratio and rise time technique for attenuation measurement: Geophysical Prospecting, v. 35, p. 668-680.

54. Tittman, B.R., Abdel-Gawad, M., and Housley, R.M., 1972, Elastic velocity and Q factor measurements on Apollo 12, 14 and 15 rocks: Proc. 3rd Lunar Science Conference, v. 3, p. 2565-2575.

55. Tittman, B.R., 1977, Internal friction measurements and their implications in seismic Q structure models of the crust, in the Earth's crust: Geophys, Monogr. 20, AGU, p.127-213.

56. Toksoz, M.N. Johnston, D.H., and Timur, A., 1979, Attenuation of seismic waves in dry and saturated rocks: 1. Laboratory mechanisms: Geophysics v. 44, p. 681-690.

57. Tonn, R., 1991, The determination of the seismic quality factor Q from VSP data: a comparison of different computational methods: Geophysical Prospecting, v. 39, p. 1-27.

58. Tullos, F.N., Reid, A.C., 1969, Seismic attenuation of Gulf Coast sediments: Geophysics, v. 34, p. 516-528.

59. Walsh, J.B., 1966, seismic wave attenuation in rock due to friction: Journal of Geophysical Research, v. 71, p. 2591-2599.

60. Winkler, K.W., Nur, A., 1979, Pore fluids and seismic attenuation in rocks: Geophysical Research Letters v. 6, p. 1-4.

61. Winkler, K.W., Nur, A., 1982, Seismic attenuation: Effects of pore fluids and frictional sliding: Geophysics, v. 47, p. 1-14.

62. Wuenschel, P.C., 1965, Dispersive body waves - An experimental study: Geophysics, v. 30, p. 539-551.

63. van Sandt, D.R., Levin, F.K., 1963, A study of cased and open holes for deep hole seismic detection: Geophysics, v. 28, p. 8-13.

64. Zoeppritz, K., 1919, Uber reflexion und durchgang seismischer wellen durch Unstetigkerlsflaschen. Berlin, Uber Erdbebenwellen VIIB, Nachrichten der Koniglichen Gesellschaft der Wissenschaften zu Gottingen, Math-phys. K.1 p. 57-84.

APPENDIX 1

Details of the two surveys:

The following lists indicate the depths and number of repeated recordings for the VSP levels in each of the wells, Watson #1 and Tirrawarra #22. The depths marked with an asterisk, after editing, have been omitted from the spectral ratio analysis. Elevation information is also listed for each well for completeness.

WATSON #1 VSP LEVELS

Level	Depth in feet below KB	No. of records	Level	Depth in feet below KB	No. of records
1	* 1000	3	40	3056	1
2	* 3000	3	41	3001	1
3	5500	3	42	2946	1
4	5420	1	43	2896	1
5	5340	1	44	2846	1
6	5231	1	45	2796	1
7	5122	1	46	2741	2
8	5022	1	47	2686	1
9	4922	3	48	* 2631	2
10	* 4851	1	49	2576	1
11	4780	1	50	2526	2
12	* 4713	1	51	2476	1
13	4646	1	52	2426	1
14	4579	2	53	2376	1
15	4504	2	54	2328	1
16	4429	1	55	2280	1
17	4354	1	56	2232	1
18	4291	1	57	2184	1
19	4228	1	58	* 2138	1
20	4165	1	59	2092	2
21	4105	1	60	2046	1
22	4045	3	61	2000	1
23	3985	1	62	1954	1
24	3930	1	63	1906	1
25	3875	2	64	1858	1
26	3820	1	65	1810	1
27	3765	1	66	1762	1
28	3710	2	67	1712	1
29	3655	1	68	1662	1
30	3600	1	69	1612	1
31	3545	1	70	1562	1
32	3488	1	71	1521	1
33	3431	1	72	1480	1
34	* 3374	1	73	1439	1
35	* 3322	1	74	1398	1
36	3270	1	75	1357	1
37	3218	1	76	1316	1
38	3166	1	77	1275	1
39	3111	1	78	1234	1

Level	Depth in feet below KB	No. of records	Level	Depth in feet below KB	No. of records
79	1193	2	95	589	1
80	1154	2	96	* 555	1
81	1115	1	97	* 521	1
82	1076	1	98	* 487	2
83	1037	1	99	* 453	1
84	998	1	100	* 419	1
85	959	1	101	* 385	1
86	920	1	102	* 352	1
87	881	1	103	* 319	1
88	842	1	104	* 286	1
89	803	1	105	* 253	1
90	764	1	106	* 220	2
91	729	1	107	* 187	2
92	694	1	108	* 155	1
93	659	1	109		
94	624	1			

Elevation of KB = 293.15 Ft

Elevation of Ground Level = 274.15 Ft

TIRRAWARRA #22 VSP LEVELS

Record Number	Depth in feet below KB	No. of records	Record Number	Depth in feet below KB	No. of records
1	* 1500	2	40	6800	3
2	* 6000	2	41	* 6727	2
3	9800	8	42	* 6700	3
4	* 9741	4	43	* 6595	4
5	9700	4	44	6500	2
6	* 9636	5	45	6400	2
7	9600	3	46	6300	2
8	9500	3	47	6200	2
9	9400	4	48	6100	2
10	9300	3	49	6000	2
11	* 9200	3	50	* 5900	2
12	* 9149	2	51	* 5882	3
13	9100	3	52	* 5880	4
14	9000	3	53	* 5700	3
15	8900	3	54	* 5668	2
16	* 8860	2	55	* 5600	2
17	8800	2	56	* 5522	1
18	* 8740	3	57	5500	2
19	8700	3	58	5400	2
20	8600	2	59	5300	2
21	8500	3	60	5200	2
22	8400	2	61	5100	2
23	* 8300	3	62	5000	3
24	8200	3	63	4900	2
25	8100	2	64	4800	2
26	8000	3	65	4700	2
27	7900	3	66	4600	2
28	7800	2	67	4500	2
29	* 7700	2	68	4400	2
30	* 7685	3	69	4300	2
31	7600	2	70	4200	2
32	7500	2	71	4100	2
33	7400	2	72	4000	2
34	7300	2	73	3900	2
35	7200	2	74	3800	2
36	7100	2	75	3700	2
37	7000	2	76	3600	2
38	* 6900	3	77	3500	2
39	* 6863	4	78	3400	2

TIRRAWARRA #22 VSP LEVELS (CONT)

Record Number	Depth in feet below KB	No. of records	Record Number	Depth in feet below KB	No. of records
79	3300	2	95	1700	2
80	* 3200	2	96	* 1600	2
81	* 3100	4	97	* 1500	2
82	* 3000	3	98	* 1400	2
83	* 2900	2	99	* 1300	2
84	* 2800	2	100	* 1200	2
85	* 2700	2	101	* 1100	2
86	2600	2	102	1000	2
87	* 2500	2	103	900	1
88	2400	2	104	800	2
89	2300	2	105	700	2
90	2200	2	106	* 600	2
91	2100	2	107	* 500	2
92	2000	2			
93	1900	2			
94	* 1800	2			

Elevation of KB = 139.4 Ft

Elevation of Ground Level = 123.2 Ft

APPENDIX 2

Laboratory Attenuation Measurements

1A. Laboratory Techniques

The use of laboratory techniques to obtain information on attenuation, additional to that using in-situ techniques, has been essential in understanding the process of attenuation. In the laboratory, with controlled conditions, it has been possible to identify and quantify the effects of temperature, confining pressure, porosity, pore fluid and frequency on attenuation. It is necessary however to relate the laboratory results to the in-situ conditions of burial at depth. This appendix is not intended as a complete description of laboratory techniques, but to briefly outline some of these and to highlight some of the results that relate to the in-situ measurements.

Johnson and Toksoz (1981), separate laboratory techniques into the following four categories.

1. free vibration
2. forced vibration
3. wave propagation
4. observation of stress-strain curves

The method used determines the frequencies at which measurements are made. For the free vibrations this is generally less than 100 Hz, for forced vibration the range is between 100 Hz and 100 kHz; for wave propagation the range is in the ultrasonic frequencies greater than 100 kHz: Stress-strain methods allow measurements at less than 1 Hz.

1. Free Vibration

A torsion pendulum described by Peselnick and Outerbridge (1961) is one method that may be used. A rod of the material under investigation is suspended vertically, with a mass having a large moment of inertia attached to its lower end. The pendulum is put into oscillation, and the decay of the free oscillations after the initial deflection is recorded.

For an oscillating system in free decay the logarithmic decrement δ is given by equation 9 in section 3.2. By recording the decay of the system oscillating at its resonant frequency f_o, over a time interval Δt, the logarithmic decrement is given by;

$$\delta = \ln (A_t/A_{t+\Delta t})/(\Delta t f_o) \qquad \ldots 33$$

and Q can be calculated from equation 12.

In using the above technique, extreme care must be taken to isolate the system from extraneous vibrations and magnetic fields. The effect of clamping the sample at one end is to effectively reduce the length of the sample and is assumed to be negligible. Loss of energy not associated with free decay must be accounted for. This is the result of air damping and energy loss to the supports and frame of the system. Finally, and critical to all laboratory techniques, is the preparation of the sample.

2. Forced Vibration

These methods are based on forcing cylindrical samples to vibrate in the extensional or torsional mode. Estimates of Q can be made in two ways: i) by exciting the system to resonance, and then turning off the driving source and monitoring the subsequent decay of the vibrations ii) by measuring the amplitude of vibration of a standing wave at, and close to the

resonant frequency of the sample. The bluntness of the resonant peak is proportional to the logarithmic decrement d as given below (Gardner et al. 1964).

$$\delta = \pi \Delta f / f_o \qquad \ldots 34$$

Here Δf is the difference between the two frequencies at which the amplitude is 1/ 0.707 times the peak amplitude, and f_o is the resonant frequency.

Using forced vibration methods, sometimes referred to as the resonant bar technique, attenuation estimates can be made under different conditions of confining pressure, water saturation, and frequency. In calculating results the effect of energy radiating into the surrounding medium, and the effect of a confining jacket placed around the sample must be taken into account.

3. Wave propagation

The use of wave propagation through rock samples allows a measurement and calculation of attenuation to be made that is directly comparable with in-situ measurements. Two methods are in common use: i) the pulse-echo method, and ii) the through transmission method. Each method may use a pulse of a significant bandwith, or alternatively a single frequency tone. Problems arise due to losses through edge effects, beam spreading, coupling, diffraction, and mode conversion. By careful design and analysis these effects can be minimized. The frequencies used tend to be in the ultrasonic range, and analysis can be carried out using the spectral ratio technique. Wave propagation methods are applicable to samples confined in a jacket to examine the effects of both saturation and confining pressure.

4. Stress-Strain relationships

A sample of the material being investigated is subjected to a cyclic loading and unloading, and recordings of the related stresses and strains are made. The cycle may be

either sinusoidal or saw-toothed with a very wide range in periodicity and amplitude. The results are plotted as hysteresis curves. The loss of energy to the system, due to internal friction, is equal to the area between the loading and unloading curves. The relative attenuation is calculated from the loss of energy divided by the area under the loading curve. This method requires careful preparation of samples, the ability to measure strains of very small amplitude (down to 10^{-10}), and calibration against a known sample (generally a high Q steel).

1B Laboratory Results

With an increasing awareness of the possible benefits in being able to estimate attenuation in-situ, a large volume of literature on laboratory techniques and results has been published. Johnston and Toksoz (1981) compiled a set of papers that outline the major techniques and results. It is the intention here to highlight some of the results from laboratory experiments, particularly those which measure the effect of pressure, pore fluids, saturation and temperature.

Born (1941), using resonant bar techniques on dry rocks, observed constant Q attenuation between 500 Hz and 4 kHz. Peselnick and Outerbridge (1961) observed frequency-independent Q between 8.2 and 18.6 kHz (Table 11). However there is evidence that values obtained using different techniques give different attenuation values. For example, table 9 shows a decrease by a factor of 3 between Q values measured using the bar-resonance technique at 18.6 kHz and the pulse-echo technique at 9 MHz.

Method	Frequency	δ (nepers/wavelength)	Q
Free Vibration Sample A	3.8 Hz	$3.4\text{-}4.1\text{x}10^{-3}$	924-766
Free Vibration Sample B	6.52 Hz	$4\text{x}10^{-3}$	785
Forced Vibration Sample C	8200 Hz	$5\text{x}10^{-3}$	628
Forced Vibration Sample C	16400 Hz	$5\text{x}10^{-3}$	628
Forced Vibration Sample B	9500 Hz	$5\text{x}10^{-3}$	628
Forced Vibration Sample B	18600 Hz	$5\text{x}10^{-3}$	628
Wave propagation sample S1	9 MHz	$17\text{x}10^{-3}$	185

Table 9, Laboratory Results

Jones (1986) has shown that in saturated rocks there is some dependence of Q on frequency. This supports the work of Nur and Winkler (1980) who observed a constant Q attenuation in dry Berea Sandstone, but some frequency dependence of Q when saturated (Figure 65). Taken as a whole, there appears to be some ambiguity over the dependence of Q on frequency. However, over the seismic band, evidence suggests that it is independent of frequency.

Mavko et al (1979), state that one of the first observations of lunar seismology is that seismic waves propagate with much less attenuation on the moon (Q of 3000-5000), than observed in samples in the laboratory (Q of 100 at room temperature). Attenuation rates therefore, are affected by temperature and/or the vacuum conditions found on the moon. Decreasing the temperature to -200°C results in an increase in Q of 2-3 times, in both terrestrial and lunar rocks (Tittman et al 1972). Tittmann (1977) shows that the Q of a low-porosity dry olivine basalt ranges from 100 in normal laboratory conditions to over 2000 when outgassed at moderate temperatures in a high vacuum. Q returns to its previous value when the basalt is re-exposed to air.

Most laboratory experiments confirm that attenuation depends strongly on effective pressure, with attenuation in both dry and saturated rocks decreasing with applied pressure. Winkler and Nur (1982) suggest that applied pressure closes the pores and cracks within the rock, which stiffens the rock frame and leaves a smaller number of fluid-filled cracks to absorb energy. Velocity depends on pressure in a similar fashion.

Attenuation is strongly dependent upon fluid saturation, and is observed to be higher in both saturated and partially saturated rocks than in dry rocks. The relationship between saturation and attenuation is also dependent on the type of fluid. O'Hara (1989) presents attenuation measurements for four different fluids. The results are shown in Figure 65, where P_f refers to the pore fluid pressure and P_{eff} is the effective stress on the sample (the result of subtracting P_f from the external confining pressure). The attenuation in the brine saturated rock is approximately double that of the samples saturated with other fluids, and therefore attenuation is also dependent on the pore fluid-matrix chemistry. Laboratory measurements show that attenuation depends not only upon the fluid saturation, but also on the product of frequency and viscosity, which peaks between the seismic and sonic bands (Jones, 1986). The viscosity of a fluid also changes with temperature.

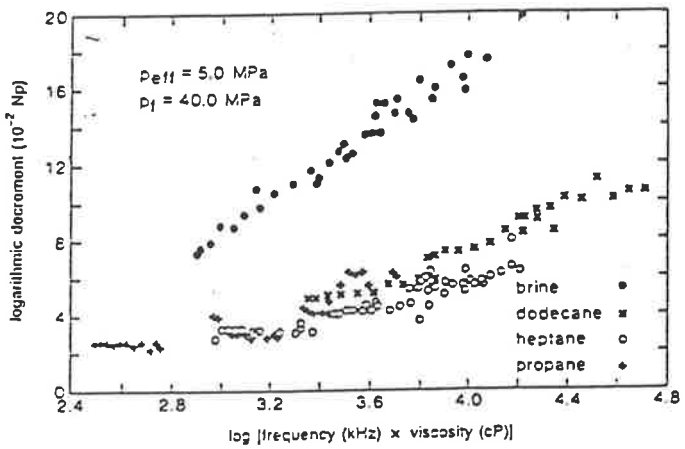

Fig.65

Logarithmic decrement in fluid saturated Berea Sandstone, versus the logarithm of the product of extensional wave frequency and fluid viscosity (O'Hara, 1989)

Recent work on compressional wave attenuation in 42 sandstone samples (Klimentos and McCann, 1990) has shown that clay content effects attenuation, possibly by the viscous interaction between the pore fluid and the clay particles. With many of the 42 samples having a small range of grain size and pore size, permeability has been shown to be related to clay content and consequently to attenuation. The results, determined using frequencies between 0.5 and 1.5 MHz under a pressure of 5MPa, show an increase in attenuation with increasing clay content and a possible, but not conclusive, decrease in attenuation with increasing permeability. As with all laboratory techniques, experiments must be performed to test these results using seismic frequencies and the confining pressures prevailing at depth.

Laboratory techniques have allowed parameters such as pressure, saturation, and temperature to be varied whilst measuring attenuation. The frequency range accessible in the laboratory far exceeds the conventional seismic band of approximately 10-100Hz. Some ambiguity still remains over the constancy of Q, but relationships between attenuation and several other parameters have been resolved.